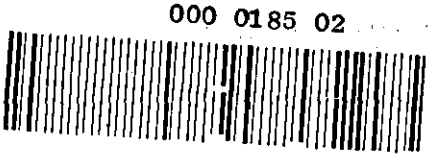

WIND-INDUCED OSCILLATIONS OF CIRCULAR CYLINDRICAL SHELLS

by

C.B. SHARMA

A Thesis Submitted for the Degree of

Doctor of Philosophy of

Loughborough University of Technology

Supervisor : Prof. D.J. Johns

Department of Transport Technology

September 1970

ACKNOWLEDGEMENTS

The author wishes to express his deep sense of gratitude to his supervisor, Professor David J. Johns for his valuable time and counsel during this study. Financial support was provided by the Ministry of Technology (U.K.) under Contract No. PD/1170/05. The author is also grateful for the assistance rendered by Messrs. R. Payne, J. Court, N. Randall and J.E. Smith during experimental work.

The author is deeply indebted to Dr. Kevin Forsberg, Head, Solid Mechanics, Lockheed Palo Alto Research Laboratory, California for providing some of his theoretical results to compare with the present work.

Special thanks are due to Mrs. Brown for her care and patience in typing the manuscript.

Finally, with both pride and appreciation the author acknowledges the patience and understanding of his wife, Padma, and his children, Sanjay and Seema during the course of this study.

GENERAL INTRODUCTION

In recent years, considerable interest has been shown in the elastic stability and vibration characteristics of circular cylindrical shells because of the widespread use of this or similar type structures in air, space, and water craft.

In general, in the determination of the modal characteristics of thin cylindrical shells, sixteen sets of homogeneous boundary conditions can be examined at each end of the shell. The present study is concerned with shells clamped at the base and with free, ring stiffened or simply-supported upper end i.e. structures typical of a chimney stack. In particular, the problem is to study wind-induced oscillations of tall chimneys.

The problem in wind-induced swaying oscillations of tall chimneys and other similar cylindrical shell structures is now well documented and methods of prediction and prevention of such phenomena are believed to be well understood.

The corresponding problem of wind-induced ovalling and breathing oscillations has occurred less frequently but certain incidents have been attributable to this cause:

In 1964 during a typhoon, ovalling oscillations were observed of a 150 ft. high, 10ft diameter steel chimney in Hongkong. The chimney material was mild steel of $^{5}/_{16}$ inch thickness. The nature of the oscillations was of an ovalling (n = 2) mode at a frequency of about 1.6 - 2.4 Hz. After some time the sole stiffening ring at the top end of the chimney broke away from the basic shell whereupon the amplitude of the vibrations increased violently prior to collapse.

The present investigation was prompted by the above incident. The study was done in two different phases described in the form of Part A and Part B. Preliminary studies had been previously conducted at Loughborough into this problem and, already, significant advances had been made which had clarified some of the unknowns and highlighted the need for a more comprehensive investigation of which this study is the result.

Part A is concerned with the theoretical part of the present investigation. A fairly general theoretical analysis for free vibration characteristics of clamped-free and clamped ring stiffened circular cylindrical shells has been developed and programmed for digital computer solution. The treatment is comprehensive in the sense that the Flugge's thin shell equations of motion have been used, three translational shell inertia components are included. Also included are the effects of stiffening ring geometry, eccentricity, mass and rotary inertia.

The analysis is capable of handling vibration characteristics of cylindrical shells, in the swaying (cantilever mode, $n = 1$) as well as in the ovalling or breathing modes ($n \geq 2$, n is circumferential wave number) with arbitrary length-to-radius ratio and radius-to-thickness ratio. In the case of a shell with an end ring it also allows for variation in the non-dimensional ring characteristics e.g. ring breadth/shell radius, ring depth/shell radius.

After the introductory chapter 1, chapter 2 of Part A deals with the analytical investigation. Here, by using Flugge's thin shell equations expressions for strain and kinetic energies are derived. General expressions for ring strain and kinetic energies (including ring eccentricity and rotary inertia) are also derived. Various mode shapes are chosen e.g. polynomial function, trigonometric function, characteristic beam function etc. by allowing variation in longitudinal mode functions. The frequency equations are then derived by using the Rayleigh-Ritz procedure and the degree of this equation depends upon the degrees of freedom in the choice of mode shapes. These equations are solved by using various numerical techniques. The effect of the assumption of zero hoop and shear strain is seen to reduce the degree of the frequency equation.

Chapter 3 consists of a discussion of the analytical results. This is subdivided in two parts i) clamped-free shell and ii) clamped-ring stiffened shell. The effect of zero hoop and shear strain on the frequency spectrum is assessed in both the cases. The dependence of frequency on the number of axial waves and circumferential waves is also examined. In case (ii) the

effects of ring mass, eccentricity and stiffness on the frequency spectrum are also discussed.

In chapter 4, for a few typical shell geometrics of interest, the results of the present theory are compared with the results of exact and more complicated vibration analyses for thin cylindrical shells with clamped-free or clamped-ring stiffened ends. The main points of the exact analysis are given in the Appendix V.

Conclusions of the foregoing analysis are given in chapter 5.

Appendix I gives pertinent details of a preliminary analysis concerning an investigation of the vibration characteristics of a vertical, cantilevered shell, with its lower edge restrained against displacement and its upper edge supported on a stiff reinforcing ring.

Appendix II contains properties and tables of characteristic functions representing normal modes of vibration of a beam. Appendix III gives expressions for the integrals, involving characteristic beam functions and their derivatives, encountered in the analysis.

Appendix IV contains the flow charts of the main computer programmes used along with the flowchart for the Regula-Falsi iteration procedure.

Appendix V gives the summary of an exact analytical approach for clamped-free and clamped-ring stiffened shells. The results of this theory are compared with the present theory.

Part B contains mainly the results of the experimental programme carried out for the aforesaid problem. After an introductory chapter 1, vortex shedding phenomena are discussed in chapter 2 followed by a discussion on vortex-induced vibrations in chapter 3.

Chapters 4 and 5 describe the construction of model shells, experimental rigs and instrumentation. General test procedures are given for the wind tunnel tests on model stacks and model excitation by electromechanical shaker.

The comparisons of analytical and experimental vibration frequencies is given in chapter 6. The results by using a mechanical shaker as the excitation device are reported in the first part. In this part the structural dampi ng

characteristics have been measured experimentally for various modes of vibration. In the second part of chapter 6 the test results of model stacks in the wind are compared with "predicted" analytical results. Many model stacks have been tested for the purpose of correlation of analytical results with the experimental ones.

Chapter 7 contains the main conclusions of the experimental programme.

Appendix I contains the observations made on a particular shell with helical strakes on upper one third of it. The effect of helical strakes is analysed.

In the Appendix II the results of measured structural damping are given in a table form for a particular shell with one or two layers of 0.005" thick fablon. Fablon was used to increase the structural damping of the shell.

WIND-INDUCED OSCILLATIONS OF CIRCULAR CYLINDRICAL SHELLS

PART A

A THEORETICAL ANALYSIS

ABSTRACT

A theoretical analysis for the free vibration of clamped/free and clamped/ring stiffened cylindrical shells has been developed and programmed for digital computer solution. The analysis is capable of handling vibration characteristics of cylindrical shells, in the swaying (cantilever mode n=1) as well as in the ovalling or breathing modes ($n \geq 2$; n is circumferential wave number), with arbitrary length to radius ratio and radius to thickness ratio. In the case of a shell with an end ring it also allows for variation in the non-dimensional ring characteristics (ring breadth/shell radius, ring depth/shell radius).

Three translational shell inertia components are included and the effects of ring eccentricity and mass and rotary inertia are examined.

The paper examines the accuracy of various engineering approximations as compared with more exact solutions from Flügge's thin shell equations and discusses the error in terms of a non-dimensional frequency parameter.

It is interesting to note that for tall shells the assumption of zero hoop and shear strain leads to considerable simplification in the analysis without introducing any significant error in the minimum natural frequency.

The problem is formulated using the energy method and the Rayleigh-Ritz technique is employed to obtain an approximate solution. The choice of the modal shape is varied and it includes a longitudinal modal component approximated alternately by polynomial, trigonometric or "exact" beam vibration functions chosen to satisfy prescribed end conditions. Specially for the shell clamped at the base and ring stiffened at the top, the combination of two beam vibrations modes (clamped/free and clamped/simply supported) is taken for the longitudinal displacement component.

Numerical results are found in each case and compared with one another and the choice of mode shape thus assessed. Results are also compared to the existing theories and experiments for the clamped/free cylindrical shell. The analyses are then substantiated later by comparing the results with the exact solution of Flügge's equations of motion.

CONTENTS

CONTENTS (contd)

LIST OF FIGURES

LIST OF TABLES

NOTATION

a	radius to shell midsurface
A_{ij}	elements of stiffness matrix in frequency equation
A_R	area of the ring section
$A_R^{(r)}$	rth moment of area of ring section about skin median.
A_1, A_2 ; B_1, B_2 ; C_1, C_2 ;	generalized coordinates in displacement functions
B_{ij}	elements of mass matrix in frequency equation
b_R	net breadth of ring section
c_r, d_r	eigenvalue properties of beam (see appendix II)
d_R	net depth of ring section
E	Youngs modulus
$e_{xx}, e_{\theta\theta}, e_{x\theta}$	strains
$\bar{e}_{xx}, \bar{e}_{\theta\theta}; \bar{e}_{x\theta}$	extensions; shear strain
h	shell thickness
$I_R^{(r)}$	rth moment of mass of ring per unit circumference at skin median, about skin median.
I_1, I_2, I_3 I_4, I_5, I_6	integrals defined in Appendix III for longitudinal mode functions.
k_x, k_θ	changes of curvature
$k_{x\theta}$	twist
L	length of the cylinder
ℓ ; $\bar{\ell}$	axial mode parameter; ℓ/L
m	longitudinal mode number (see fig. 2)
M_1, M_2	values of longitudinal beam vibration functions at a specific distance $x = x_i$
M_3, M_4	values of derivatives of longitudinal beam vibration functions at a specific distance $x = x_i$

NOTATION (contd)

n	circumferential mode number (see fig. 2).
N_1, N_2, N_3, N_4 N_5, N_6, N_7, N_8	constants for rings defined in equation (38)
p_r, q_r	beam eigenvalues
T	kinetic energy (see eq. (12) and (16))
t	time
U	strain energy in shell and rings
u, v, w	longitudinal, circumferential, and radial (or normal) displacements, respectively of the shell mid-plane.
x, θ, z	longitudinal, circumferential and radial coordinates (see fig. 1)
$\bar{x}$	x/L
$\phi(x)$, $\psi(x)$	assumed longitudinal vibration modes for shell
$\phi_r(x)$, $\psi_r(x)$	characteristic beam vibration functions in longitudinal direction for clamped-free and clamped-simply supported beam respectively.
β	$h^2/12a^2$
λ_r	$p_r a$
μ_r	$q_r a$
ν	Poisson's ratio
ρ	mass density
ω	natural frequency (circular)
Δ	frequency parameter, $\frac{\rho u^2(1-\nu^2)\omega^2}{E}$
$\sigma_{xx}, \sigma_{x\theta}, \sigma_{\theta\theta}$	stresses

Subscripts:

s	refers to shell
R	refers to ring

A comma followed by subscripts denotes partial differentiation with respect to the subscripts, e.g. $u_{,x}$ denotes $\frac{\partial u}{\partial x}$ and $w_{,\theta\theta}$ denotes $\partial^2 w / \partial \theta^2$.

A dot (.) above a quantity denotes time derivative of the quantity; e.g. $\dot{u}$ denotes $\frac{\partial u}{\partial t}$.

1. INTRODUCTION

The problem of the determination of the in-vacuo dynamic characteristics of thin cylindrical shells has been studied extensively by many research workers.

However only a few papers are devoted to the study of the vibration characteristics of cylindrical shells with different boundary conditions at the two ends. Forsberg [1] has made a detailed study of the effect of end boundary conditions on the modal characteristic of thin cylindrical shells.

In this study we have dealt with the vibration characteristics of a cylindrical shell clamped at one end and either free or stiffened by an elastic ring at the other. In particular the problem is studied for shells, typical of slender welded steel chimneys, with lower edge fully restrained and the upper edge either free or supported on a stiff reinforcing ring. This investigation is prompted by the recent collapse of such a shell in the form of a tall slender chimney stack when subjected to a high sustained lateral wind. The stack was observed to oscillate in an ovalling mode of large amplitude prior to collapse.

The problem of a clamped-free shell has received very little attention and that of clamped ring stiffened shell still less. Weingarten [2] has calculated the natural frequency for a particular shell with clamped-free end conditions using a Donnell-type equation. Watkins and Clary [3] give a comparison of results of an experimental investigation into the vibration characteristics of thin circular cylindrical shells with results obtained by using simple analytical methods. Similar work was done by Sewall & Naumann [4] who made comparisons of analytical and experimental frequencies and mode shapes of eccentrically stiffened and unstiffened cylindrical shells with various end support conditions.

The major purpose of the present report is to show the dependence of the lower natural frequencies of such cylindrical shells on the geometrical and material properties of the shell, e.g. length/radius; thickness/radius, Young's modulus, density etc. The following are the phases of this problem which have been dealt with thoroughly:

(a) Choice of appropriate shell equations of motion.

(b) Choice of modal forms, influence of boundary conditions.

(c) Rotary and Inplane inertia effects.

(d) The assumption of zero hoop and shear strain.

The equations of motion developed by Flügge [5] are used here. Flügge derived equations for cylindrical shells which retain terms of higher order than the Timoshenko-Love theory, yet are computationally tractable. They have become an accepted standard to which other theories are referred for accuracy. Many other investigators (Novozhilov, Vlasov and Koiter) have presented shell theories intended to remove all inconsistencies as compared to Love's first approximation. These theories increase the complexities of the problem but not necessarily the accuracy. Naghdi [6] has indicated that none of these is superior to Flügge's theory. In general one cay say that the wide variety in the resulting equations arises basically from small differences in the formulation of the strain displacement relationships, and the discrepancies occur only in terms which numerically have little significance. As long as the limitations of the thin shell theory are observed, the various formulations generally give identical numerical results within engineering accuracy. An excellent account of this fact is given by Warburton [7] where it is remarked that for a wide range of parameters the effect of various different shell theories on the natural frequencies are very small.

The modal deflection functions that have been assumed in the past satisfy part or all of the end boundary conditions. The different mode shapes correspond to differences in the functional dependence of the deflections on the axial coordinate x. These include polynomial expressions as taken by Johns and Allwood [9], trigonometric functions in x, as well as the case in which the longitudinal modal components are approximated by elementary beam vibration functions chosen to satisfy all the end conditions.

Also the effect upon the frequency parameter of including transverse shear deformation and rotary inertia in the analysis are relatively small for the parameter studied in reference [8] but these effects increase rapidly for radius/thickness ratio < 20. Such effects are not included in the present study. Included in the present analysis are the radial, axial and circumferential inertia terms and the ring rotary inertia.

The analysis by Johns and Allwood [9] considered that for tall shells the assumption of zero hoop and shear strain leads to considerable simplification without introducing any significant error in the minimum natural frequency. This is extended here to cover a wide range of cases and for short shells this assumption is thought to lead to error such that the frequencies may be increased considerably

above the more exact results. Some valuable comments have been made by Warburton[7] on Ref. 9 which also indicate the errors involved in various approximations.

A further report is to follow which will deal more fully with the correlation of theoretical and experimental vibration data for circular shells and with the results of wind-tunnel studies into wind-excited oscillations of such shells.

2. ANALYTICAL INVESTIGATION

2.1 General

Analytical shell frequencies presented in this paper were obtained by application of the well known energy method employing the Rayleigh-Ritz procedure. The general approach of the method is outlined below.

Firstly, the expressions for the kinetic and potential energies are written for a cylindrical shell and for a ring. For a clamped/ring stiffened shell these expressions are combined to give the total kinetic and potential energies. Next, mode shapes are assumed with undetermined coefficients, which satisfy the appropriate end conditions. These assumed displacement functions are then substituted into the energy expressions and application of Rayleigh-Ritz procedure yields frequency equations which on solution will give desired natural frequencies.

2.2 Analysis

The energy expressions are written first in terms of strain, then strain-displacement relations are used to give these expressions in terms of displacement of the middle surface of the shell. Included are the radial and in-plane inertia terms (axial and circumferential). Eccentricity effects due to the ring centroid being not coincident with shell median plane are explicitly taken into account. The rotary inertia of the shell is believed to be negligible but, however, rotary inertia is taken into account in the kinetic energy expressions for the rings..

2.3 Strain Energies

The coordinate system are notation used in the anlysis are defined in Fig. (1). A circular cylindrical shell of length L, mean radius a, and uniform thickness h is considered. Coordinate axes, x, θ, z, correspond to the axial, circumferential and radial directions respectively. The strain displacement-relationships considered for a cylindrical shell with the coordinate system given in figs (1) are those derived by Flügge [5] as

$$
\begin{aligned}
e_{xx} &= u_{,x} - z w_{,xx} \\
e_{\theta\theta} &= \frac{v_{,\theta}}{a} - \frac{z w_{,\theta\theta}}{a(a+z)} + \frac{w}{a+z} \qquad (1) \\
e_{x\theta} &= \frac{u_{,\theta}}{a+z} + \frac{a+z}{a} v_{,x} - \left(\frac{z}{a} + \frac{z}{a+z}\right) w_{,x\theta}
\end{aligned}
$$

where a comma before the variable used as a subscript denotes partial differentiation with respect to the variable (i.e. $u_{,x} = \frac{\partial u}{\partial x}$ etc.). These relationships are referred to as Flügge's exact strain displacement relations, and assume that normals to the middle surface remain normal after straining and that all the displacements are very small i.e. that they are negligible compared with radius of curvature of the middle surface and that their first derivatives, the slopes, are negligible compared with unity.

Although equations (1) may appear to be complicated it is quite easy to give them a mechanical interpretation. Equations (1) may also be cast into another form by introducing a set of quantities describing the deformation of an element of the middle surface. These are:

the extensions: $\bar{e}_{xx} = u_{,x}$, $\bar{e}_{\theta\theta} = \frac{1}{a}(v_{,\theta} + w)$

the shear strain: $\bar{e}_{x\theta} = \frac{u_{,\theta}}{a} + v_{,x}$

together with the changes of curvature $k_x = w_{,xx}$, $k_\theta = \frac{1}{a^2}(w + w_{,\theta\theta})$

and the twist $k_{x\theta} = \frac{1}{a}\left(w_{,x\theta} + \frac{1}{2a}u_{,\theta} - \frac{1}{2}v_{,x}\right)$

The strain energy of the shell is calculated by considering a small element in a thin shell. Provided the shell is considered to be thin, it is assumed that the small element is in plane stress ($\sigma_{zz} = 0$, $\sigma_{xz} = \sigma_{\theta z} = 0$). Thus Hookes Law in this case is:

$$\sigma_{xx} = \frac{E}{(1-\nu^2)}(e_{xx} + \nu e_{\theta\theta})$$

$$\sigma_{\theta\theta} = \frac{E}{(1-\nu^2)}(e_{\theta\theta} + \nu e_{xx}) \qquad (2)$$

$$\sigma_{x\theta} = \frac{E}{2(1+\nu)}e_{x\theta}$$

The incremental strain energy density is

$$dU = \sigma_{xx}\, de_{xx} + \sigma_{\theta\theta}\, de_{\theta\theta} + \sigma_{x\theta}\, de_{x\theta} \qquad (3)$$

Substituting (2) into (3) and integrating gives strain energy density·

$$U = \frac{E}{1-\nu^2}\left[\frac{1}{2}(e^2_{xx} + e^2_{\theta\theta}) + \nu e_{xx}e_{\theta\theta} + \frac{1-\nu}{4}e^2_{x\theta}\right] \qquad (4)$$

The total strain energy is found by integrating the above expression over the entire shell volume

$$U_s = \int_V U\,dV$$

$$= \frac{E_s}{2(1-\nu^2)} \int_{-h/2}^{h/2} \int_0^{2\pi} \int_0^L \left[e^2_{xx} + e^2_{\theta\theta} + 2\nu\, e_{xx}\, e_{\theta\theta} + \frac{(1-\nu)}{2}\, e^2_{x\theta} \right] (a+z)\, dx\, d\theta\, dz \qquad (5)$$

Here $(a+z)\, dx\, d\theta\, dz$ is a volume element and E_s is the Young's modulus of the shell material. The strain displacement relations (1) can be used to give the strain energy in terms of the displacements u, v, w of the middle surface of the shell. Integrating over the shell thickness the potential energy of the cylindrical shell is written as

$$U_s = \frac{E_s a h}{2(1-\nu^2)} \int_0^{2\pi} \int_0^L \Big[u_{,x}^2 + \frac{1}{a^2} (w + v_{,\theta})^2 + \frac{2\nu}{a} u_{,x} (v_{,\theta} + w) + \frac{1}{2a^2} (1-\nu) (u_{,\theta} + a v_{,x})^2 + \beta \Big\{ a^2 w_{,xx}^2 + \frac{1}{a^2} (w + w_{,\theta\theta})^2 - 2a\, u_{,x}\, w_{,xx} + 2\nu\, w_{,xx} (w_{,\theta\theta} - v_{,\theta}) + \frac{1}{2} (1-\nu) \Big(\frac{1}{a^2} u_{,\theta}^2 + 3\, v_{,x}^2 + 4\, w_{,x\theta}^2 + \frac{2}{a} u_{,\theta}\, w_{,x\theta} - 6\, v_{,x}\, w_{,x\theta} \Big) \Big\} \Big] dx d\theta \qquad (6)$$

where $\beta = h^2/12a^2$. Hence $\frac{E_s h}{(1-\nu^2)}\,\beta = \frac{E_s h^3}{12(1-\nu^2)a^2}$

The above expression (6) is a combination of the shell extensional and the shell bending energy; $\frac{E_s h}{1-\nu^2}$ being the extensional stiffness and $\frac{E_s h^3}{12(1-\nu^2)}$ being the bending stiffness.

To arrive at the above expression (6) the infinite series in $\frac{h}{a}$ were truncated by neglecting fifth and higher powers of h/a e.g.

$$\ln \frac{a + h/2}{a - h/2} \approx \frac{h}{a} + \frac{h^3}{12a^3}$$

The potential energy expression for the rings will be developed assuming that these are uniform along their circumferential length and have an asymmetric cross-section. Further, it is assumed that only circumferential strain is relevant for calculating the strain energy in this case; also that the cross sectional planes do not warp. The compatibility requirements are easily satisfied by the assumption that the ring is integral with the shell at a single common line of attachment. This assumption is more easily justified if the ring is welded, bolted, riveted or integrally machined with the shell. Derivations for the ring energies are based on an analysis in Ref. [10]

For a ring neglecting σ_{xx} , σ_{zz} and taking $\sigma_{\theta\theta} = E_R e_{\theta\theta}$ (7)

$$U_R = \frac{1}{2} E_R \int_0^{2\pi} \int_{d_R} b_R e^2_{\theta\theta} (a+z) \, d\theta \, dz \tag{8}$$

where b_R is breadth of the ring and d_R the depth. Substitution for $e_{\theta\theta}$ from equation (1) gives on integrating over the ring depth,

$$U_R = \frac{E_R}{2a} \int_0^{2\pi} \left\{ A_R (v,_\theta + w)^2 + \frac{A_R^{(1)}}{a} (v,^2_\theta - w^2 - 2v,_\theta w,_{\theta\theta} - 2w w,_{\theta\theta}) + \frac{A_R^{(2)}}{a^2} (w + w,_{\theta\theta})^2 - \frac{A_R^{(3)}}{a^3} (w + w,_{\theta\theta})^2 + \ldots \right\} d\theta \tag{9}$$

where

$A_R = \int_{d_R} b_R \, dz$ = area of the ring section.

$A_R^{(r)} = \int_{d_R} Z^r \, b_R \, dz$ = r^{th} moment of area of ring section about skin median plane.

The eccentricity effects are explicitly accounted for by taking these energies in terms involving the distance z. Thus for r odd, $A_R^{(r)}$ is to be taken negative when the ring is an internal one. In the case of a ring at the top of the shell (x=L) the expression (9) is

$$U_R = \frac{E_R}{2a} \int_0^{2\pi} \left\{ A_R (v,_\theta + w)^2 + \frac{A_R^{(1)}}{a} (v,^2_\theta - w^2 - 2v,_\theta w,_{\theta\theta} - 2ww,_{\theta\theta}) + \frac{A_R^{(2)}}{a^2} (w + w,_{\theta\theta})^2 - \frac{A_R^{(3)}}{a^3} (w + w,_{\theta\theta})^2 + \ldots \right\}_{x=L} d\theta \tag{10}$$

The total potential energy due to several rings at various positions of the shell is given by

$$U_R = \sum_{i=1}^{N} \frac{E_{R_r}}{2a} \int_0^{2\pi} \Big\{ A_{R_i} (v_{,\theta} + w)^2 + \frac{A_{R_i}^{(1)}}{a} (v_{,\theta}^2 - w^2 - 2v_{,\theta} w_{,\theta\theta} - 2 w w_{,\theta\theta}) + \frac{A_{R_i}^{(2)}}{a^2} (w + w_{,\theta\theta})^2 - \frac{A_{R_i}^{(3)}}{a^3} (w + w_{,\theta\theta})^2 + \ldots \Big\}_{x = x_i} d\theta \tag{11}$$

where the total number of the rings is N and $x_1, x_2, \ldots, x_n$ are the distances of the ring stations from the clamped end of the shell. Quantities E_{R_r} A_{R_r}, $A_{R_r}^{(1)} \ldots$ etc. correspond to r^{th} ring.

In the case of many closely spaced rings these are not necessarily considered as discrete elements and a 'smeared' analysis similar to that of Mikulas and McElman [11] may be used. Because of the different end conditions and because of provision for the effects of inplane inertia terms and ring rotary inertia the present paper is broader in scope. For a 'smeared' stiffener analysis the summation sign in equation (11) is replaced by an integration over the entire length of the shell. An assessment of the validity of 'smeared' analyses compared with discrete stiffener analyses is given by Parthan and Johns [12].

2.4. Kinetic Energies

Neglecting the rotary inertia, the kinetic energy of the shell may be written as

$$T_S = \frac{1}{2} \rho_s a h \int_0^{2\pi} \int_0^{L} \left[(\dot{u})^2 + (\dot{v})^2 + (\dot{w})^2 \right] d\theta dx \tag{12}$$

where dot above the variable denotes differentiation w.r.t. time, ρ_s is the mass density of the shell material. Although rotary inertia of shell is negligible the rotary inertia of the stiffening rings may sufficiently affect the natural frequencies of the stiffened shell as demonstrated by Parthan and Johns [12] and Huffington and Schumacker [13]. Thus the kinetic energy of one ring is given by

$$T_R = \frac{1}{2} \int_0^{2\pi} \int_{d_R} (a + z) \rho_R b_R \left\{ (\dot{u} - z\dot{w}_{,x})^2 + \left(\frac{r}{a} \dot{v} - \frac{z}{a} \dot{w}_{,\theta} \right)^2 + \dot{w}^2 \right\} d\theta dz \tag{13}$$

where $\rho_R b_R$ is mass of the ring per unit depth and per unit circumference at a

radius = a + z. Integrating over the ring depth the kinetic energy for a ring at the free end is given by

$$T_R = \frac{a}{2}\int_0^{2\pi}\Big[m_R(\dot{u}^2+\dot{v}^2+\dot{w}^2)+\frac{2I_R^{(1)}}{a}(\dot{v}^2-\dot{v}\dot{w}_{,\theta}-a\dot{u}\dot{w}_{,x}) + \frac{I_R^{(2)}}{a^2}\left\{a^2\dot{w}_{,x}^2+(\dot{v}-\dot{w}_{,\theta})^2\right\}\Big]_{x=L} d\theta \tag{14}$$

where

$m_R = \int_{d_R} \delta_R\, b_R \frac{a+z}{a}\, dz$ is mass of the ring per unit circumference at the reference surface

$$I_R^{(1)} = \int_{d_R} \rho_R\, b_R \frac{a+z}{a}\, z\, dz$$

$$I_R^{(2)} = \int_{d_R} \rho_R\, b_R \frac{a+z}{a}\, z^2\, dz$$

If $\bar{\rho}_R$ is taken as the ring density averaged over the entire ring section the above can be expressed using previously defined quantities (equation (9)) as

$$\begin{aligned} m_R &\approx \bar{\rho}_R\left\{A_R + \frac{1}{a} A_R^{(1)}\right\} \\ I_R^{(1)} &\approx \bar{\rho}_R\left\{A_R^{(1)} + \frac{1}{a} A_R^{(2)}\right\} \\ I_R^{(2)} &\approx \rho_R\left\{A_R^{(2)} + \frac{1}{a} A_R^{(3)}\right\} \end{aligned} \tag{15}$$

The kinetic energy due to rings at various positions of the shell is given by

$$T_R = \sum_{i=1}^{N}\frac{a}{2}\int_0^{2\pi}\Big[m_{R_i}(\dot{u}^2+\dot{v}^2+\dot{w}^2)+\frac{2I_{R_i}^{(1)}}{a}(\dot{v}^2-\dot{v}\dot{w}_{,\theta}-a\dot{u}\dot{w}_{,x}) + \frac{I_{R_i}^{(2)}}{a^2}\left\{a^2\dot{w}_{,x}^2+(\dot{v}-\dot{w}_{,\theta})^2\right\}\Big]_{x=x_i} d\theta \tag{16}$$

The corresponding expression for the potential and kinetic energies used by Johns & Allwood [9] are given in the appendix (I) for comparison.

2.5 Modal Functions

2.5.1 General

The general expressions chosen for the inplane and radial displacements u, v and w are

$$\begin{aligned} u &= \left\{ A_1 \phi'(x) + A_2 \psi'(x) \right\} \cos n\theta \cos \omega t \\ v &= \left\{ B_1 \phi(x) + B_2 \psi(x) \right\} \sin n\theta \cos \omega t \\ w &= \left\{ C_1 \phi(x) + C_2 \psi(x) \right\} \cos n\theta \cos \omega t \end{aligned} \tag{17}$$

where $\phi(x)$ and $\psi(x)$ are axial mode functions and $\phi'(x) = \frac{1}{P}\frac{d\phi}{dx}$ and $\psi'(x) = \frac{d\psi}{dx}\cdot\frac{1}{q}$

Fig. 2 shows typical modal forms for a circular shell with identical boundary conditions at each end. The modes are assumed in the present study to satisfy part or all of the boundary conditions which are in general different at each end as is seen in Fig. 3. The following sets of axial mode functions $\phi(x)$ and $\psi(x)$ have been incorporated in this present analysis.

2.5.2 Johns and Allwood [9] chose a polynomial expression in x for the axial mode functions for a clamped-free or clamped ring-stiffened shell viz.

$$\begin{aligned} \phi(x) &= \bar{x}^2 (\bar{x} - 3) \text{ , where } \bar{x} = x/L \\ \psi(x) &= \bar{x}^2 (\bar{x}^2 - 6) \end{aligned} \tag{18}$$

These correspond to an encastre and axially-clamped base and approximately to zero axial stress and edge moment at the ring stiffened, or free, upper end.

2.5.3 In the second case the modal dependence on the axial co-ordinate x is chosen (for the shell clamped at the base and free at the top) so that w, the radial deflection varies from zero with x up to a certain length ℓ (not predetermined) of the shell from the clamped end and then it becomes constant for the rest of the length of the shell.

$$\phi(x) = \begin{cases} 1 - \cos \pi \bar{x}/\bar{\ell} & 0 < \bar{x} < \bar{\ell} \\ 2 & \bar{\ell} < \bar{x} < 1 \end{cases} \tag{19}$$

where $\ell/L = \bar{\ell}$

2.5.4 In the third case (again for clamped-free shells which are typical of unstiffened chimney stacks) the modal function is a beam vibration function chosen to satisfy the prescribed set of end conditions i.e. of clamped base and free upper end. In this case,

$$\phi_r(x) = \cosh p_r x - \cos p_r x - c_r (\sinh p_r x - \sin p_r x) \quad (20)$$

where p_r is given by the roots of the transcendental equation

$$\cosh p_r L \cos p_r L + 1 = 0 \quad (21)$$

and

$$c_r = \frac{\sinh p_r L - \sin p_r L}{\cosh p_r L + \cos p_r L} \quad (22)$$

2.5.5 In the last case (for the cylindrical shell clamped at the base and with an elastic ring at the upper end), the longitudinal modal component cannot be represented by the clamped free beam vibration function alone. Hence the combination of clamped-free [given by equation (20)] and clamped-simply supported beam vibration functions has been taken to approximate the longitudinal modal component in this case. The clamped-simply supported beam vibration function is given by

$$\psi_r(x) = \cosh q_r x - \cos q_r x - d_r (\sinh q_r x - \sin q_r x) \quad (23)$$

where q_r is given by the transcendental equations

$$\sin q_r L \cosh q_r L - \sinh q_r L \cos q_r L = 0 \quad (24)$$

and

$$d_r = \cot q_r L = \coth q_r L \quad (25)$$

The properties and numerical values of ϕ_r, p_r, c_r and ψ_r, q_r, d_r are tabulated by Bishop & Johnson [14]. The choice of a beam mode functions for $\phi_r(x)$ and $\psi_r(x)$ allows some simplification in the analysis through the orthogonality properties e.g

$$\int_0^L \phi_r(x)\, \phi_s(x)\, dx = \int_0^L \phi''_r(x)\, \phi''_s(x)\, dx = 0 \quad (r \neq s) \quad (26)$$

and similar for ψ.

where $\phi''_r(x) = \frac{1}{p_r^2} \frac{d^2\phi_r(x)}{dx^2}$, $\psi''_s(x) = \frac{1}{q_s^2} \frac{d^2\psi_s(x)}{dx^2}$ etc

The detailed account of these functions and their properties is given in the appendix II.

2.6 The Assumption of zero hoop and shear strain

The assumption of zero hoop and shear strain directly simplifies the mode shapes and the subsequent analysis i.e. if

$$\begin{aligned} v_{,\theta} \quad + w &= 0 \\ v_{,x} \quad + \frac{u_{,\theta}}{a} &= 0 \end{aligned} \tag{27}$$

the modal forms (17) are reduced to the following simplified form:

$$\begin{aligned} u &= -\frac{a}{n^2}\left\{C_1 \ \phi'(x) + C_2 \ \psi'(x)\right\} \cos n\theta \quad \cos \omega t \\ v &= -\frac{1}{n}\left\{C_1 \ \phi(x) + C_2 \ \psi(x)\right\} \sin n\theta \quad \cos \omega t \\ w &= \left\{C_1 \ \phi(x) + C_2 \ \psi(x)\right\} \cos n\theta \quad \cos \omega t \end{aligned} \tag{28}$$

Thus it is easy to see that the number of amplitude functions is reduced to one-third from three to one for a clamped-free shell with A_2, B_2, C_2 neglected; from six to two for a shell with A_2, B_2, C_2 retained as well as A_1 B_1 C_1. The resulting simplification in the various frequency equations and the effect of this on the final results is discussed in the following sections.

2.7 Frequency Equations

2.7.1 General

Substituting an assumed set of modal forms into the expression for total strain energy (U) and total kinetic energy (T) and assuming the motion to be simple harmonic of frequency ω, the equations of motion are obtained from relations of the following type:

$$\begin{aligned} \frac{\partial}{\partial A_1}\left[U(x,\theta) - \omega^2 T(x,\theta)\right] &= \frac{\partial}{\partial A_2}\left[U(x,\theta) - \omega^2 T(x,\theta)\right] = 0 \\ \frac{\partial}{\partial B_1}\left[U(x,\theta) - \omega^2 T(x,\theta)\right] &= \frac{\partial}{\partial B_2}\left[U(x,\theta) - \omega^2 T(x,\theta)\right] = 0 \\ \frac{\partial}{\partial C_1}\left[U(x,\theta) - \omega^2 T(x,\theta)\right] &= \frac{\partial}{\partial C_2}\left[U(x,\theta) - \omega^2 T(x,\theta)\right] = 0 \end{aligned} \tag{29}$$

The operations represented by these equations lead to the familiar eigenvalue-eigenvector formulation which may be expressed in different forms for different set of mode shapes for different kind of boundary conditions.

General expressions for the integrals present in the energy expression are given in Appendix III.

2.7.2. Clamped-Free shell

In this case U and T are taken as the strain and kinetic energies of the shell alone.

If the longitudinal modal function given by (19) is taken and the energy expressions are those given in the appendix I*, application of Rayleigh-Ritz procedure yields an expression for the natural frequency ω. The assumption of zero hoop and shear strain gives the following as the simplified frequency equation

$$\Delta = \frac{\beta n^2}{n^2+1}\left[(n^2-1)^2 + \frac{\pi^2 (n^2-1)^2 (q-s)}{-10\bar{\ell}^2 + 12\bar{\ell} + \pi^2 r}\right] \qquad (30)$$

where $\beta = \dfrac{h^2}{12a^2}$, $\Delta = \dfrac{\rho_s a^2 (1-\nu^2)\,\omega^2}{E_s}$

The value of the constant $\bar{\ell}$ in equations (19) and (30) is determined to give the minimum value of the frequency ω . $\bar{\ell}$ is obtained from the solution of the quartic

$$\bar{\ell}^4 - .8\bar{\ell}^3 + 2\frac{p\pi^2}{q-s}\bar{\ell}^2 - \frac{2.4\,p\pi^2}{q-s}\bar{\ell} - \frac{.2\,p\pi^4 r}{q-s} = 0 \qquad (31)$$

where $e = a/L$

$$p = \frac{e^4}{(n^2-1)^2}\left\{1 + \frac{1}{\beta n^4}\right\}$$

$$r = \frac{e^2}{n^2(n^2+1)}$$

$$q = \frac{2e^2(1-\nu)}{n^2} - r$$

$$s = \frac{2e^2\nu}{1-n^2}$$

---

*` The approach of Johns and Allwood with various relevant expressions is given in the appendix I .

In another case the longitudinal modal function given by (20) is taken and the energy expressions given by (6) and (12). Applying the Rayleigh-Ritz procedure the resulting frequency equation in determinantal form is given by

$$\begin{vmatrix} A_{11} - \Delta I_2 & A_{12} & A_{13} \\ A_{21} & A_{22} - \Delta & A_{23} \\ A_{31} & A_{32} & A_{33} - \Delta \end{vmatrix} = 0 \qquad (32)$$

Here $A_{11} = \lambda_r^2 + (1 + \beta) \frac{(1 - \nu)}{2} n^2 I_2$

$A_{12} = A_{21} = - \nu n \lambda_r I_1 - \frac{1}{2} (1 - \nu) n \lambda_r I_2$

$A_{13} = A_{31} = -\nu \lambda_r I_1 + \beta \lambda_r \left\{ - \lambda_r^2 + \frac{1}{2} (1 - \nu) n^2 I_2 \right\}$

$A_{22} = n^2 + \frac{1}{2} (1 - \nu) \lambda_r^2 I_2 (1 + 3\beta)$

$A_{23} = A_{32} = n + \beta n \lambda_r^2 \left\{ \nu I_1 + \frac{3}{2} (1 - \nu) I_2 \right\}$

$A_{33} = 1 + \beta \left\{ \lambda_r^4 + (n^2 - 1)^2 + 2 \nu \lambda_r^2 n^2 I_1 + 2 (1 - \nu) n^2 \lambda_r^2 I_2 \right\}$

where $\lambda_r = p_r a$

$$I_1 = \frac{1}{L} \int_0^L p_r^2 \left\{ \int \phi_r(x)\, dx \right\}^2 dx$$

$$I_2 = \frac{1}{L} \int_0^L \left\{ \phi'_r(x) \right\}^2 dx$$

Explicit expressions for these integrals are derived from Appendix II and given in the appendix III .

The frequency equation (32) above is a cubic in Δ , but often only the lowest value of Δ is of structural interest.

The assumption of zero hoop and shear strain in this case reduces the cubic frequency equation to a very simple linear equation in Δ ,

$$\Delta = \frac{\lambda_r^4 + \beta n^2 \lambda_r^2 \left[\lambda_r^2 n^2 + 2\nu n^2 (n^2-1) I_1 + 2(1-\nu)(n^2-1)^2 I_2\right] + \beta n^4 (n^2-1)^2}{\lambda_r^2 I_2 + n^2 (n^2+1)} \tag{33}$$

It should be noted that both equations (30) and (33) reduce for an infinitely long shell to give

$$\Delta = \beta n^2 (n^2-1)^2/(n^2+1) \tag{34}$$

This expression corresponds to a well-known ring formula for purely circumferential modes which is also derived in Appendix I.

2.7.3. Clamped-Ring stiffened shell

For this case the axial mode function is taken using both equations (20) and (23) in equations (17). The strain and kinetic energies are given by

$$\begin{aligned} U &= U_s + U_R \\ T &= T_s + T_R \end{aligned} \tag{35}$$

where U_s, U_R and T_s, T_R are given respectively by (6), (10) and (12), (14). In case of several discrete rings in intermediate axial positions the expressions for U_R and T_R are taken as given by equations (11) and (16) respectively. Finally substitution of equations (17) into equations (35) and application of the Rayleigh-Ritz variational procedure to this system yields the frequency equation which may be represented in the following determinantal form

$$\left| \begin{bmatrix} A_{11} & A_{12} & A_{13} & A_{14} & A_{15} & A_{16} \\ A_{12} & A_{22} & A_{23} & A_{24} & A_{25} & A_{26} \\ A_{13} & A_{23} & A_{33} & A_{34} & A_{35} & A_{36} \\ A_{14} & A_{24} & A_{34} & A_{44} & A_{45} & A_{46} \\ A_{15} & A_{25} & A_{35} & A_{45} & A_{55} & A_{56} \\ A_{16} & A_{26} & A_{36} & A_{46} & A_{56} & A_{66} \end{bmatrix} - \Delta \begin{bmatrix} B_{11} & B_{12} & 0 & 0 & B_{15} & B_{16} \\ B_{12} & B_{22} & 0 & 0 & B_{25} & B_{26} \\ 0 & 0 & B_{33} & B_{34} & B_{35} & B_{36} \\ 0 & 0 & B_{34} & B_{44} & B_{45} & B_{46} \\ B_{15} & B_{25} & B_{35} & B_{45} & B_{55} & B_{56} \\ B_{16} & B_{26} & B_{36} & B_{46} & B_{56} & B_{66} \end{bmatrix} \right| = 0 \tag{36}$$

Stiffness matrix — Mass matrix

where A_{ij} and B_{ij} $(i = 1, 6\ ;\ j = 1, 6)$ are given by

$$A_{11} = \lambda_r^2 + \frac{n^2(1-\nu)}{2} I_2 (1+\beta)$$

$$A_{12} = \frac{\lambda_r^3}{\mu_r} I_5 + \frac{n^2(1-\nu)}{2} \frac{\lambda_r^2}{\mu_r^2} I_6 (1+\beta)$$

$$A_{13} = -n\lambda_r \left\{ \nu I_1 + \tfrac{1}{2}(1-\nu) I_2 \right\}$$

$$A_{14} = -\frac{n}{2}(1+\nu) \frac{\lambda_r^2}{\mu_r} I_6$$

$$A_{15} = -\nu \lambda_r I_1 + \beta \lambda_r \left\{ -\lambda_r^2 + \frac{n^2}{2}(1-\nu) I_2 \right\}$$

$$A_{16} = -\nu \frac{\lambda_r^2}{\mu_r} I_6 + \beta \lambda_r^2 \left\{ -\lambda_r I_5 + \frac{n^2}{2}(1-\nu) \frac{1}{\mu_r} I_6 \right\}$$

$$A_{22} = \frac{\lambda_r^3}{\mu_r} I_5 + \frac{n^2(1-\nu)}{2} \frac{\lambda_r^2}{\mu_r^2} I_6 (1+\beta)$$

$$A_{23} = -n \left\{ \nu \frac{\mu_r^2}{\lambda_r} + \tfrac{1}{2}(1-\nu) \frac{\lambda_r^3}{\mu_r^2} \right\} I_6$$

$$A_{24} = -n \mu_r \left\{ \nu I_3 + \tfrac{1}{2}(1-\nu) I_4 \right\}$$

$$A_{25} = -\nu \frac{\mu_r^2}{\lambda_r} I_6 + \beta \frac{\lambda_r^3}{\mu_r^2} \left\{ -\lambda_r \mu_r I_5 + \frac{n^2}{2}(1-\nu) I_6 \right\}$$

$$A_{26} = -\nu \mu_r I_3 + \beta \mu_r \left\{ -\mu_r^2 + \frac{n^2}{2}(1-\nu) I_4 \right\}$$

$$A_{33} = n^2 + n^2 (N_1 + N_4) M_1^2 + \tfrac{1}{2}(1-\nu) \lambda_r^2 I_2 (1+3\beta)$$

$$A_{34} = n^2 I_5 + n^2 M_1 M_2 (N_1 + N_4) + \tfrac{1}{2}(1-\nu) \frac{\lambda_r^3}{\mu_r} I_6 (1+3\beta)$$

$$A_{35} = n + \beta n \lambda_r^2 \left\{ \nu I_1 + \frac{3}{2} (1 - \nu) I_2 \right\} + n M_1^2 (N_1 + n^2 N_4)$$

$$A_{36} = n I_5 + n M_1 M_2 (N_1 + n^2 N_4) + \beta n \left\{ \nu \frac{\mu_r^3}{\lambda_r} + \frac{3}{2} (1 - \nu) \frac{\lambda_r^3}{\mu_r} \right\} I_6$$

$$A_{44} = n^2 + n^2 M_2^2 (N_1 + N_4) + \tfrac{1}{2} (1 - \nu) \mu_r^2 I_4 (1 + 3\beta)$$

$$A_{45} = n I_5 + \frac{\beta n \lambda_r^3}{2 \mu_r} I_6 (3 - \nu) + n M_1 M_2 (N_1 + n^2 N_4)$$

$$A_{46} = n + \beta n \mu_r^2 \left\{ \nu I_3 + \frac{3}{2} (1 - \nu) I_4 \right\} + n M_2^2 (N_1 + n^2 N_4)$$

$$A_{55} = 1 + \beta \left[\lambda_r^4 + (n^2 - 1)^2 + 2n^2 \lambda_r^2 \left\{ \nu I_1 + (1 - \nu) I_2 \right\} \right] + M_1^2 \left\{ N_1 + N_4 (2n^2 - 1) + (n^2 - 1)^2 (N_2 - N_5) \right\}$$

$$A_{56} = I_5 + \beta \left[\left\{ \lambda_r^4 + (n^2 - 1)^2 \right\} I_5 + \nu n^2 I_6 \left(\frac{\lambda_r^3}{\mu_r} + \frac{\mu_r^3}{\lambda_r} \right) + 2n^2 \frac{\lambda_r^3}{\mu_r} (1 - \nu) I_6 \right] + M_1 M_2 \left\{ N_1 + N_4 (2n^2 - 1) + (n^2 - 1)^2 (N_2 - N_5) \right\}$$

$$A_{66} = 1 + \beta \left[\mu_r^4 + (n^2 - 1)^2 + 2n^2 \mu_r^2 \left\{ \nu I_3 + (1 - \nu) I_4 \right\} \right] + M_2^2 \left\{ N_1 + N_4 (2n^2 - 1) + (n^2 - 1)^2 (N_2 - N_5) \right\}$$

$$B_{11} = I_2 + (N_3 + N_6) M_3^2$$

$$B_{12} = \frac{\lambda_r^2}{\mu_r^2} I_6 + (N_3 + N_6) M_3 M_4$$

$$B_{15} = -M_3^2 \lambda_r (N_6 + N_7)$$

$$B_{16} = - \mu_r M_3 M_4 (N_6 + N_7)$$

$$B_{22} = I_4 + (N_3 + N_6) M_4^2$$

$$B_{25} = -\lambda_r M_3 M_4 (N_6 + N_7)$$

$$B_{26} = -\mu_r M_4^2 (N_6 + N_7)$$

$$B_{33} = 1 + M_1^2 (N_3 + 3N_6 + 3N_7 + N_8)$$

$$B_{34} = I_5 + M_1 M_2 (N_3 + 3N_6 + 3N_7 + N_8)$$

$$B_{35} = n M_1^2 (N_6 + 2N_7 + N_8)$$

$$B_{36} = n M_1 M_2 (N_6 + 2N_7 + N_8)$$

$$B_{44} = 1 + M_2^2 (N_3 + 3N_6 + 3N_7 + N_8)$$

$$B_{45} = n M_1 M_2 (N_6 + 2N_7 + N_8)$$

$$B_{46} = n M_2^2 (N_6 + 2N_7 + N_8)$$

$$B_{55} = 1 + M_1^2 (N_3 + N_6 + n^2 N_7 + n^2 N_8) + \lambda_r^2 M_3^2 (N_7 + N_8)$$

$$B_{56} = I_5 + M_1 M_2 (N_3 + N_6) + (N_7 + N_8)(\lambda_r \mu_r M_3 M_4 + n^2 M_1 M_2)$$

$$B_{66} = 1 + M_2^2 (N_3 + N_6 + n^2 N_7 + n^2 N_8) + \mu_r^2 M_4^2 (N_7 + N_8)$$

Here

$$\lambda_r = p_r a \quad , \quad \mu_r = q_r a$$

$$I_1 = \frac{1}{L} \int_0^L p_r^2 \left\{ \int \phi_r(x)\, dx \right\}^2 dx$$

$$I_2 = \frac{1}{L} \int_0^L \left\{ \phi_r'(x) \right\}^2 dx \qquad (37)$$

contd...

$$I_3 = \frac{1}{L} \int_0^L q_r^2 \left\{ \int \psi_r(x)\, dx \right\}^2 dx \qquad (37)$$

$$I_4 = \frac{1}{L} \int_0^L \left\{ \psi'_r(x) \right\}^2 dx$$

$$I_5 = \frac{1}{L} \int_0^L \phi_r(x)\, \psi_r(x)\, dx$$

$$I_6 = \frac{1}{L} \int_0^L \left[\left\{ p_r \int \phi_r(x)\, dx \right\} \left\{ q_r \int \psi_r(x)\, dx \right\} \right] dx$$

In the above expressions use has been made of the orthogonality properties of characteristic functions of beam vibration as given by equation (26). All the explicit expressions for the above integrals are detailed in the Appendix III.

Also for N discrete rings stationed at the points $x_1, x_2, \ldots, x_N$

$$M_1 = \sum_{i=1}^{N} \phi_r(x_i), \qquad M_2 = \sum_{i=1}^{N} \psi_r(x_i)$$

$$M_3 = \sum_{i=1}^{N} \phi'_r(x_i), \qquad M_4 = \sum_{i=1}^{N} \psi'_r(x_i)$$

$$N_1 = \sum_{i=1}^{N} \frac{E_{R_i} A_{R_i} (1 - \nu^2)}{E_s h L}$$

$$N_2 = \sum_{i=1}^{N} \frac{E_{R_i} A^{(2)}_{R_i} (1 - \nu^2)}{E_s a^2 h L}$$

$$N_3 = \sum_{i=1}^{N} \frac{\rho_{R_i} A_{R_i}}{\rho_s h L}$$

$$N_4 = \sum_{i=1}^{N} \frac{E_{R_i} A^{(1)}_{R_i} (1 - \nu^2)}{E_s a h L}$$

$$N_5 = \sum_{i=1}^{N} \frac{E_{R_i} A^{(3)}_{R_i} (1 - \nu^2)}{E_s a^3 h L} \qquad (38)$$

contd..

$$N_6 = \sum_{i=1}^{N} \frac{\rho_{R_i} A_{R_i}^{(1)}}{\rho_s a h L}$$

$$N_7 = \sum_{i=1}^{N} \frac{\rho_{R_i} A_{R_i}^{(2)}}{\rho_s a^2 h L}$$

$$N_8 = \sum_{i=1}^{N} \frac{\rho_{R_i} A_{R_i}^{(3)}}{\rho_s a^3 h L}$$

where ρ_{R_i}, E_{R_i}, A_{R_i} and $A_{R_i}^{(r)}$ are the density, Youngs modulus, area of cross section and r^{th} moment of area of cross section about the skin median for the ring stationed at $x = x_i$ along the shell generator.

Frequency equation (36) is a sextic in the frequency parameter Ω. As is observed in the next section its solution involves obviously a more complicated analysis and more digital computer time. Moreover the sextic could not be solved exactly in the mathematical sense. So if in this case (especially when tall cylindrical shells are considered) the assumption of zero hoop and shear strain is made, the ensuing analysis is simplified and the sextic is reduced to a quadratic in Ω, which in turn could be solved exactly. The procedure is as follows.

The reduced form of the modal displacement function (28) is considered. This is substituted into the expressions for the strain and kinetic energies of the shell and the ring as given in the Appendix [I]. Then the Rayleigh-Ritz method is applied to yield the frequency equation

$$\left| \begin{bmatrix} A_{11} & A_{12} \\ A_{12} & A_{22} \end{bmatrix} - \Omega \begin{bmatrix} B_{11} & B_{12} \\ B_{12} & B_{22} \end{bmatrix} \right| = 0 \qquad (39)$$

where

$$A_{11} = \lambda_r^4 + \beta n^2 \lambda_r^2 + \left\{ n^2 \lambda_r^2 + 2\nu n^2 (n^2 - 1) I_1 + 2(1 - \nu)(n^2 - 1)^2 I_2 \right\}$$

$$+ n^4 (n^2 - 1)^2 (\beta + N_2 M_1^2)$$

$$A_{12} = \lambda_r^4 I_5 + \beta n^2 \left\{ n^2 \lambda_r^4 I_5 + \nu (n^2 - 1) n^2 I_6 \left(\frac{\lambda_r^3}{\mu_r} + \frac{\mu_r^3}{\lambda_r} \right) \right.$$

$$\left. + 2 (1 - \nu)(n^2 - 1)^2 \frac{\lambda_r^3}{\mu_r} I_6 \right\} + n^4 (n^2 - 1)^2 (\beta I_5 + N_2 M_1 M_2)$$

$$A_{22} = \mu_r^4 + \beta n^2 \mu_r^2 \left\{ n^2 \mu_r^2 + 2\nu n^2 (n^2 - 1) I_3 + 2 (1 - \nu) (n^2 - 1)^2 I_4 \right\}$$

$$+ n^4 (n^2 - 1)^2 (\beta + N_2 M_2^2)$$

$$B_{11} = n^2 (n^2 + 1) (1 + N_3 M_1^2) + \lambda_r^2 (I_2 + N_3 M_3^2)$$

$$B_{12} = n^2 (n^2 + 1) (I_5 + N_3 M_1 M_2) + \frac{\lambda_r}{\mu_r} (\lambda_r^2 I_6 + \mu_r^2 N_3 M_3 M_4)$$

$$B_{22} = n^2 (n^2 + 1) (1 + N_3 M_2^2) + \mu_r^2 (I_4 + N_3 M_4)^2$$

The equation (39) was derived by using the energy expression for the ring and the shell as given by Johns and Allwood [9] . There the ring was symmetric and the rotary inertia of the ring was also not taken into account. To complete the solution the ring eccentricity and rotary inertia has been included. Also in allowing for the effect of zero hoop and shear strain for the ring stiffened shell the energy expressions derived in the previous section have been used. Again employing the variational technique by Rayleigh-Ritz a frequency equation similar to (39) results with different elements A'_{11} , A'_{12} , A'_{22}, B'_{11} , B'_{12} . B'_{22} .

$$\left| \begin{bmatrix} A'_{11} & A'_{12} \\ A'_{12} & A'_{22} \end{bmatrix} - \Delta \begin{bmatrix} B'_{11} & B'_{12} \\ B'_{12} & B'_{22} \end{bmatrix} \right| = 0 \qquad (40)$$

$$A'_{11} = A_{11} + 2 n^2 \beta \lambda_r^4 - n^4 (n^2 - 1)^2 N_5 M_1^2$$

$$A'_{12} = A_{12} + 2 n^2 \beta \lambda_r^4 I_5 - n^4 (n^2 - 1)^2 N_5 M_1 M_2$$

$$A'_{22} = A_{22} + 2 n^2 \beta \mu_r^4 - n^4 (n^2 - 1)^2 N_5 M_2^2$$

$$B'_{11} = B_{11} + \lambda_r^2 M_3^2 \left\{ (2n^2 + 1) N_6 + n^2 (n^2 + 2) N_7 + n^4 N_8 \right\}$$
$$+ n^2 M_1^2 \left\{ (3 - n^2) N_6 + (n^2 - 3)(n^2 - 1) N_7 + (n^2 - 1)^2 N_8 \right\}$$

$$B'_{12} = \lambda_r \mu_r M_3 M_4 \left\{ (2n^2 + 1) N_6 + n^2 (n^2 + 2) N_7 + n^4 N_8 \right\}$$
$$+ n^2 M_1 M_2 \left\{ (3 - n^2) N_6 + (n^2 - 3)(n^2 - 1) N_7 + (n^2 - 1)^2 N_8 \right\}$$

$$B'_{22} = \mu_r^2 M_4^2 \left\{ (2n^2 + 1) N_6 + n^2 (n^2 + 2) N_7 + n^2 N_8 \right\}$$
$$+ n^2 M_2 \left\{ (3 - n^2) N_6 + (n^2 - 3)(n^2 - 1) N_7 + (n^2 - 1)^2 N_8 \right\}$$

It should be obvious of course that these analyses may also be applied to a clamped free shell by the simple expedient of putting E_R , ρ_R equal to zero. Such results are shown in Table 1.

3. ANALYTICAL RESULTS

3.1 General

The major purpose of the present report is to show the dependence of the natural frequencies of cylindrical shells on the geometrical and material properties e.g. length-to-radius ratio (L/a), radius-to-thickness ratio (a/h), Youngs modulus (E), density (ρ) etc.

As derived in the last section the algebraic equations solved here are of 1st, 2nd, 3rd, 4th and 6th degree. Equations of first, second, third and fourth degree can be solved exactly, whereas an iteration procedure has been adopted to solve the sixth degree equation in Δ given by equation (36).

For the sextic, a specified set of shell geometries and ring characteristics, an assumed number of circumferential waves n, and a specified set of boundary conditions at each end, is selected. The effect of specified boundary conditions at each end is incorporated by choosing the data for the beam vibration functions, ϕ_r ψ_r. An iteration scheme is then used to compute Δ . Starting from some initial estimate for the frequency parameter Δ , the determinant is evaluated for successive values of Δ until there is a change in its sign, indicating that a zero has been bracketed between two successive frequency parameter estimates. Regula falsi procedure is then employed to locate the zero to some preselected accuracy. The entire range of the problems of interest can be covered by varying the initial input to the determinant, i.e. by changing a/h, L/a, ν , n, b_R/a etc. The number of iterations required for convergence is greatly reduced if close initial estimates of the frequency parameter are available. Here the solutions developed for the clamped-free shell case have been used as initial estimates for the clamped-ring stiffened shell case.

3.2 Clamped-Free Shell

3.2.1 General

For any fixed values of n and axial wave number m (see Fig. 2) there are three natural frequencies corresponding to three different values of the amplitude ratios A_1 ; B_1 ; C_1. In general, two of these three frequencies are several orders of magnitude higher than the minimum value and hence the lowest value of frequency corresponding to mainly radial motion, is of structural interest.

These higher frequencies will arise only if inplane as well as radial inertia terms are retained in the equations of motion. Although these higher frequencies are not to be studied here, all three inertia terms have been retained in developing the results presented herein.

Also, for a fixed number of circumferential waves the frequency increases monotonically with an increasing number of axial half waves. This holds for entire range of shell parameters (a/h, L/a, ν) and for all boundary conditions. Because of this fact the Figs. 4 et seq. are all drawn for m = 1, i.e. for the fundamental longitudinal mode shape.

The behaviour is quite different when the number of circumferential waves n is varied as is indicated in Fig. 4. The value of n which corresponds to a mode shape having the minimum frequency depends strongly upon the length-to-radius ratio of the shell. This fact is obvious from the Figs. 4 et.seq.

In order to direct attention to the significant findings of the present study, in many cases only the frequency envelopes are examined. Frequency envelope is lower bound to the frequency spectrum for a given value of a/h, and for m = 1 and $n \geq 1$.

Figs. 4 - 5 which are based on the cubic equation (32) show the envelopes of frequency parameter curves for constant values of circumferential wave number n and length-to-radius ratio (L/a), indicated by heavy line in the graph. Fig. 4 corresponds to a/h = 200 and Fig. 5 to a/h = 100. It is to be noted that for shells of large length-to-radius ratio (L/a) the minimum frequency will correspond to n = 1 i.e. to swaying oscillations. The values of L/a for which the change from n = 2 to n = 1 takes place depend upon a/h. For a/h = 20, this occurs for L/a = 8 to 10, for a/h = 5000, it occurs for L/a > 100.

Fig. 6 shows in more detail part of the frequency spectrum for n = 1 (or swaying modes only). It is obvious that except for very short shells the curve is independent of the radius-to-thickness ratio, which may be deduced from the governing equations easily. For swaying the long shell behaves more as a beam and membrane action predominates over bending action of the shell wall.

The solid line represents the frequency spectrum for a clamped-free shell as found by the cubic frequency equation (32) and the dotted line is that due to the quadratic frequency equation (40) for which the assumption of zero hoop and shear strain was taken. It is clear from Fig. 6 that for long shells this assumption

does not introduce any significant change in the frequency parameter but for short shells it raises the frequency considerably.

3.2.2. Effect of Zero hoop and shear

It is interesting to note that for tall shells the assumption of zero hoop and shear strain expressed by equation (27) leads to considerable simplification in the frequency equation as contemplated by Johns and Allwood [9] without introducing any significant error in the minimum natural frequency. The ovalling frequency (n = 2) for a particular shell geometry is given in Table 1 employing various sets of mode shapes determined by equations (18), (19), (20), (23) with or without zero hoop and shear strain. The order of the frequency equations in each of these cases is indicated and it is seen that with zero hoop and shear strain assumed, the cubic and sextic equations are reduced to linear and quadratic forms. In both these cases for this particular geometry the difference in the natural frequency is less than a few tenth of a percent.

For different shell geometries of interest to the designer (as indicated in Ref. [15]) of steel chimney the influence of zero hoop and shear strain is seen by comparing Tables 2 and 3 for the sextic and quadratic frequency equations employing Flügge theory. For n = 1 the difference is nearly 15 to 18% for all the shell geometries considered but for n = 2 the maximum difference is nearly 14% for short thin shells (e.g. L/a = 10, a/h = 300) whereas it is negligible for long shells.

In Fig. 7 the frequency envelopes for a clamped-free shell are drawn for different radius-to-thickness ratios (20, 100, 500, 5000). The continuous curves represent the envelopes corresponding to the cubic frequency equation (32) and the broken ones correspond to the quadratic frequency equation (40). As length-to-radius ratio increases the results agree closely with the quadratic frequency results (equation (40)) being slightly higher than those for the cubic (32). For the shells of small length-to-radius ratio the difference is more considerable. This increase in frequency parameter (Δ) of the quadratic (40) over the cubic (32) may be attributed mainly to the assumption of zero hoop and shear in the former analysis which, clearly, for short shells raises the frequency parameter considerably. The inclusion of the clamped-pinned characteristic beam function ψ_r in the quadratic analysis has made no significant difference to the results obtained for the clamped-free shell as was seen previously in the results of Table 1.

3.2.3 Dependence of frequency on circumferential wave number

Figs. 4 and 5 showed the variation of frequency factor Δ with L/a for various values of n and at a given value of L/a the dependence on n is seen to be large.

Fig. 8 shows this dependence of the frequency factor Δ on the circumferential wave number in an alternative way. The three different curves correspond to three different values of L/a, (1, 10, 100) and for a/h = 100. It is clear that the lower the length-to-radius ratio of the shell the higher the value of n corresponding to the minimum frequency. For L/a = 1, the minimum frequency corresponds to a breathing mode with n = 6 whereas for L/a = 10 the ovalling frequency with n = 2 is more critical and a value of L/a as 100 the sway frequency (n = 1) is the one which is critical. Here the dotted curve is due to the quadratic (40) and the continuous curve is due to the cubic (32). The difference in the results from these two equations is again more marked in case of low length-to-radius ratio than in case of high length-to-radius ratio. For high values of n the frequency parameter seems to be independent of L/a which is shown in the studies of Reference [1] .

3.2.4. Dependence of frequency on axial wave number

Further study indicates that as m increases the frequency increases with the lowest frequency spectrum being for m = 1. This is shown in Fig. 9. Also in this figure the predicted results of the present theory are compared with measured results of Ref [4] . The agreement appears to be quite satisfactory.

The diminishing influence of higher axial wave number m, at the higher values of circumferential wave number n on the frequency parameter is clearly seen here.

Fig. 10 also shows a comparison between the results from present theory and measured frequency parameters from Ref. [3] . The agreement is again quite good. . The two curves for each cylinder tested correspond to m = 1, 2.

3.2.5. Detailed Results

The values of frequency parameters, for those shells which may be of interest to the designers of chimneys (as indicated in Reference [15]) are given in form of table 2 - 3. Table 1 showed that the results from sextic frequency equation (36) give the best approximation to the frequency parameter from all the analyses considered in this paper at least for one geometry. Table 2 gives more detailed sextic results and the corresponding results due to cubic frequency equation (32). The approach in both these cases was based on Flügge theory.

The sextic results are lower than those of the cubic.

For n = 1 the numerical difference in the results of both analyses appears to diminish as length-to-radius ratio (L/a) increases but the proportional difference remains essentially constant.

In the case of ovalling with n = 2 the agreement of both sets of results is better for all a/h considered and particularly for large values of L/a. For example for L/a = 10 the difference between the two sets of results is less than a percent but for L/a = 50 the difference in the values is almost negligible. Thus for a clamped-free shell the inclusion of the mode $\psi_r(x)$ (equation (23)) which raises the order of the frequency equation from a cubic to a sextic has no major significant effect.

Table 3 gives the frequency parameters for the clamped-free shells using identical mode shapes but the energy expression due to Flügge theory in the one case and those due to Timoshenko-Love in the other case. Previous studies (references [7 & 8]) have shown that for some modes of practical cylindrical shells the effect on frequency of using different energy expressions is very small. Comparing the frequencies obtained with the different energy expressions the percentage difference between the extreme values of $\Delta^{\frac{1}{2}}$ for the modes chosen was less than $\frac{1}{2}$ percent for all geometries considered (involving a wider range of values of L/a and a/h than that shown in Tables 2 - 3) It is seen that this difference is even smaller for those geometries considered in Table 3; being detectable only for low values of L/a and a/h i.e. only for the values a/h = 50, n = 1, L/a = 10, 15 and a/h = 100, n = 2, L/a = 10. Also shown in the Tables 2 - 3 are the values of frequency parameter for an infinitely long shell (L/a = ∞). For n = 2 the increase in frequency parameter as L/a decreases is a measure of the constraint effect of the clamped base. Thus the error in calculating the ovalling frequency for a short shell from the simple ring formula of equation (34) may be considerable.

3.3 Cylindrical Shell with Ring Stiffened Upper End

3.3.1 General

Figure 11 shows frequency envelopes for a clamped-free shell (indicated as a continuous curve) and for a shell with a clamped and a ring stiffened upper end (indicated as a broken curve). Two values of a/h (= 100, 5000) are taken and the ring characteristics are $b_R/a = .03$ and $d_R/a = .09$ (i.e. a slender ring).

Clearly the ring has had a significant effect in raising the frequencies for $n \geq 2$ as may also be seen by comparing Tables 2 and 4. For n = 1 effect is to slightly lower the frequencies.

Reference [16] noted that the behaviour of such a shell can be considered in the following three regions:

Region I : where $0 \leq n < n_1$, the attached rings simply add mass to the system and thus constitute more inertia than stiffness so that the natural frequency of the system is slightly lower than the corresponding frequency of unstiffened shell at least for the fundamental mode. Comparing the Tables 2 - 3 with Tables 4 - 8 it is clear that the frequency parameter for n = 1 is lowered by the addition of a stiffening ring.

Region II : where $n_1 < n < n_2$, the attached ring contributes the dominant stiffness, causing an abrupt upsweep in the frequency spectrum as compared to an unstiffened shell. For thinner shells this rise is higher than for thicker shells as is evident in Tables 4 - 7. For example in Tables 4 - 6 for eccentric ring for L/a = 10, n = 2 the frequency parameter goes on decreasing for a/h = 50 - 200 and then it starts increasing for a/h = 250, 300.

Region III : where $n > n_2$ the ring motion becomes so small, compared to inter ring panel motion, that the frequency of the system approaches asymptotically to that of a clamped-clamped panel, and the mode shape becomes predominantly one of panel vibration. In this region, the equivalent orthotropic analysis are evidently not applicable and the frequency curve may become flat and may have a second minimum resulting in numerous resonances in a narrow frequency band.

3.3.2 Effect of zero hoop and shear strain

The effect of zero hoop and shear strain in the case of a ring stiffened shell can be studied from the Tables 4 and 5 and Tables 6 and 7. Tables 4 and 6 correspond to the sextic frequency equation (36) and Tables 5 and 7 correspond to the quadratic frequency equation (40). This quadratic is reduced from the sextic by assuming zero hoop and shear strain.

It is observed that this assumption increases the value of frequency parameter. This increase is more marked for the shell of small length-to-radius ratio than for the shells of large length-to-radius ratio (radius-to-thickness ratio being held constant). From Tables 4 and 5 for the eccentric ring when a/h = 50 and n = 2, the increase in frequency is 3.5% for L/a = 10 and 0.15% for L/a = 50. Secondly for

a/h = 300 and n = 2, the increase in frequency due to this assumption is nearly 20% for L/a = 10 and 5 % for L/a = 50.

3.3.3 Effect of Ring Mass

As shown in Figure 12 omitting the ring mass increases the frequency parameter. This increase is considerable only for very short shells and decreases rapidly with increasing length-to-radius ratio (L/a).

3.3.4 Effect of Ring Eccentricity

This effect can directly be studied by observing Tables 4 - 5. Table 4 gives the frequency parameter for sextic with eccentric ring (indicated by 'SFE') and sextic with symmetric ring (indicated by 'SFS'). Table 5 gives similar results for quadratic indicated 'QFE' and 'QFS' for eccentric and symmetric ring respectively. The effect of eccentricity with the smaller ring (I), shown in Table 4, 5 is highly significant in increasing the frequencies and should clearly be included in shell analyses. Its effect increases with a/h and decreases with L/a. For example when L/a = 10, n = 2 and a/h = 300 the externally stiffened shell has a frequency almost 30% higher than the symmetrically stiffened shell.

The corresponding results for the larger ring (II) as in Tables 6, 7 show less beneficial effects of eccentricity in general. In particular eccentricity may be seen to lower the frequency as compared to symmetrically stiffened shell.

The reasons for this have not yet been analysed in depth but it is believed that the stiffness of this larger ring has been more than sufficient to cause the fundamental mode to approximate to that of a clamped-simply supported shell in which case the end ring then makes a larger contribution to the higher inertia than it does to the stiffness and clearly higher the inertia of the eccentric ring compared to the symmetric ring would then produce a lower shell frequency.

Some further remarks about internal and external stiffening are given in References [12, 17, 18].

It is not unreasonable to expect a shell internally ring stiffened to respond differently from an externally stiffened shell. However it might be anticipated that the differences between the internal and external ring stiffening would be small as compared to their differences with a symmetrically placed ring stiffener if the eccentricity is relatively small (less, say than 5% of the shell radius).

Although the work of Hu, Gormley and Lindholm [16] indicates that there is very little effect on the frequencies due to ring eccentricity, but the present analysis, the analyses due to Sewall and Naumann [4] Mikulas and McElman [11] Egle and Soder [17] and Forsberg [18] indicate that there is a definite effect of eccentricity. This problem needs to be examined further by the means of carefully carried out experiments with integral or welded ring shell construction.

Table 9 shows the values of frequency parameters for clamped-simply supported shells. This may be compared with the values in Tables 6, 7 and 8 for the case of a stiffer ring. It is seen that in case of sextic (Table 6) the values of frequency parameter are slightly less than those of Table 9 for n = 2 case. Whereas Tables 7 - 8 give values of frequency parameter Λ which are slightly higher than Table 9 in case of ovalling (n = 2). It may be concluded that sextic gives better results than other cases. For swaying mode (n = 1) the frequency is greatly increased in case of clamped-supported shell in contrast to slight decrease in frequency in case of clamped-ring stiffened shell as compared to the clamped-free shell.

3.3.5 Influence of Ring Stiffness

For a particular shell geometry described in Table 1 the effect of a ring on the minimum frequency has been studied and the results are given in Table 10. It is found for this particular shell that only a low value of ring stiffness is needed to bring the natural frequency close to that which a very stiff ring would produce. The maximum possible increase in natural frequency of this shell with a very stiff end ring over a shell with no ring is only about 25%. Observing the results in Table 10 it is seen that as the ring stiffness increases the upper end amounts to a simply supported end.

Figure 13 shows the frequency envelopes for a/h = 100, 5000. Continuous curves correspond to less stiff ring ($b_{R/a} = .003$, $d_{R/a} = .009$) whereas broken curves correspond to more stiff ring ($b_{R/a} = .03$, $d_{R/a} = .09$, 10 times of first ring characteristics). It is seen that for thick shells (a/h = 100) a stiff ring has considerable gain in frequency parameter over a less stiff ring in the entire range of L/a (except for n = 1), where ring has predominant inertia and not stiffness) but for thin shells (a/h = 5000) the frequency parameter is more or less the same in both cases. This disparity may again be attributed to the effect of ring mass.

Figure 14 shows the dependence of frequency parameter on circumferential wave number n with a particular ring ($b_R/a = .01$, $d_R/a = .03$) and for shells of $a/h = 100$ and $L/a = 10, 100$. The broken curve corresponds to sextic (36) and continuous curve to the quadratic highlighting again the effect of zero hoop and shear strain.

4. COMPARISON WITH RESULTS FROM EXACT ANALYSIS

4.1 General

An exact solution approach for equations of motion has been developed by Forsberg [18] for the case of ring stiffened cylindrical shells. This approach is conceptually different from the one employed here. Brief descriptions for this theory are given in the Appendix V.

In order to compare the results from the exact analysis and the variational solution the following shell geometries and other parameters were selected:

Radius-to-thickness ratio (a/h) has two values 250, 600, and for each a/h there are two length-to-radius ratios i.e. 9, 12. Axial wave number m takes values 1, 2, 3 and for each value of m circumferential wave number, n varies from 0 to 10 in steps of 1. Poisson's ratio, ν is .3.

4.1.1 CLAMPED-FREE SHELL:

These boundary conditions are typical of an unstiffened chimney stack. A comparison of frequency parameters as computed by the two approaches is given in Tables 11 and 12. The agreement between the available results of these two theories is very satisfactory, especially for the minimum natural frequency parameter, which in the case of the present analysis is slightly lower, in all cases, than its counterpart by Forsberg's exact analysis. The difference between the two results is very low and in most cases it is only few tenths of a percent, e.g. for a/h = 600, L/a = 12, m = 3, n = 3 it is only 0.2%. The maximum difference in the lowest natural frequency parameter is 2.5% for a/h = 250, L/a = 12, m = 2, n = 3.

Differences between other frequency parameters than the minimum is also within 2% in most of the cases except the swaying frequency parameter. The difference seems to be more pronounced in this case for $m \geq 2$ as can be seen from tables 11 and 12.

For the fundamental axial mode (m = 1) and n = 1, the difference between the two results is not very pronounced and it decreases with increasing L/a and a/h. For a/h = 250, L/a = 9 the difference is 1.1% which is the same as for a/h = 600 and L/a = 9. For a/h = 250, L/a = 12 the difference between the sway frequency parameters given by the exact approach and the present variational approach is only about 0.4% and for a/h = 600, L/a = 12 it is only 0.35%.

When m = 2 the difference between the two results is very pronounced in contrast to m = 1. For a/h = 250, L/a = 9 it is nearly 13% but for a/h = 250, L/a = 12 it is 7% showing that it decreases with increasing L/a.

Figures 15 and 16 represent an alternative way of comparing the results of the two theories. Two figures correspond to two different values of a/h i.e. Figure 15 corresponds to a/h = 250 and figure 16 corresponds to a/h = 600. Here also it is obvious from the frequency curves from either sides of the minimum natural frequency that present variational technique gives low values of frequency parameters than the "exact" theory adopted by Forsberg [18] . Also the overall agreement is quite good as seen in the figures 15 and 16. In case of m = 2 for axisymmetric and sway modes the difference in the frequency parameters is more pronounced but it decreases with increasing L/a. For higher values of n there is virtually no effect of a change in L/a or in the axial wave number m, also the two sets of results agree very closely in that region.

4.1.2. CLAMPED-RING STIFFENED SHELLS

In case of the shell with clamped base and top stiffened by a stiff elastic ring (breadth/shell radius = 0.1 and depth/shell radius = 0.3) the results of the two theories are seen compared in figures 17 and 18 and in table 13.

In the case of sway (n = 1) oscillations the solution of both theories agree very closely where the dominant ring inertia results in reducing the frequency parameter. The results due to a sextic frequency

equation in the author's theory are slightly higher than Forsberg's [18] results by a maximum of about 5% in the cases considered for swaying oscillations.

In the case of the circumferential wave number $n \geq 2$ i.e. for ovalling and breathing, the frequency parameters given by the sextic frequency equation of present theory are lower than the corresponding results given by Forsberg's [18] method. The frequency parameters given by the quadratic frequency equation (which is obtained by reducing the sextic due to the assumption of zero hoop and shear strain) is much closer to the results given by the Forsberg [18] method than those from the sextic frequency equation as can be seen in the figures 17 and 18. For ovalling oscillations ($n = 2$) Forsberg's results lie in between the sextic and quadratic frequency equations of the present theory. For $n > 2$ the results from the present theory are slightly lower than Forsberg [18] method. This may be due to slight differences in the use of the particular ring theory, although the basic shell theory used in both the cases in that due to Flugge. For $n > 5$ in the case if the given geometries the results of both the theories agree very closely.

It may be remarked, however, that the shell having one end stiffened by a very stiff elastic ring may be approximated as having a simply supported end. Thus the frequency parameters found for a clamped-ring stiffened shell will be nearly equal to, but not greater than, the clamped-simply supported shell theoretically. The results of the sextic frequency equations of the present theory for clamped-ring stiffened shell are always lower than clamped-simply supported shell. But this is not true for the results of quadratic frequency equation of the present theory and Forsberg's method. This fact is observed by reading the table 13 where, for a clamped-ring stiffened shell (ring: $b_R/a = .1$, $d_R/a = .3$), the results from the sextic frequency equation of the present theory and Forsberg's theory [18] are compared with the results obtained for a clamped-simply supported shell from the cubic frequency equation of the present theory. It is evident from

table 13that the results of the sextic for a sufficiently stiff ring are very near to, but lower than, those for the clamped-simply supported case. Available results of Forsberg's theory are higher than those for the clamped-simply supported case.

For the shells with clamped base and with an elastic ring at the top and two intermediate rings of equal dimensions in case of L/a = 9 and three intermediate equivalent rings in case of L/a =12, the curves are given in figures 17 and 18. It is seen that in region I the swaying frequency is lowered in both the cases. This is because the attached rings contribute more inertia effect than stiffness effect. In region II where $2 \leq n \leq 8$ the attached rings contribute the dominant stiffness decreasing with n, so that the frequency parameter is much higher than that corresponding to the clamped-free or clamped-ring stiffened shell. In region III, where $n > 8$, the ring motion becomes so small compared to the inter-ring panel motion that the frequency of the system approaches asymptotically to that of clamped-ring stiffened shell.

Thus it is obvious that with many intermediate rings swaying becomes more critical but ovalling or breathing oscillations may be avoided. These results were obtained by using Forsberg analysis [18] .

The major disadvantage of the exact method by Forsberg [18] is that it must rely on an iterative technique to find zeros of a determinant. When such a zero is bracketed, the eigenvalue can be accurately computed. However there is no assurance that all of the roots of the system will be located and if the eigenvalues are very closely spaced the technique employed may well miss many pairs of roots without giving any indication that eigenvalues have been missed. This fact is obvious by looking at the tables 11, 12, 13 where for this reason not all values of frequency parameters are given using Forsberg analysis particularly for m = 3. For the present analysis . with a small finite number of degrees of freedom there are well defined mathematical techniques for finding all of the roots of the system within a specified interval. This fact is very much obvious if one looks at the tables 11, 12, 13.

Also, computer time involved in finding the exact solution is very great per eigenvalue in Forsberg's method. In the present analysis when solving the quadratic and cubic frequency equations this is negligible and a great number of frequency parameters can be calculated in seconds. Even if we use a sextic the run time is much less as compared to the exact solution because solutions corresponding to the quadratic frequency equations give really good initial estimates of frequencies.

Thus for engineering applications and for determining the variables discussed here the present analysis seems generally preferable to the exact solution outlined by Forsberg [18] . Also the input data a/h, L/a and ν, m, n, and the ring characteristics (b_R/a, d_R/a) can be handled with great ease and without any complication. It will be seen in a later section that the predicted frequency results of the present analysis very well agree with the test results. It must however be admitted that for the prediction of internal stress resultants in the shells, Forsberg's method would be more accurate than that of the present analyses.

5. CONCLUSIONS

A theoretical analysis for the free vibration of clamped-free and clamped-ring stiffened shells has been developed and implemented for digital computer solution. Flow charts of the programs are given in the Appendix [IV] . The computer used was an I.C.L. 1905. The analysis is capable of handling cylindrical shells of arbitrary length-to-radius ratio (L/a) and radius-to-thickness ratio (a/h). In the case of the stiffening ring it caters for such arbitrary ring characteristics as ring breadth (b_R) and ring depth (d_R) and their arbitrary positioning on the shell. Thus a range of shell geometries with or without stiffening rings of desired size may be handled with convenience. Due consideration has been given to such effects as:

(a) Choice of the appropriate shell equations of motion

(b) Choice of modal forms, influence of boundary conditions

(c) Rotary and inplane inertia effects

(d) Effect of zero hoop and shear strain

From the results of this study, the following conclusions appear to be valid.

1. Elementary beam vibration functions are satisfactory approximations to the longitudinal components of the mode shapes of cylindrical shells involving clamped free ends or clamped-ring stiffened ends.

2. The assumption of zero hoop and shear strain leads to considerable simplification in the analysis. In effect it lowers the degree of the frequency equation to be solved from cubic to linear or from sextic to quadratic depending on the upper end boundary condition. The influence on the frequency of this assumption is small for tall shells, but for short shells it can increase the frequencies considerably. Thus for engineering applications for tall shells such as chimneys this assumption may be made so as to avoid undue complexity in the analysis without introducing any significant error in the frequency.

3. For ring stiffened shells with a clamped base for modes involving swaying oscillations (n = 1), the ring stiffness has little influence on the frequency. The primary effect then is to add mass to the system and consequently to reduce the frequency of the shell. The eccentricity effects are also negligible for the swaying (n = 1) mode.

For modes involving higher number of circumferential waves there is a

significant effect of the ring stiffness and the ring eccentricity also has a profound influence on the frequency spectrum.

4. The ring rotary inertia, on the basis of the present study, appears to have negligible effect.

5. The contributions of the more exact Flügge shell theory show very little effect on the frequency spectrum for the shells considered in this report. In the author's opinion these minor refinements only increase the complexity of the analysis with negligible increase in the accuracy in the results as compared with the Timoshenko-Love theory.

6. Comparison with exact analysis shows that a few results of the present analysis are fractionally lower than exact results for the cases considered. The reason for this may be computational error incurred in evaluating the quantities involved e.g. the integrals involving characteristic beam functions etc. and overall computational error. Though, as one may see, the trend has not been for the worse. Also the exact analysis is not "exact" in the strictest sense of the term.

The above discrepancy is more marked in the results for the clamped-ring stiffened shell. The difference here may be attributed partly to the error in computation and partly to the difference in the structural idealisation of ring adopted in the two approaches. However, the problem remains unresolved and will be studied later.

REFERENCES

1. Forsberg, K. : Influence of Boundary Conditions on the Modal Characteristics of Thin Cylindrical shells. AIAAJ., Vol. 2, No. 12, Dec. 1964 pp. 2150-2157.
2. Weingarten, V.I. : Free Vibration of Thin Cylindrical Shells. AIAAJ., Vol.2, No. 4, April 1964 pp. 717-722.
3. Watkins, J.D. and Clary, R.L. : Vibration Characteristics of some Thin-Walled Cylindrical and Conical Frustum Shells. NASA TN D-2729, 1965.
4. Sewall, J.L. and Naumann, E.C. : An Experimental and Analytical Vibration study of Thin Cylindrical Shells with and without Longitudinal Stiffeners. NASA TN D-4705, 1968.
5. Flügge, Wilhelm : Stresses in Shells. Fourth printing, Springer-Verlag (Berlin), 1967.
6. Naghdi, M. : Foundations of Elastic Shell Theory, Progress in Solid Mechanics, Vol. IV, Ed. I.N. Sneddon and R. Hill. North Holland (Amsterdam) 1963.
7. Warburton, G.B. : Comments on "Vibration Studies of a Ring-Stiffened Circular Cylindrical Shell" J. Sound Vib. Vol. 9, No. 2, 1969 pp 349-352.
8. Warburton, G.B. : Contribution to discussion of "The Strain-Energy Expression for Thin Elastic Shells". J.Appl.Mech., Vol. 26, No. 2, June 1959 pp. 315.
9. Johns, D.J. and Allwood, R.J. : Vibration Studies of a Ring-Stiffened Circular Cylindrical Shell. J. Sound. Vib., Vol. 8, No.1, 1968, pp. 147-155.
10. Miller, P.R. : Free Vibrations of a Stiffened Cylindrical Shell. A.R.C. Technical Report, R. & M.N. No. 3154, HMSO (London), 1960.
11. Mikulas, M.M. Jr.,; McElman, J.A. : On Free Vibrations of Eccentrically Stiffened Cylindrical Shells and Flat Plates. NASA TN D-3010, 1965.
12. Parthan, S. and Johns, D.J. : Effects of In-plane and Rotary Inertia on the Frequencies of Eccentrically Stiffened Cylindrical Shells. AIAA Paper. New Orleans, April 1969.
13. Huffington, N.J. Jr. and Schumacher, R.N. : Flexure of Parallel Stiffened Plates. R R-59, Jan. 1965, Research Dept., Martin Co., Baltimore, Md.

14. Bishop, R.E.D., and Johnson, D.C. : The Mechanics of Vibration. Cambridge Univ.Press, 1960.

15. Johns, D.J. and Sharma, C.B. : The Structural Design of Self-supporting Steel Chimneys: Deduced from B.S. 4076 : 1966. Report T.T. 6915, Loughborough Univ. of Technology, 1969.

16. Hu, W.C.L., Gormley, J.F. and Lindholm U.S. : An Analytical and Experimental Study of Vibrations of Ring-Stiffened Cylindrical Shells. Technical Report No. 9, Southwest Research Institute, San Antonio, Texas (June 1967).

17. Egle, D.M. and Soder, K.E. Jr., : A Theoretical Analysis of the Free Vibration of Discretely Stiffened Cylindrical Shells with Arbitrary End Conditions. Final Report (Part I) NASA Research Grant NGR-37-003-035, School of Aerospace and Mechanical Engineering, University of Oklahoma, Norman, Oklahoma (August 1968).

18. Forsberg, K. : Exact Solution for Natural Frequencies of Ring Stiffened Cylinders, AIAA/ASME 10th Structures, Structural Dynamics and Material Conference, New Orleans, Louisiana / April 14-16, 1969.

APPENDIX I

This appendix contains pertinent details of the analysis carried out by Johns and Allwood in reference [9] The problem concerns an investigation of the vibration characteristics of a vertical, cantilevered shell, with its lower edge restrained against displacement and its upper edge supported on a stiff reinforcing ring (Fig. 3). The investigation was prompted by the recent collapse of such a shell in the form of a tall, slender chimney stack when subjected to a high, sustained lateral wind. The stack was observed to oscillate in an ovalling mode of large amplitude prior to collapse.

BASIC THEORY

Expression for the strain energy (U_s) and kinetic energy (T_s) in a thin uniform shell are given by Timoshenko-Love theory as:-

$$U_s = \int_0^{2\pi}\int_0^{L} \frac{E_s h}{2(1-\nu^2)} \left\{ u_{,x}^2 + \frac{1}{a^2}(v_{,\theta} + w)^2 + \right.$$

$$\tfrac{1}{2}(1-\nu)(v_{,x} + \frac{1}{a}u_{,\theta})^2 + \frac{h^2}{12}\left[w_{,xx}^2 + \frac{1}{a^4}(w_{,\theta\theta} - v_{,\theta})^2\right.$$

$$\left.\left. + \frac{2\nu}{a^2} w_{,xx}(w_{,\theta\theta} - v_{,\theta}) + \frac{2(1-\nu)}{a^2}(w_{,x\theta} - v_{,x})^2\right]\right\} a\,d\theta\,dx \qquad (I.1)$$

$$T_s = \int_0^{2\pi}\int_0^{L} \tfrac{1}{2}\rho_s h \left[\dot{u}^2 + \dot{v}^2 + \dot{w}^2\right] a\,d\theta\,dx \qquad (I.2)$$

where displacements u, v, w are denoted in Figure 3.

The corresponding equations for U_R and T_R, for a uniform, circular ring at any position $x = \ell$ along the above shell are

$$U_R = \int_0^{2\pi}\left[\frac{E_R A_R}{2a^2}(v_{,\theta} + w)_\ell^2 + \frac{E_R I_R}{2a^4}(w_{,\theta\theta} - v_{,\theta})_\ell^2\right] a\,d\theta \qquad (I.3)$$

$$T_R = \int_0^{2\pi} \frac{\rho_R A_R}{2}\left[\dot{u}^2 + \dot{v}^2 + \dot{w}^2\right]_\ell a\,d\theta \qquad (I.4)$$

In the analyses which follow it is assumed that any stiffening ring is symmetrically disposed about the mid-plane of the shell and no effects due to ring eccentricity are introduced.

Vibration of Shells Fully Clamped at One End and Ring Stiffened at the Other

It is shown that

(a) simplified eighth order equations in w of the Donnell type are not generally acceptable,

(b) the effects of axial constraints are important (ref. 1),

(c) the assumption (or not) of zero axial slope ($w_{,x} = 0$) at $x = 0$ will introduce little error;

(d) the assumption of zero hoop and shear strain for long shells can probably be justified, i.e. relations

$$\begin{aligned} v_{,\theta} + w &= 0 \\ v_{,x} + \frac{1}{a} u_{,\theta} &= 0 \end{aligned} \qquad (I.5)$$

may be assumed for tall shells, and these cause considerable simplification to eqns. (I.1) and (I.3).

Assuming the above results and for a radial mode of the type

$$w = C\ f(x) \cos n\theta \sin \omega t, \qquad (I.6)$$

the following expressions can be obtained, by using equations (I.5), for the axial and circumferential modes:

$$u = -\frac{Ca}{n^2} f'(x) \cos n\theta \sin \omega t \qquad (I.7)$$

$$v = -\frac{C}{n} f(x) \sin n\theta \sin \omega t \qquad (I.8)$$

Substitution (I.6 - I.8) into equations (I.1) and (I.2) yields the following expressions for the strain and kinetic energies of the shell:

$$U_s = \frac{E_s \pi L h^3 (1-n^2)^2}{24 (1-\nu^2) a^3} \left\{ \frac{e^4}{(1-n^2)^2} \left(\frac{12 a^2}{n^4 h^2} + 1 \right) X_1 + 2e^2 \frac{(1-\nu)}{n^2} X_2 + \frac{2e^2 \nu}{(1-n^2)} X_4 + X_3 \right\}; \qquad (I.9)$$

$$T_s = \omega^2 \pi \frac{\ell_s a h}{2} L \frac{(1+n^2)}{n^2} \left\{ \frac{e^2}{n^2(1+n^2)} X_2 + X_3 \right\} ; \qquad (I.10)$$

where

$$X_1 = \int_0^1 (f,_{\bar{x}\bar{x}})^2 \, d\bar{x}$$

$$X_2 = \int_0^1 (f,_{\bar{x}})^2 \, d\bar{x} ,$$

$$X_3 = \int_0^1 f^2 \, d\bar{x}$$

$$X_4 = \int_0^1 f. f,_{\bar{x}\bar{x}} \, d\bar{x} \quad \text{and} \quad \bar{x} = x/L , \quad e = a/L$$

The strain and kinetic energies of the ring, which is at the end of the shell corresponding to $\bar{x} = 1$, are given by the following expressions assuming that the centroid of the ring lies on the mid-plane of the shell:

$$U_R = \frac{E_R I_R \pi}{2 a^3} (1 - n^2)^2 \left[f_{\bar{x}} = 1 \right]^2 ; \qquad (I.11)$$

$$T_R = \frac{\omega^2 \pi \ell_R A_R a}{2} \left(\frac{1+n^2}{n^2} \right) \left[f_{\bar{x}} = 1 \right]^2 \qquad (I.12)$$

The function chosen for f (x) expressed in terms of $\bar{x} = x/L$ was

$$f = \bar{A} \bar{x}^2 (\bar{x} - 3) + \bar{B} \bar{x}^2 (\bar{x}^2 - 6) \qquad (I.13)$$

which satisfies the following boundary conditions:

$$x = 0 \, (\bar{x} = 0) \quad u = v = w = w,_x = v,_x = 0 ;$$

$$x = L \, (\bar{x} = 1) \quad u,_x = w,_{xx} = 0$$

These correspond to an encastre and axially-clamped base and approximately to zero axial stress and edge moment at the ring-stiffened end.

Forsberg [1] shows that for a shell supported at both ends the minimum natural frequency is always associated with an axial half-wave length equal to the length of the shell. The function given in equation (I.13) allows the half-wave length to take a value larger than the shell length.

The energies of the ring and shell given in equations (I.9 - I.12) have been evaluated for the function (I.13) yielding an expression for the natural frequency ω in terms of the constants $\bar{A}$ and $\bar{B}$. The values of the constants have been determined to give the minimum value of frequency ω and the result is given below in terms of α, where $\alpha = \bar{A} / \bar{B} + 2.5$;

$$\Delta = \frac{\beta\, n^2 (1-n^2)^2}{1+n^2} \left[1 + \frac{d_1 \alpha^2 + b_1 \alpha + c_1}{d_2 \alpha^2 + b_2 \alpha + c_2} \right] \qquad (I.14)$$

where $\beta = h^2/12a^2$, and

$$d_1 = 4(R - \bar{R}) + e^2(24q + 6s) + 12 e^4 p ,$$

$$b_1 = e^2(2q + 3s) ,$$

$$c_1 = \frac{3}{7} e^2 (q - s) + \frac{9}{5} e^4 p ;$$

$$d_2 = 4\bar{R} + \frac{33}{35} + \frac{24}{5} \frac{e^2}{n^2(1+n^2)} ,$$

$$b_2 = \frac{-17}{140} + \frac{2}{5} \frac{e^2}{n^2(1+n^2)} ,$$

$$c_2 = \frac{19}{2520} + \frac{3}{35} \frac{e^2}{n^2(1+n^2)} ,$$

where

$$e = a/L$$

$$R = \frac{12 E_R I_R (1-\nu^2)}{E_s L h^3} .$$

$$\bar{R} = \frac{\rho_R A_R}{\rho_s h L} ,$$

$$q = \frac{2(1-\nu)}{n^2} - \frac{1}{5n^2(1+n^2)} ,$$

$$s = \frac{2\nu}{5(1-n^2)} ,$$

$$p = \frac{1}{(1-n^2)^2} \left[\frac{12 a^2}{n^4 h^2} + 1 \right]$$

and α is obtained from the solution of quadratic

$$\alpha^2 (d_1 b_2 - b_1 d_2) + 2\alpha (d_1 c_2 - c_1 d_2) + (b_1 c_2 - c_1 b_2) = 0 \qquad \text{(I.15)}$$

In case of practical steel chimneys of L/a of 20 or more the radius-to-thickness ratio is commonly greater than 100 and the minimum frequency in ovalling is associated with n = 2. Chimneys have been observed ovalling in this mode when subject to steady wind conditions creating an exciting force by vortex shedding.

If a shell of these proportions has no stiffening, equation (I.14) simplifies to

$$\Delta = \left\{ 1 + 1.24\, e^2 (1 + 10\, e^2 p) \right\} \quad \beta \frac{n^2 (1-n^2)^2}{(1+n^2)} \qquad \text{(I.16)}$$

It may be seen that for values of the parameter $R/e^4 p$ greater than 200 the ring is sufficiently stiff to amount to a simple support and it may be shown generally that for this range of practical chimneys equation (I.14) then simplifies to

$$\Delta = \left\{ 1 + 240p \right\} \quad \beta \frac{n^2 (1-n^2)^2}{(1+n^2)} \qquad \text{(I.17)}$$

For very long shells eqns. I.14, I.16 and I.17 all yield

$$\Delta = \beta n^2 (n^2 - 1)^2 / (n^2 + 1) \qquad \text{(I.18)}$$

which is the well-known formula for 'ring' circumferential vibration modes.

APPENDIX II

Tables of Characteristic Functions Representing Normal Modes of Vibration of a Beam.

In the following are given characteristic functions of beam vibration which have been mainly used in the analyses. For each frequency there is a definite shape in which the beam will deflect while vibrating harmonically; this shape is called a normal mode of vibration of the beam. The mathematical expressions which define the normal modes are called characteristic functions.

The purpose of this appendix is to provide tables of the characteristic functions for the type of end conditions which are used in the analysis i.e. (a) clamped-free (b) clamped-supported. Such tables are needed in obtaining complete numerical solutions of the problem.

The detailed derivation, properties and numerical values of these characteristic functions are tabulated in the book by Bishop and Johnson [14] . Only the relevant data for these two types of boundary conditions will be presented in the following. It is shown in the above reference [14] that each of the functions for a given set of boundary conditions satisfies the differential equation

$$\frac{d^4 \phi_r}{dx^4} = p_r^4 \phi_r \quad \text{or} \quad \phi_r^{iv} = \phi_r \tag{II.1}$$

It is also shown that the set of characteristic functions $\phi_r(x)$, $(r = 1, 2, 3, \ldots)$ satisfy the so-called orthogonality relations, e.g.

$$\frac{I}{L} \int_0^L \phi_r(x)\, \phi_s(x)\, dx = \delta_{rs} \tag{II.2}$$

where δ_{rs} is Kronecker delta. Consequently the set of function is orthogonal in the interval $0 \leq x \leq L$

DATA FOR CLAMPED-FREE BEAM

Characteristic function and its derivatives

$$\phi_r(x) = \cosh p_r x - \cos p_r x - c_r (\sinh p_r x - \sin p_r x)$$

$$\frac{1}{p_r}\frac{d\phi_r}{dx} = \phi'_r(x) = \sinh p_r x + \sin p_r x - c_r (\cosh p_r x - \cos p_r x)$$

$$\frac{1}{p_r^2}\frac{d^2\phi_r}{dx^2} = \phi''_r(x) = \cosh p_r x + \cos p_r x - c_r (\sinh p_r x + \sin p_r x) \qquad \text{(II.3)}$$

$$\frac{1}{p_r^3}\frac{d^3\phi}{dx^3} = \phi'''_r(x) = \sinh p_r x - \sin p_r x - c_r (\cosh p_r x + \cos p_r x)$$

Boundary values

$$\phi_r(0) = \phi'_r(0) = 0$$

$$\phi''_r(L) = \phi'''_r(L) = 0$$

p_r and c_r are given by the transcendental equations

$$\cosh p_r L \cos p_r L + 1 = 0 \qquad \text{(II.4)}$$

$$c_r = \frac{\sinh p_r L - \sin p_r L}{\cosh p_r L + \cos p_r L} \qquad \text{(II.5)}$$

DATA FOR CLAMPED-SUPPORTED BEAM

Characteristic Functions and its derivatives

$$\psi_r(x) = \cosh q_r x - \cos q_r x - d_r (\sinh q_r x - \sin q_r x)$$

$$\frac{1}{q_r}\frac{d\psi_r}{dx} = \psi'_r(x) = \sinh q_r x + \sin q_r x - d_r (\cosh q_r x - \cos q_r x)$$

$$\frac{1}{q_r^2}\frac{d^2\psi_r}{dx^2} = \psi''_r(x) = \cosh q_r x + \cos q_r x - d_r (\sinh q_r x + \sin q_r x) \qquad \text{(II.6)}$$

$$\frac{1}{q_r^3}\frac{d^3\psi_r}{dx^3} = \psi'''_r(x) = \sinh q_r x - \sin q_r x - d_r (\cosh q_r x + \cos q_r x)$$

Boundary Values

$$\psi_r(0) = \psi'_r(0) = 0$$

$$\psi_r(L) = \psi''_r(L) = 0$$

q_r and d_r are given by the transcendental equations

$$\sin q_r L \cosh q_r L - \sinh q_r L \cos q_r L = 0 \qquad \text{(II.7)}$$

$$d_r = \cot q_r L = \coth q_r L \qquad \text{(II.8)}$$

Values of p_r, c_r and q_r, d_r

r	$p_r L$	c_r	$q_r L$	d_r
1	1.8751 041	0.7340 955	3.9266 023	1.0007 7730
2	4.6940 9113	1.0184 6644	7.0685 8275	1.0000 0144
3	7.8547 5743	0.9992 2450	10.2101 7613	1.0000 0000
4	10.9955 4074	1.0000 33553	13.3517 6878	1.0000 0000
5	14.1371 6839	0.9999 985501	16.4933 6143	1.0000 0000

For $r > 5$

$$p_r L \approx (2r - 1)\ \pi/2 \quad , \qquad q_r L \approx (4r + 1)\ \pi/4 \ ,$$
$$c_r \approx 1.0 \quad , \qquad d_r \approx 1.0$$

Characteristic functions and their first derivatives are tabulated in the Tables II.1 - II.5 for these two cases.

TABLE II.1

CHARACTERISTIC FUNCTIONS AND DERIVATIVES

First Mode

$\frac{x}{L}$	ϕ_1	$\phi'_1 = \frac{1}{p_1}\frac{d\phi_1}{dx}$	ψ_1	$\psi'_1 = \frac{1}{q_1}\frac{d\psi_1}{dx}$
0.00	0.00000	0.00000	0.00000	0.00000
0.02	0.00139	0.07397	0.00600	0.15089
0.04	0.00557	0.14588	0.02333	0.28944
0.06	0.01231	0.21572	0.05114	0.41566
0.08	0.02168	0.28350	0.08834	0.52955
0.10	0.03355	0.34921	0.13400	0.63116
0.12	0.04784	0.41286	0.18715	0.72055
0.14	0.06449	0.47446	0.24685	0.79778
0.16	0.08340	0.53400	0.31214	0.86296
0.18	0.10452	0.59148	0.38208	0.91623
0.20	0.12774	0.64692	0.45574	0.95776
0.22	0.15301	0.70031	0.53221	0.98775
0.24	0.18024	0.75167	0.61058	1.00643
0.26	0.20936	0.80100	0.68999	1.01410
0.28	0.24030	0.84832	0.76953	1.01105
0.30	0.27297	0.89364	0.84852	0.99764
0.32	0.30730	0.93696	0.92601	0.97427
0.34	0.34322	0.97831	1.00129	0.94137
0.36	0.38065	1.01771	1.07363	0.89940
0.38	0.41952	1.05516	1.14233	0.84886
0.40	0.45977	1.09070	1.20675	0.79029
0.42	0.50131	1.12435	1.26626	0.72427
0.44	0.54408	1.15612	1.32032	0.65138
0.46	0.58800	1.18606	1.36841	0.57226
0.48	0.63301	1.21418	1.41006	0.48755
0.50	0.67905	1.24052	1.44486	0.39794
0.52	0.72603	1.26512	1.47245	0.30410
0.54	0.77392	1.28801	1.49253	0.20675
0.56	0.82262	1.30924	1.50485	0.10661
0.58	0.87209	1.32884	1.50922	0.00440
0.60	0.92227	1.34685	1.50550	- 0.09915
0.62	0.97309	1.36334	1.49363	- 0.20332
0.64	1.02451	1.37834	1.47357	- 0.30736
0.66	1.07646	1.39191	1.44537	- 0.41057
0.68	1.12889	1.40410	1.40913	- 0.51224
0.70	1.18175	1.41497	1.36493	- 0.61167
0.72	1.23500	1.42459	1.31313	- 0.70820
0.74	1.28859	1.43302	1.25334	- 0.80117
0.76	1.34247	1.44032	1.18741	- 0.88996
0.78	1.39660	1.44656	1.11418	- 0.97400
0.80	1.45096	1.45182	1.03457	- 1.05270
0.82	1.50549	1.45617	0.94899	- 1.12556
0.84	1.56016	1.45968	0.85795	- 1.19210
0.86	1.61496	1.46245	0.76194	- 1.25187
0.88	1.66985	1.46455	0.66151	- 1.30448
0.90	1.72480	1.46607	0.55724	- 1.34960
0.92	1.77980	1.46710	0.44974	- 1.38693
0.94	1.83483	1.46773	0.33962	- 1.41621
0.96	1.88988	1.46805	0.22752	- 1.43727
0.98	1.94494	1.46817	0.11410	- 1.44996
1.00	2.00000	1.46819	0.00000	- 1.45420

TABLE II.2

CHARACTERISTIC FUNCTIONS AND DERIVATIVES

Second Mode

$\frac{x}{L}$	ϕ_2	$\phi'_2 = \frac{1}{p_2}\frac{d\phi_2}{dx}$	ψ_2	$\psi'_2 = \frac{1}{q_2}\frac{d\psi_2}{dx}$
0.00	0.00000	0.00000	0.00000	0.00000
0.02	0.00853	0.17879	0.01904	0.26276
0.04	0.03301	0.33962	0.07241	0.48557
0.06	0.07174	0.48253	0.15446	0.66857
0.08	0.12305	0.60754	0.25958	0.81207
0.10	0.18526	0.71475	0.38223	0.91666
0.12	0.25670	0.80428	0.51697	0.98325
0.14	0.33573	0.87631	0.65851	1.01310
0.16	0.42070	0.93108	0.80176	1.00789
0.18	0.51002	0.96892	0.94192	0.96966
0.20	0.60211	0.99020	1.07449	0.90088
0.22	0.69544	0.99539	1.19534	0.80411
0.24	0.78852	0.98502	1.30078	0.68345
0.26	0.87992	0.95970	1.38759	0.54152
0.28	0.96827	0.92013	1.45308	0.38242
0.30	1.05227	0.86707	1.49510	0.21017
0.32	1.13068	0.80136	1.51208	0.02894
0.34	1.20236	0.72389	1.50305	- 0.15704
0.36	1.26626	0.63565	1.46765	- 0.34350
0.38	1.32141	0.53764	1.40611	- 0.52625
0.40	1.36694	0.43094	1.31923	- 0.70122
0.42	1.40209	0.31665	1.20839	- 0.86456
0.44	1.42619	0.19593	1.07550	- 1.01270
0.46	1.43871	0.06995	0.92292	- 1.14243
0.48	1.43920	- 0.06012	0.75348	- 1.25090
0.50	1.42733	- 0.19307	0.57035	- 1.33577
0.52	1.40289	- 0.32772	0.37700	- 1.39515
0.54	1.36578	- 0.46291	0.17715	- 1.42770
0.56	1.31600	- 0.59748	- 0.02536	- 1.43265
0.58	1.25365	- 0.73034	- 0.22661	- 1.40978
0.60	1.17895	- 0.86040	- 0.42268	- 1.35944
0.62	1.09222	- 0.98667	- 0.60973	- 1.28256
0.64	0.99384	- 1.10821	- 0.78413	- 1.18058
0.66	0.88431	- 1.22416	- 0.94244	- 1.05549
0.68	0.76419	- 1.33373	- 1.08158	- 0.90972
0.70	0.63410	- 1.43624	- 1.19882	- 0.74612
0.72	0.49475	- 1.53113	- 1.29186	- 0.56793
0.74	0.34687	- 1.61791	- 1.35888	- 0.37866
0.76	0.19123	- 1.69625	- 1.39858	- 0.18205
0.78	0.02865	- 1.76592	- 1.41019	0.01800
0.80	- 0.14007	- 1.82682	- 1.39351	0.21752
0.82	- 0.31409	- 1.87901	- 1.34890	0.41256
0.84	- 0.49261	- 1.92267	- 1.27726	0.59923
0.86	- 0.67484	- 1.95814	- 1.18004	0.77383
0.88	- 0.86004	- 1.98590	- 1.05919	0.93283
0.90	- 1.04750	- 2.00658	- 0.91715	1.07323
0.92	- 1.23660	- 2.02097	- 0.75676	1.19208
0.94	- 1.42680	- 2.03002	- 0.58122	1.28706
0.96	- 1.61764	- 2.03483	- 0.39406	1.35629
0.98	- 1.80877	- 2.03666	- 0.19902	1.39839
1.00	- 2.00000	- 2.03693	0.00000	1.41251

TABLE II.3

CHARACTERISTIC FUNCTIONS AND DERIVATIVES

Third Mode

$\frac{x}{L}$	ϕ_3	$\phi'_3 = \frac{1}{p_3}\frac{d\phi_3}{dx}$	ψ_3	$\psi'_3 = \frac{1}{q_3}\frac{d\psi_3}{dx}$
0.00	0.00000	0.00000	0.00000	0.00000
0.02	0.02339	0.28953	0.03886	0.36672
0.04	0.08839	0.52979	0.14410	0.65020
0.06	0.18727	0.72099	0.29879	0.85122
0.08	0.31238	0.86367	0.48626	0.97168
0.10	0.45614	0.95879	0.69037	1.01491
0.12	0.61120	1.00785	0.89584	0.98593
0.14	0.77049	1.01291	1.08857	0.89148
0.16	0.92728	0.97665	1.25604	0.74002
0.18	1.07535	0.90237	1.38759	0.54152
0.20	1.20901	0.79394	1.47476	0.30725
0.22	1.32324	0.65580	1.51147	0.04939
0.24	1.41376	0.49285	1.49419	- 0.21934
0.26	1.47707	0.31040	1.42202	- 0.48616
0.28	1.51056	0.11405	1.29662	- 0.73864
0.30	1.51248	- 0.09041	1.12212	- 0.96520
0.32	1.48203	- 0.29711	0.90489	- 1.15556
0.34	1.41931	- 0.50026	0.65324	- 1.30107
0.36	1.32534	- 0.69422	0.37703	- 1.39512
0.38	1.20196	- 0.87368	0.08727	- 1.43330
0.40	1.05185	- 1.03374	- 0.20439	- 1.41364
0.42	0.87841	- 1.17003	- 0.48616	- 1.33665
0.44	0.68568	- 1.27881	- 0.74658	- 1.20525
0.46	0.47822	- 1.35704	- 0.97504	- 1.02471
0.48	0.26103	- 1.40747	- 1.16223	- 0.80234
0.50	0.03937	- 1.41366	- 1.30050	- 0.54726
0.52	- 0.18130	- 1.39004	- 1.38422	- 0.26994
0.54	- 0.39555	- 1.33188	- 1.41001	0.01818
0.56	- 0.59802	- 1.24030	- 1.37687	0.30522
0.58	- 0.78359	- 1.11723	- 1.28624	0.57929
0.60	- 0.94753	- 0.96533	- 1.14194	0.82907
0.62	- 1.08556	- 0.78797	- 0.95000	1.04422
0.64	- 1.19398	- 0.58908	- 0.71844	1.21582
0.66	- 1.26974	- 0.37310	- 0.45691	1.33678
0.68	- 1.31055	- 0.14479	- 0.17628	1.40210
0.70	- 1.31485	0.09085	0.11174	1.40906
0.72	- 1.28189	0.32872	0.39519	1.35742
0.74	- 1.21172	0.56380	0.66227	1.24931
0.76	- 1.10515	0.79124	0.90189	1.08924
0.78	- 0.96375	1.00656	1.10404	0.88387
0.80	- 0.78975	1.20575	1.26035	0.64175
0.82	- 0.58594	1.38540	1.36432	0.37294
0.84	- 0.35563	1.54236	1.41160	0.08860
0.86	- 0.10245	1.67629	1.40025	- 0.19943
0.88	0.16974	1.78480	1.33072	- 0.47918
0.90	0.45702	1.86854	1.20590	- 0.73004
0.92	0.75558	1.92871	1.03099	- 0.96820
0.94	1.06189	1.96766	0.81303	- 1.15713
0.96	1.37287	1.98892	0.56168	- 1.29798
0.98	1.68610	1.99721	0.28680	- 1.38490
1.00	2.00000	1.99845	0.00000	- 1.41429

TABLE II.4

CHARACTERISTIC FUNCTIONS AND DERIVATIVES

Fourth Mode

$\frac{x}{L}$	ϕ_4	$\phi_4' = \frac{1}{p_4}\frac{d\phi_4}{dx}$	ψ_4	$\psi_4' = \frac{1}{q_4}\frac{d\psi_4}{dx}$
0.00	0.00000	0.00000	0.00000	0.00000
0.02	0.04482	0.39147	0.06496	0.46278
0.04	0.16510	0.68645	0.23451	0.78357
0.06	0.33974	0.88606	0.47104	0.96521
0.08	0.54801	0.99298	0.73820	1.01441
0.10	0.77002	1.01194	1.00204	0.94270
0.12	0.98714	0.94994	1.23237	0.76664
0.14	1.18256	0.81633	1.40407	0.50751
0.16	1.34177	0.62264	1.49825	0.19041
0.18	1.45299	0.38230	1.50306	- 0.15704
0.20	1.50758	0.11017	1.41422	- 0.50624
0.22	1.50027	- 0.17801	1.23502	- 0.82944
0.24	1.42928	- 0.46624	0.97582	- 1.10140
0.26	1.29634	- 0.73895	0.65324	- 1.30107
0.28	1.10643	- 0.98164	0.28879	- 1.41295
0.30	0.86774	- 1.18154	- 0.09274	- 1.42807
0.32	0.59073	- 1.32813	- 0.46510	- 1.34455
0.34	0.28808	- 1.41368	- 0.80250	- 1.16772
0.36	- 0.02621	- 1.43351	- 1.08150	- 0.90963
0.38	- 0.33748	- 1.38622	- 1.28266	- 0.58823
0.40	- 0.63112	- 1.27376	- 1.39201	- 0.22602
0.42	- 0.89330	- 1.10126	- 1.40200	0.15152
0.44	- 1.11166	- 0.87643	- 1.31209	0.51780
0.46	- 1.27592	- 0.61115	- 1.12877	0.84697
0.48	- 1.37836	- 0.31690	- 0.86513	1.11580
0.50	- 1.41424	- 0.00819	- 0.53994	1.30530
0.52	- 1.38199	0.30012	- 0.17628	1.40210
0.54	- 1.28336	0.59316	0.20000	1.39937
0.56	- 1.12327	0.85675	0.56222	1.29734
0.58	- 0.90964	1.07812	0.88466	1.10326
0.60	- 0.65299	1.24643	1.14445	0.83092
0.62	- 0.36594	1.35339	1.32317	0.49963
0.64	- 0.06264	1.39357	1.40813	0.13289
0.66	0.24191	1.36469	1.39330	- 0.24329
0.68	0.53258	1.26772	1.27973	- 0.60226
0.70	0.79478	1.10676	1.07546	- 0.91854
0.72	1.01518	0.88888	0.79497	- 1.16974
0.74	1.18226	0.62370	0.45814	- 1.33802
0.76	1.28688	0.32290	0.08884	- 1.41146
0.78	1.32262	- 0.00039	- 0.28676	- 1.38486
0.80	1.29608	- 0.33228	- 0.64202	- 1.26010
0.82	1.17687	- 0.65890	- 0.95176	- 1.04602
0.84	0.99762	- 0.96717	- 1.19405	- 0.75779
0.86	0.75368	- 1.24552	- 1.35168	- 0.41585
0.88	0.45270	- 1.48463	- 1.41351	- 0.04443
0.90	0.10407	- 1.67809	- 1.37513	0.33014
0.92	- 0.28179	- 1.82294	- 1.23928	0.68130
0.94	- 0.69409	- 1.92012	- 1.01558	0.98416
0.96	- 1.12317	- 1.97482	- 0.71989	1.21727
0.98	- 1.56035	- 1.99672	- 0.37317	1.36409
1.00	- 2.00000	- 2.00007	0.00000	1.41421

TABLE II.5

CHARACTERISTIC FUNCTIONS AND DERIVATIVES

Fifth Mode

$\frac{x}{L}$	ϕ_5	$\phi'_5 = \frac{1}{p_5}\frac{d\phi_5}{dx}$	ψ_5	$\psi'_5 = \frac{1}{q_5}\frac{d\psi_5}{dx}$
0.00	0.00000	0.00000	0.00000	0.00000
0.02	0.07241	0.48557	0.09685	0.55098
0.04	0.25958	0.81207	0.33974	0.88607
0.06	0.51697	0.98325	0.65851	1.01311
0.08	0.80177	1.00789	0.98717	0.95000
0.10	1.07449	0.90089	1.26755	0.72628
0.12	1.30078	0.68346	1.45308	0.38243
0.14	1.45309	0.38243	1.51700	- 0.03274
0.16	1.51709	0.02895	1.42950	- 0.46599
0.18	1.46767	- 0.34348	1.20840	- 0.86454
0.20	1.31925	- 0.70119	0.86819	- 1.18105
0.22	1.07553	- 1.01267	0.44239	- 1.37825
0.24	0.75353	- 1.25086	- 0.02533	- 1.43261
0.26	0.37706	- 1.39509	- 0.48616	- 1.33665
0.28	- 0.02529	- 1.43257	- 0.89158	- 1.09954
0.30	- 0.42257	- 1.35934	- 1.19872	- 0.74602
0.32	- 0.78399	- 1.18045	- 1.37505	- 0.31360
0.34	- 1.08140	- 0.90954	- 1.40200	0.15152
0.36	- 1.29162	- 0.56770	- 1.27698	0.59950
0.38	- 1.39826	- 0.18174	- 1.01369	0.98227
0.40	- 1.39310	0.21794	- 0.64067	1.25871
0.42	- 1.27670	0.59978	- 0.09828	1.39912
0.44	- 1.05846	0.93361	0.26570	1.38846
0.46	- 0.75579	1.19304	0.70119	1.22792
0.48	- 0.39273	1.35757	1.06118	0.93487
0.50	0.00170	1.41421	1.30682	0.54093
0.52	0.39632	1.35855	1.41161	0.08861
0.54	0.75976	1.19508	1.36423	- 0.37331
0.56	1.06317	0.93686	1.16977	- 0.79500
0.58	1.28253	0.60450	0.84919	- 1.13100
0.60	1.40051	0.22452	0.43706	- 1.34505
0.62	1.40786	- 0.17276	- 0.02218	- 1.41408
0.64	1.30418	- 0.55561	- 0.47902	- 1.33063
0.66	1.09793	- 0.89337	- 0.88421	- 1.10371
0.68	0.80582	- 1.15889	- 1.19405	- 0.75779
0.70	0.45146	- 1.33065	- 1.37513	- 0.33015
0.72	0.06355	- 1.39446	- 1.40793	0.13308
0.74	- 0.32634	- 1.34448	- 1.28892	0.58196
0.76	- 0.68626	- 1.18368	- 1.03091	0.96809
0.78	- 0.98631	- 0.92352	- 0.66175	1.24983
0.80	- 1.20090	- 0.58289	- 0.22123	1.39680
0.82	- 1.31066	- 0.18651	0.24314	1.39315
0.84	- 1.30378	0.23723	0.68130	1.23928
0.86	- 1.17672	0.65878	1.04600	0.95178
0.88	- 0.93411	1.05011	1.29790	0.56165
0.90	- 0.58801	1.38736	1.40985	0.11096
0.92	- 0.15633	1.65332	1.36978	- 0.35170
0.94	0.33937	1.83959	1.18201	- 0.77644
0.96	0.87658	1.94824	0.86678	- 1.11745
0.98	1.43502	1.99300	0.45809	- 1.33797
1.00	2.00000	2.00000	0.00000	- 1.41421

APPENDIX III

In applying the Rayleigh-Ritz method it becomes necessary to evaluate integrals containing the characteristic beam functions and their derivatives. This appendix gives the analytical expressions for the integrals, I_1, I_2, I_3, I_4, I_5, I_6 (equation (37)) encountered in the analysis. The orthogonality properties of characteristic beam functions and other properties of the parameters involved in these functions given in Appendix II have been used to arrive at the following expressions:

$$I_1 = \frac{1}{L}\int_o^L p_r^2 \left\{\int \phi_r(x)\,dx\right\}^2 dx$$

$$= \frac{1}{4p_rL}\Big[(1+c_r^2)\sinh 2p_rL - (1-c_r^2)\sin 2p_rL - 2c_r(\cosh 2p_rL + \cos 2p_rL) + 4c_r(p_rLc_r+5) + 4(1+c_r^2)\sinh p_rL\cos p_rL - 4(1-c_r^2)\cosh p_rL\sin p_rL\Big] \quad \text{(III.1)}$$

$$I_2 = \frac{1}{L}\int_o^L \left\{\phi_r'(x)\right\}^2 dx$$

$$= \frac{1}{4p_rL}\Big[(1+c_r^2)\sinh 2p_rL - (1-c_r^2)\sin 2p_rL - 2c_r(\cosh 2p_rL + \cos 2p_rL) + 4c_r(p_rLc_r-3) + 4(1-c_r^2)\cosh p_rL\sin p_rL - 4(1+c_r^2)\sinh p_rL\cos p_rL\Big] \quad \text{(III.2)}$$

$$I_3 = \frac{1}{L}\int_o^L q_r^2 \left\{\int \psi_r(x)\,dx\right\}^2 dx$$

$$= \frac{1}{4q_rL}\Big[(1+d_r^2)\sinh 2q_rL - (1-d_r^2)\sin 2q_rL - 2d_r(\cosh 2q_rL + \cos 2q_rL) + 4d_r(q_rLd_r+3)\Big] \quad \text{(III.3)}$$

$$I_4 = \frac{1}{L} \int_0^L \left\{ \psi'_r(x) \right\}^2 dx$$

$$= \frac{1}{4q_rL} \left[(1 + d_r^2) \sinh 2q_rL - (1 - d_r^2) \sin 2q_rL \right.$$

$$\left. - 2d_r (\cosh 2q_rL + \cos 2q_rL) + 4d_r (q_rL d_r - 1) \right] \qquad \text{(III.4)}$$

$$I_5 = \frac{1}{L} \int_0^L \phi_r(x) \psi_r(x) dx$$

$$= \frac{1}{L} \left[\tfrac{1}{2} \frac{1 + c_r d_r}{p_r + q_r} \sinh (p_r + q_r) L + \tfrac{1}{2} \frac{1 - c_r d_r}{p_r - q_r} \sinh (p_r - q_r) L \right.$$

$$- \frac{q_r + p_r c_r d_r}{p_r^2 + q_r^2} \cosh p_r L \sin q_r L - \frac{p_r - q_r c_r d_r}{p_r^2 + q_r^2} \sinh p_r L \cos q_r L$$

$$- \frac{p_r + q_r c_r d_r}{p_r^2 + q_r^2} \cosh q_r L \sin p_r L - \frac{q_r - p_r c_r d_r}{p_r^2 + q_r^2} \sin q_r L \cos p_r L$$

$$+ \tfrac{1}{2} \frac{1 - c_r d_r}{p_r + q_r} \sin (p_r + q_r) L + \tfrac{1}{2} \frac{1 + c_r d_r}{p_r - q_r} \sin (p_r - q_r) L$$

$$- \tfrac{1}{2} \frac{c_r + d_r}{p_r + q_r} \cosh (p_r + q_r) L - \tfrac{1}{2} \frac{c_r - d_r}{p_r - q_r} \cosh (p_r - q_r) L$$

$$+ \frac{q_r c_r + p_r d_r}{p_r^2 + q_r^2} \sin p_r L \sinh q_r L - \frac{p_r c_r - q_r d_r}{p_r^2 + q_r^2} (\cosh q_r L \cos p_r L - 1)$$

$$+ \frac{q_r c_r + p_r d_r}{p_r^2 + q_r^2} \sinh p_r L \sin q_r L + \frac{p_r c_r - q_r d_r}{p_r^2 + q_r^2} (\cosh p_r L \cos q_r L - 1)$$

$$\left. + \tfrac{1}{2} \frac{c_r + d_r}{p_r + q_r} \cos (p_r + q_r) L + \tfrac{1}{2} \frac{c_r - d_r}{p_r - q_r} \cos (p_r - q_r) L \right] \qquad \text{(III.5)}$$

$$I_6 = \frac{1}{L}\int_0^L \left[\left\{p_r \int \phi_r(x)\,dx\right\}\left\{q_r \int \psi_r(x)\,dx\right\}\right] dx$$

$$= \frac{1}{L}\left[\tfrac{1}{2}\,\frac{1+c_r d_r}{p_r+q_r}\sinh(p_r+q_r)L - \tfrac{1}{2}\,\frac{1-c_r d_r}{p_r-q_r}\sinh(p_r-q_r)L\right.$$

$$+ \frac{q_r+p_r c_r}{p_r^2+q_r^2}\sinh p_r L\cos q_r L - \frac{p_r-q_r d_r}{p_r^2+q_r^2}\cosh p_r L\sin q_r L$$

$$- \frac{q_r-p_r c_r d_r}{p_r^2+q_r^2}\cosh p_r L\sin p_r L + \frac{p_r+q_r c_r d_r}{p_r^2+q_r^2}\sinh q_r L\cos p_r L$$

$$+ \tfrac{1}{2}\,\frac{1+c_r d_r}{p_r-q_r}\sin(p_r-q_r)L - \tfrac{1}{2}\,\frac{1-c_r d_r}{p_r+q_r}\sin(p_r+q_r)L$$

$$- \tfrac{1}{2}\,\frac{c_r+d_r}{p_r+q_r}\cosh(p_r+q_r)L + \tfrac{1}{2}\,\frac{c_r-d_r}{p_r-q_r}\cosh(p_r-q_r)L$$

$$- \frac{p_r c_r - q_r d_r}{p_r^2+q_r^2}\sin p_r L\sinh q_r L - \frac{q_r c_r + p_r d_r}{p_r^2+q_r^2}(\cosh q_r L\cos p_r L - 1)$$

$$+ \frac{p_r c_r - q_r d_r}{p_r^2+q_r^2}\sinh p_r L\sin q_r L - \frac{q_r c_r + p_r d_r}{p_r^2+q_r^2}(\cosh p_r L\cos q_r L - 1)$$

$$- \tfrac{1}{2}\,\frac{c_r+d_r}{p_r+q_r}\cos(p_r+q_r)L + \tfrac{1}{2}\,\frac{c_r-d_r}{p_r-q_r}\cos(p_r-q_r)L$$

$$\left. - \frac{2(q_r c_r - p_r d_r)}{p_r^2-q_r^2}\right] \qquad \text{(III.6)}$$

APPENDIX IV

FLOW CHART OF MAIN COMPUTER PROGRAMME

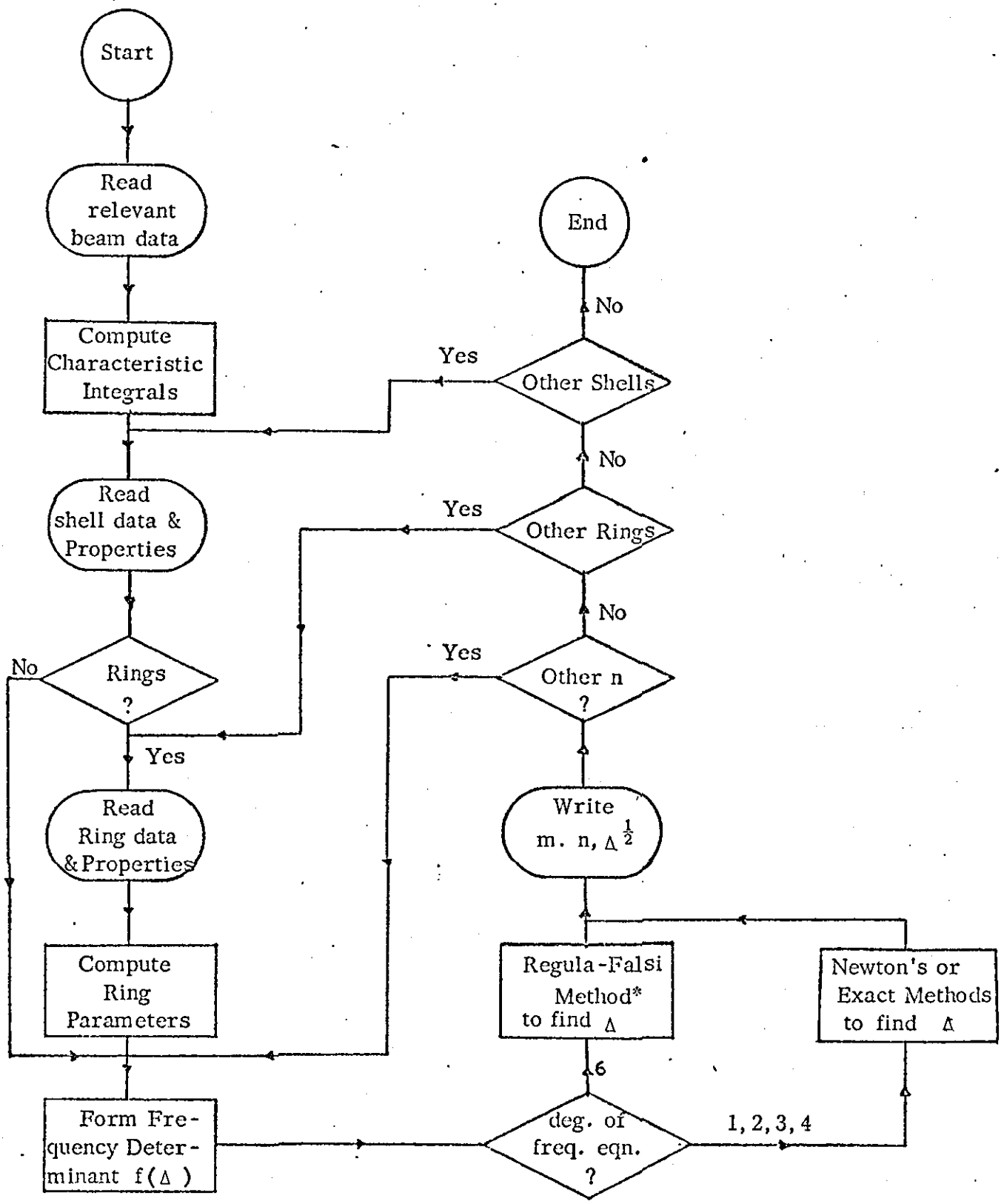

* Flow Chart for Regula-Falsi Method is given on following page.

FLOW CHART FOR REGULA-FALSI ITERATION PROCEDURE

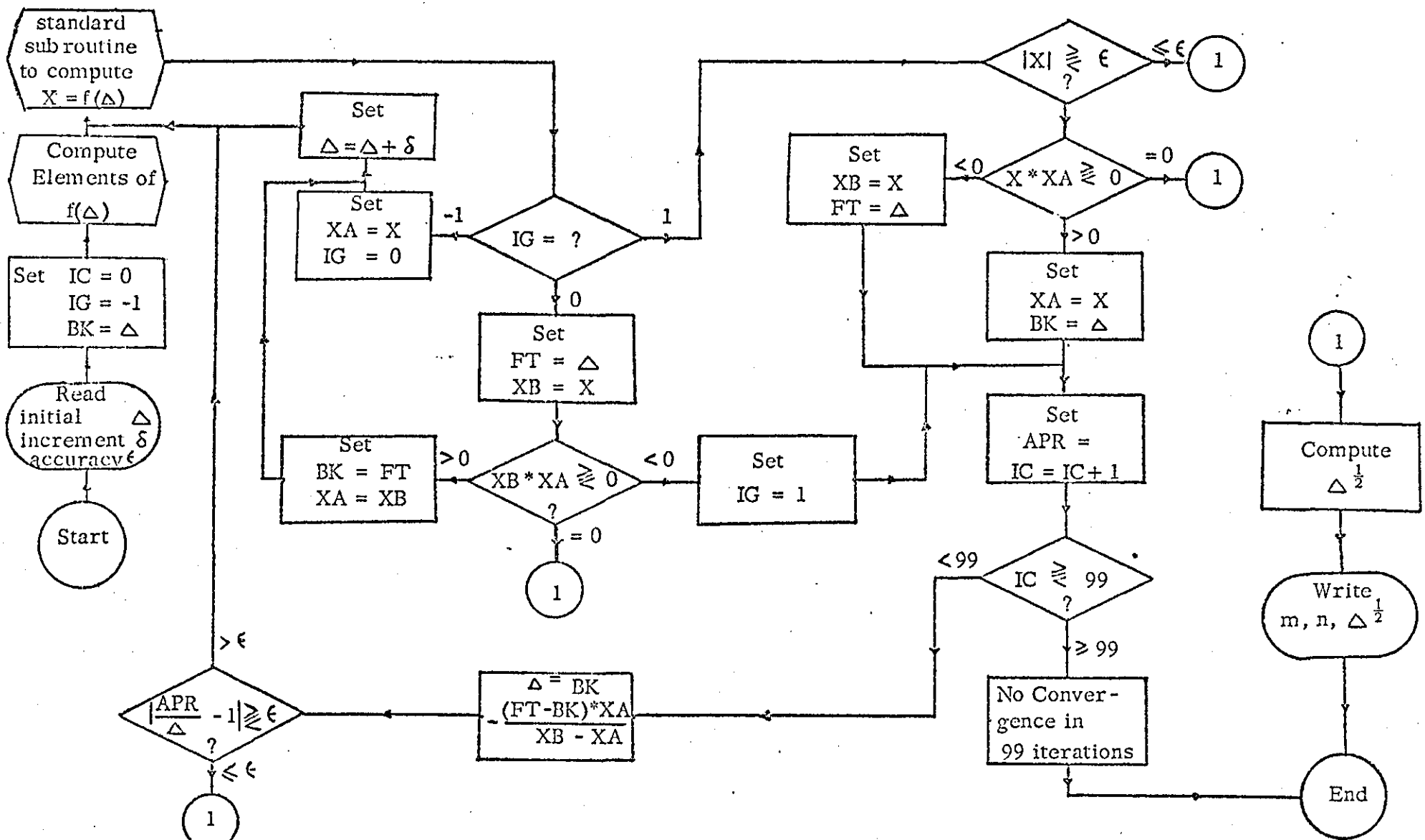

APPENDIX V

EXACT ANALYSIS FOR VIBRATION CHARACTERISTICS OF CIRCULAR CYLINDRICAL SHELLS.

Following is the brief account of the exact analysis used by Forsberg [18] for solution of natural frequencies of ring-stiffened cylindrical shells.

GENERAL COMMENTS - An analysis of the modal characteristics of a tandem series of cylinders has been developed. Each of the component cylinders is assumed to have the same mean radius a, but each may be of different length, have a different thickness and may be made of a different material. Rings may be located at each of the juncture points between cylinders as well as at both ends of the tandem series. Each of these rings is assumed to have its own set of axially-symmetric section properties and may be eccentrically attached to the cylinder in the sense that the radius of the cylinder need not be equal to the radius of the centroid of the ring cross-section. Additionally, all rings must have a "compact cross-section" in which the shear centre and the centroid coincide and the product of inertia vanishes.

EQUATIONS OF MOTION FOR SHELLS WITHOUT RINGS

Consider a tandem series of cylinders joined directly (without rings at the junctions). For each cylinder the general solution for modal vibration can be written in the form

$$\begin{Bmatrix} u \\ v \\ w \end{Bmatrix} = \sum_{s=1}^{8} e^{\lambda_{sn} x} \begin{Bmatrix} A_{sn} \cos n\theta \\ B_{sn} \sin n\theta \\ C_{sn} \cos n\theta \end{Bmatrix} e^{i\omega_n t} \qquad (V.1)$$

For modal motion it can be shown that each cylinder in the tandem series of shells must have the same circumferential wave number n. The equation used to describe the motion of the cylindrical shell segments are those given by Flügge. These equations have constant coefficients and are of the form

$$\left[L_{ij}\right] \quad \left[\phi_j\right] \quad = \quad \frac{a^2 \rho_s (1-\nu^2)}{E_s} \quad \frac{\partial^2}{\partial t^2} \quad \left[\phi_j\right] \qquad (V.2)$$

where ϕ_j are midsurface displacement components u, v, w and L_{ij} represent linear differential operators in x and θ. Substitution of expressions (V.1) into the equations of motion (V.2) yields k matrix equations (one for each cylinder) of the form

$$\left[a_{ij}\right] \begin{bmatrix} \alpha_{sn} \\ \beta_{sn} \\ 1 \end{bmatrix} = 0 \qquad (V.3)$$

where

$$\alpha_{sn} = A_{sn} / C_{sn} \quad \text{and} \quad \beta_{sn} = B_{sn} / C_{sn} \qquad (V.4)$$

The elements a_{ij} of the k^{th} matrix are functions of the circumferential wave number, n, frequency, ω, and the elastic and geometric parameters of the k^{th} cylinder. The solution to each of (V.3) will be non-trivial only if the determinant of the coefficients vanishes (i.e., $\left| a_{ij} \right| = 0$). For each component cylinder this condition leads to an eighth-order polynomial equation in λ_{sn}:

$$\lambda_{sn}^8 + g_{sn}^{(6)} \lambda_{sn}^6 + g_{sn}^{(4)} \lambda_{sn}^4 + g_{sn}^{(2)} \lambda_{sn}^2 + g_{sn}^{(0)} = 0 \qquad (V.5)$$

The roots provide the permissible values of λ_{sn} to be used in (V.1) and once they are determined one can return to (V.3) and obtain α_{sn} and β_{sn}. The 8k complex constants C_{sn} are evaluated by solving a system of 8k equations, of which 8(k-1) represent compatibility of displacements, forces, and moments between adjoining cylinders. The remaining 8 equations arise from 4 specified boundary conditions at each end of the overall shell.

There are sixteen possible sets of homogeneous boundary conditions which can be specified independently at each end of the shell.

These consist of all combinations of the following:

$$w = 0 \quad \text{or} \quad S_x = Q_x + (1/a)\ \partial M_{x\theta} / \partial\theta = 0 \tag{V.6a}$$

$$\partial w/\partial x = 0 \quad \text{or} \quad M_x = 0 \tag{V.6b}$$

$$u = 0 \quad \text{or} \quad N_x = 0 \tag{V.6c}$$

$$v = 0 \quad \text{or} \quad T_x = N_{x\theta} - (1/a)\ M_{x\theta} = 0 \tag{V.6d}$$

The detailed statement of these compatibilities and boundary conditions leads directly to the matrix:

$$\begin{array}{c} \begin{matrix} \text{1st cyl} & \text{2nd cyl} & & \text{kth cyl} \end{matrix} \\ \begin{bmatrix} [4 \times 8] & 0 & & \\ [8 \times 8] & [8 \times 8] & & \\ 0 & [8 \times 8] & & \\ & & [8 \times 8] \quad 0 & \\ & & [8 \times 8] \quad [8 \times 8] & \\ & & 0 \quad\ [4 \times 8] & \end{bmatrix} \end{array} \begin{bmatrix} C_{1n} \\ C_{2n} \\ \\ \\ \\ C_{8kn} \end{bmatrix} = 0 \tag{V.7}$$

For a non-trivial solution, the determinant of the coefficients must vanish. Since λ_{sn} in equation (V.1) depends upon the eigenvalues ω of the determinant, it is not possible to express the equation in a standard form (e.g. $(A - \omega^2 B)\ Y = 0$). Thus, at this point in the analysis a numerical evaluation of the solution is introduced. Although a numerical solution is required to find the eigenvalues, the solution is exact in the same sense that a numerical solution of the transcendental frequency equation for a beam yields an exact solution.

One now selects a specified set of shell geometries, as assumed number of circumferential waves n, and a specified set of boundary conditions at each end. An iteration scheme is then used to find the eigenvalues. The determinant is evaluated for successive values of the frequency until there is a change in its sign, indicating that a zero has been bracketed between two successive frequency estimates. Regula-falsi is employed to locate the eigenvalue to some preselected accuracy. This method has been used to

compute eigenvalues which are less than .1% apart. After the eigenvalue is determined the eigenvector is computed. The eigenvector is then substituted into the equation system to check that the equations are satisfied to the desired accuracy. If the eigenvectors do not check, computation is terminated.

EQUATIONS OF MOTION OF THE RING

The equation of motion for the rings can be written in terms of four displacement quantities: w_R, v_R, u_R and β_R. The eccentricity and the finite width, b_R, of the ring are included in the analysis.

When two cylindrical shells are joined by a ring, the forces and moments between the shells can be replaced by an equivalent force couple system acting together with the ring inertia forces at the centroid of the ring cross section.

The displacements of the ring centroid and rotation of the ring cross-section can be related to the displacements at the ends of the adjoining shells by kinematic considerations. When the effect of the warping of the ring cross-section due to torsion is ignored, the cross-section rotates as a rigid body through the angle β_R.

When the ring centroid displacements are expressed in terms of shell displacements, the force and moment compatibility relations for shell-ring-shell junction can be written in terms of the shell displacements at this junction. Detailed analysis and explicit expression can be found in reference [18] .

It is seen that if the rings are present at a junction between two cylinders, the elements of matrix of equation (V.7) become more involved, but the size of the matrix is not expanded.

A comparison of the frequencies as computed by the variational technique and exact approach is given in section 4 (pp. 32-36).

TABLE 1

EFFECT OF ZERO HOOP AND SHEAR STRAIN ON FREQUENCY OF A CLAMPED-FREE SHELL

(m = 1; n = 2) WITH VARIOUS MODES

LENGTH = 150 ft., RADIUS = 5 ft., THICKNESS = 5/16 in. a/h = 192

L/a = 30

YOUNGS MODULUS = 30×10^6 p.s.i.

DENSITY = 7.37×10^{-4} lb. - sec^2, POISSON'S RATIO = .3

FREQUENCY	With hoop and shear strain		Zero hoop and shear strain			
			Reduced from cubic & sextic		Other mode shapes	
	Cubic (32)*	Sextic (36)*	Linear (33)*	Quadratic (40)*	Quadratic (I.15, I.14)*	Quartic (31)*
$\Delta \frac{1}{2} \times 10^2$	.41179791	.41101781	.41329154	.41328979	.41447447	.42488354
$\omega / 2\pi$ (Hertz)	2.3103	2.3059	2.3187	2.3186	2.3253	2.3837

* Refer to the number of equations in the text.

TABLE 2. FREQUENCY PARAMETER $\Delta^{\frac{1}{2}}$ ($\times 10^2$) FOR CLAMPED-FREE SHELLS

SF : Sextic (Flügge Theory), CF : Cubic (Flügge Theory)

Length -to- radius ratio L/a		Radius-to-thickness ratio a/h											
		50		100		150		200		250		300	
		n = 1	n = 2	n = 1	n = 2	n = 1	n = 2	n = 1	n = 2	n = 1	n = 2	n = 1	n = 2
10	SF	2.0835	1.7081	2.0834	1.0351	2.0834	.8540	2.0834	.7808	2.0834	.7445	2.0834	.7240
	CF	2.2042	1.7226	2.2041	1.0619	2.2041	.8871	2.2040	.8171	2.2040	.7826	2.2040	.7632
15	SF	.9406	1.5867	.9405	.8351	.9405	.6001	.9405	.4921	.9405	.4331	.9405	.3973
	CF	.9984	1.5892	.9983	.8415	.9983	.6096	.9983	.5038	.9983	.4464	.9983	.4119
20	SF	.5320	1.5632	.5320	.7953	.5320	.5450	.5320	.4238	.5320	.3539	.5320	.3095
	CF	.5655	1.5638	.5654	.7973	.5654	.5482	.5654	.4281	.5654	.3591	.5624	.3154
25	SF	.3414	1.5560	.3414	.7838	.3414	.5288	.3414	.4030	.3414	.3290	.3414	.2907
	CF	.3631	1.5561	.3630	.7845	.3630	.5300	.3630	.4048	.3630	.3311	.3630	.2832
30	SF	.2374	1.5531	.2374	.7794	.2374	.5227	.2374	.3952	.2374	.3194	.2374	.2695
	CF	.2526	1.5531	.2526	.7797	.2526	.5232	.2526	.3960	.2526	.3204	.2526	.2706
35	SF	.1746	1.5517	.1746	.7774	.1746	.5200	.1746	.3918	.1746	.3152	.1746	.2645
	CF	.1858	1.5517	.1858	.7775	.1858	.5202	.1858	.3921	.1858	.3156	.1858	.2650
40	SF	.1339	1.5509	.1339	.7764	.1339	.5186	.1339	.3900	.1339	.3131	.1339	.2620
	CF	.1423	1.5509	.1423	.7764	.1423	.5187	.1423	.3902	.1423	.3133	.1423	.2623
45	SF	.1061	1.5504	.1061	.7758	.1061	.5179	.1061	.3891	.1061	.3120	.1061	.2607
	CF	.1125	1.5504	.1125	.7758	.1125	.5179	.1125	.3891	.1125	.3120	.1125	.2608
50	SF	.0863	1.5501	.0862	.7755	.0862	.5174	.0862	.3885	.0862	.3113	.0862	.2599
	CF	.0912	1.5501	.0912	.7755	.0912	.5174	.0912	.3885	.0912	.3113	.0912	.2599
∞	SF	0	1.5492	0	.7746	0	.5164	0	.3873	0	.3098	0	.2582

TABLE 3. FREQUENCY PARAMETER $\Delta^{\frac{1}{2}}$ ($\times 10^2$) FOR CLAMPED-FREE SHELLS

QF : Quadratic (Flügge Theory), QT : Quadratic (Timoshenko-Love Theory)

Length -to- radius ratio L/a		Radius-to-thickness ratio a/h											
		50		100		150		200		250		300	
		n = 1	n = 2	n = 1	n = 2	n = 1	n = 2	n = 1	n = 2	n = 1	n = 2	n = 1	n = 2
10	QF	2.4579	1.7528	2.4578	1.1094	2.4578	.9432	2.4578	.8776	2.4578	.8455	2.4578	.8276
	QT	2.4578	1.7528	2.4578	1.1093	2.4578	.9432	2.4578	.8776	2.4578	.8455	2.4578	.8276
15	QF	1.0994	1.5958	1.0993	.8533	1.0993	.6256	1.0993	.5230	1.0993	.4679	1.0993	.4351
	QT	1.0993	1.5958	1.0993	.8533	1.0993	.6256	1.0993	.5230	1.0993	.4679	1.0993	.4351
20	QF	.6198	1.5660	.6198	.8013	.6198	.5539	.6198	.4353	.6198	.3677	.6198	.3251
	QT	.6198	1.5660	.6198	.8013	.6198	.5539	.6198	.4353	.6197	.3677	.6917	.3251
25	QF	.3971	1.5570	.3971	.7861	.3971	.5324	.3971	.4079	.3971	.3349	.3971	.2876
	QT	.3971	1.5570	.3971	.7861	.3971	.5324	.3971	.4079	.3971	.3349	.3971	.2876
30	QF	.2759	1.5535	.2759	.7805	.2759	.5244	.2759	.3975	.2759	.3223	.2759	.2729
	QT	.2759	1.5535	.2759	.7805	.2759	.5244	.2759	.3975	.2759	.3223	.2759	.2729
35	QF	.2028	1.5519	.2028	.7780	.2028	.5209	.2028	.3929	.2028	.3167	.2028	.2663
	QT	.2028	1.5519	.2028	.7780	.2028	.5209	.2028	.3929	.2028	.3167	.2028	.2663
40	QF	.1553	1.5510	.1553	.7767	.1553	.5191	.1553	.3907	.1553	.3139	.1553	.2630
	QT	.1553	1.5510	.1553	.7767	.1553	.5191	.1553	.3907	.1553	.3139	.1553	.2630
45	QF	.1227	1.5505	.1227	.7760	.1227	.5181	.1227	.3895	.1227	.3124	.1227	.2612
	QT	.1227	1.5505	.1227	.7760	.1227	.5181	.1227	.3895	.1227	.3124	.1227	.2612
50	QF	.0994	1.5501	.0994	.7756	.0994	.5176	.0994	.3887	.0994	.3116	.0994	.2602
	QT	.0994	1.5501	.0994	.7756	.0994	.5176	.0994	.3887	.0994	.3116	.0994	.2602

TABLE 4. FREQUENCY PARAMETER $\Delta^{\frac{1}{2}}$ ($\times 10^2$) FOR CLAMPED-RING STIFFENED SHELLS

RING I ($b_R/a = .01$, $d_R/a = .03$)

SFE : Sextic (Flügge Theory) Eccentric Rings, SFS : Sextic (Flügge Theory) Symmetric Ring

Length -to- radius ratio L/a		Radius-to-thickness ratio a/h											
		50		100		150		200		250		300	
		n = 1	n = 2	n = 1	n = 2	n = 1	n = 2	n = 1	n = 2	n = 1	n = 2	n = 1	n = 2
10	SFE	2.0811	1.7602	2.0786	1.1445	2.0761	1.0148	2.0735	.9851	2.0709	.9864	2.0683	.9990
	SFS	2.0812	1.7116	2.0787	1.0557	2.0762	.8939	2.0737	.8393	2.0712	.8206	2.0686	.8167
15	SFE	.9399	1.6274	.9392	.9316	.9385	.7563	.9378	.7020	.9370	.6883	.9363	.6904
	SFS	.9399	1.5895	.9392	.8528	.9385	.6388	.9378	.5540	.9371	.5182	.9364	.5047
20	SFE	.5318	1.5935	.5315	.8664	.5312	.6617	.5309	.5830	.5306	.5496	.5303	.5351
	SFS	.5318	1.5654	.5315	.8093	.5312	.5765	.5309	.4763	.5306	.4287	.5303	.4062
25	SFE	.3413	1.5783	.3411	.8325	.3410	.6068	.3408	.5087	.3407	.4587	.3405	.4307
	SFS	.3413	1.5578	.3411	.7949	.3410	.5538	.3408	.4449	.3407	.3892	.3405	.3592
30	SFE	.2373	1.5691	.2373	.8114	.2372	.5721	.2371	.4614	.2370	.4007	.2369	.3641
	SFS	.2374	1.5547	.2373	.7885	.2372	.5426	.2371	.4279	.2370	.3658	.2369	.3296
35	SFE	.1746	1.5631	.1745	.7982	.1744	.5512	.1744	.4330	.1743	.3660	.1743	.3241
	SFS	.1746	1.5530	.1745	.7850	.1744	.5358	.1744	.4168	.1743	.3496	.1743	.3085
40	SFE	.1339	1.5591	.1339	.7901	.1338	.5387	.1338	.4164	.1338	.3456	.1337	.3003
	SFS	.1339	1.5521	.1339	.7827	.1338	.5311	.1338	.4089	.1338	.3382	.1337	.2931
45	SFE	.1061	1.5563	.1061	.7851	.1060	.5312	.1060	.4065	.1060	.3334	.1060	.2861
	SFS	.1061	1.5515	.1061	.7811	.1060	.5276	.1060	.4032	.1060	.3303	.1060	.2830
50	SFE	.0862	1.5545	.0862	.7820	.0862	.5266	.0862	.4004	.0861	.3259	.0861	.2772
	SFS	.0862	1.5511	.0862	.7799	.0862	.5250	.0862	.3991	.0862	.3248	.0861	.2762

TABLE 5. FREQUENCY PARAMETER $\Delta^{\frac{1}{2}}$ ($\times 10^2$) FOR CLAMPED-RING STIFFENED SHELLS

RING I ($b_R/a = .01$, $d_R/a = .03$)

QFE : Quadratic (Flügge Theory) Eccentric Ring , QFS : Quadratic (Flügge Theory) Symmetric Ring

Length -to- radius ratio L/a		Radius-to-thickness ratio a/h											
		50		100		150		200		250		300	
		n = 1	n = 2	n = 1	n = 2	n = 1	n = 2	n = 1	n = 2	n = 1	n = 2	n = 1	n = 2
10	QFE	2.4505	1.8217	2.4431	1.2534	2.4358	1.1535	2.4287	1.1452	2.4218	1.1643	2.4145	1.1931
	QFS	2.4507	1.7560	2.4434	1.1288	2.4363	.9800	2.4292	.9310	2.4222	.9146	2.4152	.9115
15	QFE	1.0971	1.6465	1.0949	.9765	1.0927	.8253	1.0905	.7916	1.0883	.7958	1.0862	.8142
	QFS	1.0972	1.5988	1.0950	.8725	1.0928	.6667	1.0907	.5879	1.0885	.5563	1.0864	.5457
20	QFE	.6188	1.6039	.6179	.8954	.6169	.7123	.6160	.6542	.6151	.6391	.6142	.6407
	QFS	.6189	1.5684	.6179	.8169	.6170	.5891	.6161	.4937	.6152	.4505	.6143	.4319
25	QFE	.3966	1.5860	.3961	.8559	.3956	.6488	.3951	.5685	.3947	.5338	.3942	.5183
	QFS	.3966	1.5590	.3961	.7989	.3956	.5614	.3952	.4569	.3947	.4057	.3942	.3803
30	QFE	.2756	1.5756	.2753	.8302	.2751	.6047	.2748	.5068	.2745	.4567	.2742	.4287
	QFS	.2756	1.5552	.2753	.7910	.2751	.5482	.2748	.4378	.2745	.3806	.2742	.3494
35	QFE	.2026	1.5684	.2024	.8123	.2022	.5743	.2021	.4646	.2019	.4048	.2017	.3688
	QFS	.2026	1.5533	.2024	.7868	.2022	.5405	.2021	.4256	.2019	.3635	.2017	.3272
40	QFE	.1552	1.5632	.1550	.8000	.1549	.5545	.1548	.4377	.1547	.3718	.1546	.3308
	QFS	.1552	1.5523	.1550	.7842	.1549	.5352	.1548	.4168	.1547	.3505	.1546	.3099
45	QFE	.1226	1.5595	.1225	.7920	.1225	.5419	.1224	.4209	.1223	.3512	.1222	.3069
	QFS	.1226	1.5516	.1225	.7824	.1225	.5312	.1224	.4099	.1223	.3403	.1222	.2964
50	QFE	.0993	1.5569	.0993	.7868	.0992	.5340	.0992	.4103	.0991	.3382	.0990	.2917
	QFS	.0993	1.5512	.0993	.7810	.0992	.5281	.0992	.4045	.0991	.3326	.0990	.2863

TABLE 6. FREQUENCY PARAMETER $\Delta^{\frac{1}{2}}$ ($\times 10^2$) FOR CLAMPED-RING STIFFENED SHELLS

RING II ($b_R/a = .1$, $d_R/a = .3$)

SFE : Sextic (Flügge Theory) Eccentric Ring , SFS : Sextic (Flügge Theory) Symmetric Ring

Length -to- radius ratio L/a		Radius-to-thickness ratio a/h											
		50		100		150		200		250		300	
		n = 1	n = 2	n = 1	n = 2	n = 1	n = 2	n = 1	n = 2	n = 1	n = 2	n = 1	n = 2
10	SFE	1.7376	2.9001	1.4900	2.5847	1.3210	2.5446	1.1979	2.5421	1.1035	2.5471	1.0282	2.5531
	SFS	1.7824	3.0667	1.5486	2.7915	1.3833	2.7549	1.2603	2.7478	1.1647	2.7467	1.0879	2.7469
15	SFE	.8365	1.9282	.7457	1.3741	.6766	1.2531	.6228	1.2133	.5798	1.1978	.5445	1.1916
	SFS	.8513	1.9664	.7681	1.4384	.7024	1.3271	.6501	1.2899	.6075	1.2744	.5722	1.2670
20	SFE	.4888	1.6872	.4466	1.0098	.4119	.8290	.3836	.7581	.3601	.7247	.3403	.7072
	SFS	.4952	1.6986	.4573	1.0341	.4250	.8613	.3980	.7945	.3752	.7630	.3558	.7462
25	SFE	.3197	1.6110	.2971	.8807	.2774	.6639	.2607	.5700	.2464	.5218	.2341	.4945
	SFS	.3230	1.6152	.3029	.8909	.2849	.6762	.2692	.5889	.2556	.5429	.2437	.5168
30	SFE	.2251	1.5815	.2118	.8285	.1996	.5927	.1889	.4844	.1796	.4255	.1715	.3903
	SFS	.2270	1.5833	.2153	.8333	.2043	.6004	.1944	.4946	.1857	.4376	.1779	.4037
35	SFE	.1671	1.5681	.1586	.8048	.1506	.5593	.1434	.4425	.1370	.3768	.1313	.3359
	SFS	.1683	1.5689	.1609	.8072	.1537	.5634	.1471	.4483	.1411	.3838	.1357	.3441
40	SFE	.1290	1.5612	.1232	.7929	.1177	.5422	.1126	.4207	.1080	.3507	.1039	.3061
	SFS	.1298	1.5617	.1248	.7942	.1199	.5445	.1153	.4241	.1110	.3549	.1071	.3112
45	SFE	.1026	1.5573	.0986	.7864	.0946	.5328	.0909	.4086	.0874	.3359	.0843	.2890
	SFS	.1032	1.5576	.0997	.7872	.0961	.5342	.0928	.4106	.0897	.3386	.0868	.2923
50	SFE	.0837	1.5550	.0807	.7826	.0777	.5274	.0749	.4015	.0723	.3273	.0699	.2788
	SFS	.0841	1.5552	.0815	.7831	.0789	.5283	.0764	.4028	.0740	.3290	.0718	.2810

TABLE 7. FREQUENCY PARAMETER $\Delta^{\frac{1}{2}}$ ($\times 10^2$) FOR CLAMPED-RING STIFFENED SHELLS

RING II ($b_R/a = .1$, $d_R/a = .3$)

QFE : Quadratic (Flügge Theory) Eccentric Ring , QFS: Quadratic (Flügge Theory) Symmetric Ring

Length -to- radius ratio L/a		Radius-to-thickness ratio a/h											
		50		100		150		200		250		300	
		n = 1	n = 2	n = 1	n = 2	n = 1	n = 2	n = 1	n = 2	n = 1	n = 2	n = 1	n = 2
10	QFE	1.8874	3.7780	1.5895	3.5005	1.3987	3.4371	1.2632	3.4068	1.1607	3.3861	1.0797	3.3693
	QFS	1.9447	3.7710	1.6573	3.5094	1.4681	3.4568	1.3315	3.4357	1.2271	3.4236	1.1439	3.4150
15	QFE	.9082	2.1963	.7913	1.7177	.7102	1.6124	.6497	1.5729	.6024	1.5534	.5641	1.5420
	QFS	.9291	2.1963	.8186	1.7193	.7399	1.6153	.6801	1.5770	.6328	1.5586	.5941	1.5483
20	QFE	.5336	1.7866	.4757	1.1629	.4331	1.0056	.4003	.9442	.3739	.9142	.3521	.8973
	QFS	.5635	1.7869	.4895	1.1635	.4488	1.0064	.4168	.9453	.3908	.9155	.3691	.8989
25	QFE	.3511	1.6543	.3181	.9548	.2929	.7574	.2729	.6747	.2564	.6327	.2426	.6087
	QFS	.3565	1.6546	.3261	.9550	.3023	.7577	.2830	.6751	.2670	.6332	.2534	.6092
30	QFE	.2485	1.6030	.2280	.8673	.2117	.6447	.1985	.5457	.1875	.4932	.1781	.4622
	QFS	.2518	1.6032	.2330	.8674	.2178	.6448	.2052	.5459	.1946	.4934	.1855	.4624
35	QFE	.1851	1.5799	.1715	.8266	.1604	.5896	.1512	.4797	.1435	.4192	.1368	.3823
	QFS	.1873	1.5800	.1749	.8267	.1646	.5897	.1559	.4798	.1485	.4193	.1420	.3824
40	QFE	.1433	1.5683	.1337	.8060	.1258	.5608	.1192	.4440	.1135	.3780	.1085	.3367
	QFS	.1448	1.5683	.1361	.8060	.1288	.5608	.1226	.4441	.1172	.3780	.1124	.3368
45	QFE	.1142	1.5618	.1072	.7947	.1014	.5447	.0964	.4238	.0921	.3540	.0883	.3097
	QFS	.1152	1.5619	.1090	.7947	.1036	.5448	.0990	.4238	.0949	.3541	.0913	.3097
50	QFE	.0931	1.5580	.0879	.7881	.0835	.5353	.0797	.4117	.0763	.3396	.0733	.2931
	QFS	.0939	1.5580	.0892	.7881	.0852	.5354	.0816	.4117	.0785	.3396	.0757	.2931

TABLE 8. FREQUENCY PARAMETER $\Delta^{\frac{1}{2}}$ ($\times 10^2$) FOR CLAMPED-RING STIFFENED SHELLS

RING I ($b_R/a = .01$, $d_R/a = .03$), RING II ($b_R/a = .1$, $d_R/a = .3$)

QTRI : Quadratic (Timoshenko-Love Theory) Symmetric Ring I, QTRII : Quadratic (Timoshenko-Love Theory) Symmetric Ring II

Length -to- radius ratio L/a		Radius-to-thickness ratio a/h											
		50		100		150		200		250		300	
		n = 1	n = 2	n = 1	n = 2	n = 1	n = 2	n = 1	n = 2	n = 1	n = 2	n = 1	n = 2
10	QTRI	2.4506	1.7559	2.4434	1.1288	2.4362	.9800	2.4292	.9310	2.4222	.9146	2.4152	.9115
	QTRII	1.9448	3.7714*	1.6574	3.5108*	1.4682	3.4589*	1.3316	3.4386*	1.2272	3.4273*	1.1439	3.4194*
15	QTRI	1.0971	1.5987	1.0950	.8725	1.0928	.6667	1.0907	.5879	1.0885	.5563	1.0864	.5457
	QTRII	.9290	2.1963	.8186	1.7194	.7399	1.6156	.6801	1.5774*	.6328	1.5591*	.5941	1.5489*
20	QTRI	.6188	1.5684	.6179	.8169	.6170	.5891	.6161	.4937	.6152	.4505	,6143	.4319
	QTRII	.5435	1.7869	.4895	1.1635	.4488	1.0065	.4168	.9454	.3908	.9156	.3691	.8990*
25	QTRI	.3966	1.5590	.3961	.7989	.3956	.5614	.3952	.4569	.3947	.4057	.3942	.3803
	QTRII	.3565	1.6546	,3261	.9551	.3023	.7577	.2830	.6751	.2670	.6332	.2534	.6093
30	QTRI	.2756	1.5552	.2753	.7910	.2751	.5482	.2748	.4378	.2745	.3806	.2742	.3494
	QTRII	.2518	1.6032	.2330	.8674	.2178	.6448	.2052	.5459	.1946	.4934	.1854	.4624
35	QTRI	.2026	1.5533	.2024	.7868	.2022	.5405	.2021	.4256	.2019	.3645	.2017	.3272
	QTRII	.1873	1.5800	.1749	.8267	.1646	.5897	.1559	.4798	.1485	.4193	.1420	.3824
40	QTRI	.1552	1.5523	.1550	.7842	.1549	.5352	.1548	.4168	.1547	.3505	.1546	.3099
	QTRII	.1448	1.5683	.1361	.8060	.1288	.5608	.1226	.4441	.1172	.3780	.1124	.3368
45	QTRI	.1226	1.5516	.1225	.7824	.1225	.5312	.1224	.4099	.1223	.3403	.1222	.2964
	QTRII	.1152	1.5619	.1090	.7947	.1036	.5448	.0990	.4238	.0949	.3541	.0913	.3097
50	QTRI	.0993	1.5512	.0993	.7810	.0992	.5281	.0992	.4045	.0991	.3326	.0990	.2863
	QTRII	.0939	1.5580	.0892	.7881	.0852	.5354	.0816	.4117	.0785	.3396	.0757	.2931

* Though the sway frequency is minimum, frequency for n = 3 is lower than n = 2.

TABLE 9. FREQUENCY PARAMETER $\Delta^{\frac{1}{2}}$ ($\times 10^2$) FOR CLAMPED-SIMPLY SUPPORTED SHELLS

Cubic Frequency Equation (Flügge Theory)

Length -to- radius ratio L/a	Radius-to-thickness ratio a/h											
	50		100		150		200		250		300	
	n = 1	n = 2	n = 1	n = 2	n = 1	n = 2	n = 1	n = 2	n = 1	n = 2	n = 1	n = 2
10	7.8449	3.2440	7.8445	2.9275	7.8445	2.8650	7.8444	2.8428	7.8444	2.8325	7.8444	2.8269
15	3.7910	2.0300	3.7908	1.5011	3.7908	1.3812	3.7908	1.3367	3.7908	1.3156	3.7908	1.3040
20	2.2050	1.7243	2.2049	1.0659	2.2049	.8922	2.2049	.8228	2.2049	.7886	2.2049	.7694
25	1.4345	1.6271	1.4345	.9077	1.4345	.6973	1.4345	.6067	1.4345	.5598	1.4345	.5326
30	1.0054	1.5894	1.0054	.8426	1.0053	.6113	1.0053	.5059	1.0053	.4489	1.0053	.4146
35	.7428	1.5724	.7428	.8128	.7428	.5701	.7428	.4556	.7428	.3915	.7428	.3517
40	.5708	1.5638	.5708	.7977	.5708	.5487	.5708	.4289	.5708	.3602	.5708	.3166
45	.4522	1.5589	.4522	.7894	.4522	.5371	.4522	.4140	.4522	.3423	.4522	.2961
50	.3669	1.5561	.3669	.7846	.3669	.5303	.3669	.4051	.3669	.3316	.3669	.2838

TABLE 10

(Shell Geometry is same as in Table 1)

Clamped-Simply supported Shell

$\Delta^{\frac{1}{2}}$ ($\times 10^2$) = .51851219

$\omega/2\pi$ = 2.91 Hertzs

Clamped-Ring Stiffened Shell

Effect of Ring Stiffness on the Shell with various mode shapes

m = 1 , n = 2

M.I. OF RING I_R	SEXTIC (36)*		QUADRATIC (39)*		QUADRATIC (I.15)
	$\Delta^{\frac{1}{2}}$ x 10^2	$\omega/2\pi$ (HERTZ)	$\Delta^{\frac{1}{2}}$ x 10^2	$\omega/2\pi$ (HERTZ)	$\omega/2\pi$ (HERTZ)
0.0	.41101781	2.3059	.41328963	2.3186	2.325
.96	.48566582	2.7247	.50009295	2.8056	2.785
1.91	.48858661	2.7411	.52660181	2.9544	2.944
3.83	.49042674	2.7514	.54246953	3.0434	3.040
7.622	.49150295	2.7574	.55021507	3.0868	3.088
15.316	.49228575	2.7618	.55403181	3.1082	3.120
6750.00	.49402877	2.7716	.55760417	3.1283	.....
	... ...	... ...	... ...	... ...	3.135

* REFER TO NUMBER OF EQUATION IN THE TEXT.

TABLE 11. Comparison of frequency parameter $\Delta^{\frac{1}{2}}$ ($\times 10^2$) given by exact Forsberg Analysis with present theory

CLAMPED-FREE SHELL

a/h = 250	L/a = 9						L/a = 12					
n	m = 1		m = 2		m = 3		m = 1		m = 2		m = 3	
	Present	Forsberg	Present	Forsberg	Present	Forsberg	Present	Forsberg	Present	Forsberg	Present	Forsberg
0	14.1715		37.4263		57.7934		10.6286		28.0697		43.3451	
1	2.7001	2.6660	14.2590	12.4200	31.4284		1.5465	1.5530	8.6181	7.9980	20.5465	
2	.9382	.9510	5.2647	5.1780	13.7674		.5886	.5971	3.0220	3.0660	8.1987	
3	.9761		2.6969	2.7510	7.0861		.9105	.9101	1.6933	1.7400	4.1538	
4	1.7034		2.2632	2.2950	4.5125		1.6891		1.8944	1.9080	2.9334	
5	2.7281		2.9200	2.9260	3.9137		2.7223		2.6936	2.7910	3.1735	
6	3.9942		4.0849	4.0760	4.5137		3.9905		4.0286	4.0790	4.1867	
7	5.4938		5.5530		5.7680		5.4906		5.5187	5.5100	5.6034	
8	7.2251		7.2730		7.4051		7.2221		7.2467		7.3042	
9	9.1877		9.2310		9.3283		9.1848		9.2080		9.2543	
10	11.3814		11.4226		11.5039		11.3785		11.4011		11.4423	

TABLE 12. Comparison of frequency parameter $\Delta^{\frac{1}{2}}$ ($\times 10^2$) given by exact Forsberg Analysis with present theory

CLAMPED-FREE SHELL

a/h = 600	L/a = 9						L/a = 12					
n	m = 1		m = 2		m = 3		m = 1		m = 2		m = 3	
	Present	Forsberg	Present	Forsberg	Present	Forsberg	Present	Forsberg	Present	Forsberg	Present	Forsberg
0	14.1715		37.4262		57.7933		10.6286		28.0697		43.3450	
1	2.7001	2.6650	14.2589	12.2400	31.4283		1.5465	1.5520	8.6180		20.5465	
2	.8937	.9074	5.2556	5.1060	13.7629		.5157	.5258	3.0074	3.0170	8.1925	
3	.5571	.5635	2.5658	2.5950	7.0315		.4358	.4384	1.4839	1.5240	4.0675	
4	.7428	.7434	1.6353	1.6720	4.2132		.7145	.7143	1.0915	1.1150	2.4732	
5	1.1455	1.1320	1.4938	1.5130	2.9581		1.1371		1.2623	1.2700	1.9259	1.9300
6	1.6672		1.8068	1.8130	2.5586		1.6636		1.7129	1.7140	2.0016	
7	2.2903		2.3566	2.3560	2.7247		2.2881		2.3132		2.4448	
8	3.0110		3.0498	3.0460	3.2397		3.0094		3.0257		3.0940	
9	3.8285		3.8558	3.8500	3.9648		3.8271		3.8397		3.8811	
10	4.7424		4.7645		4.8352		4.7411		4.7521		4.7811	

TABLE 13. Comparison of frequency parameter $\Delta^{\frac{1}{2}}$ (x 10^2) given by exact Forsberg Analysis with present theory

CR: Clamped-ring stiffened shell (Ring: $b_R/a = .1$, $d_R/a = .3$) ; CS: Clamped-Simply supported shell
(Sextic) (Cubic)

m = 1	a/h = 250						a/h = 600					
n	L/a = 9			L/a = 12			L/a = 9			L/a = 12		
	Present CR	Forsberg CR	Present CS	Present CR	Forsberg CR	Present CS	Present CR	Forsberg CR	Present CS	Present CR	Forsberg CR	Present CS
0												
1	1.3707	1.3080	9.3866	0.8731	0.8406	5.6932	0.9554	0.9063	9.3866	0.6217	0.5930	5.6932
2	3.3519	3.6980	3.4596	1.9419	2.2180	2.0022	3.3425	3.7540	3.4469	1.9374	2.2640	1.9811
3	1.8573	2.2390	1.8938	1.2780	1.5010	1.2974	1.6809	2.2320	1.7099	1.0021	1.3550	1.0163
4	1.9440	2.1640	1.9574	1.7726		1.7783	1.1871	1.5890	1.2001	0.8867	1.036	0.8925
5	2.8031		2.8103	2.7496		2.7525	1.2954	1.4960	1.3031	1.1883	1.2650	1.1914
6	4.0259		4.0326	4.0037		4.0065	1.7204		1.7273	1.6817		1.6846
7	5.5109		5.5187	5.4991		5.5024	2.3105		2.3184	2.2954		2.2987
8	7.2355		7.2452	7.2284		7.2324	3.0177		3.0274	3.0121		3.0162
9	9.1938		9.2058	9.1894		9.1945	3.8280		3.8400	3.8273		3.8324

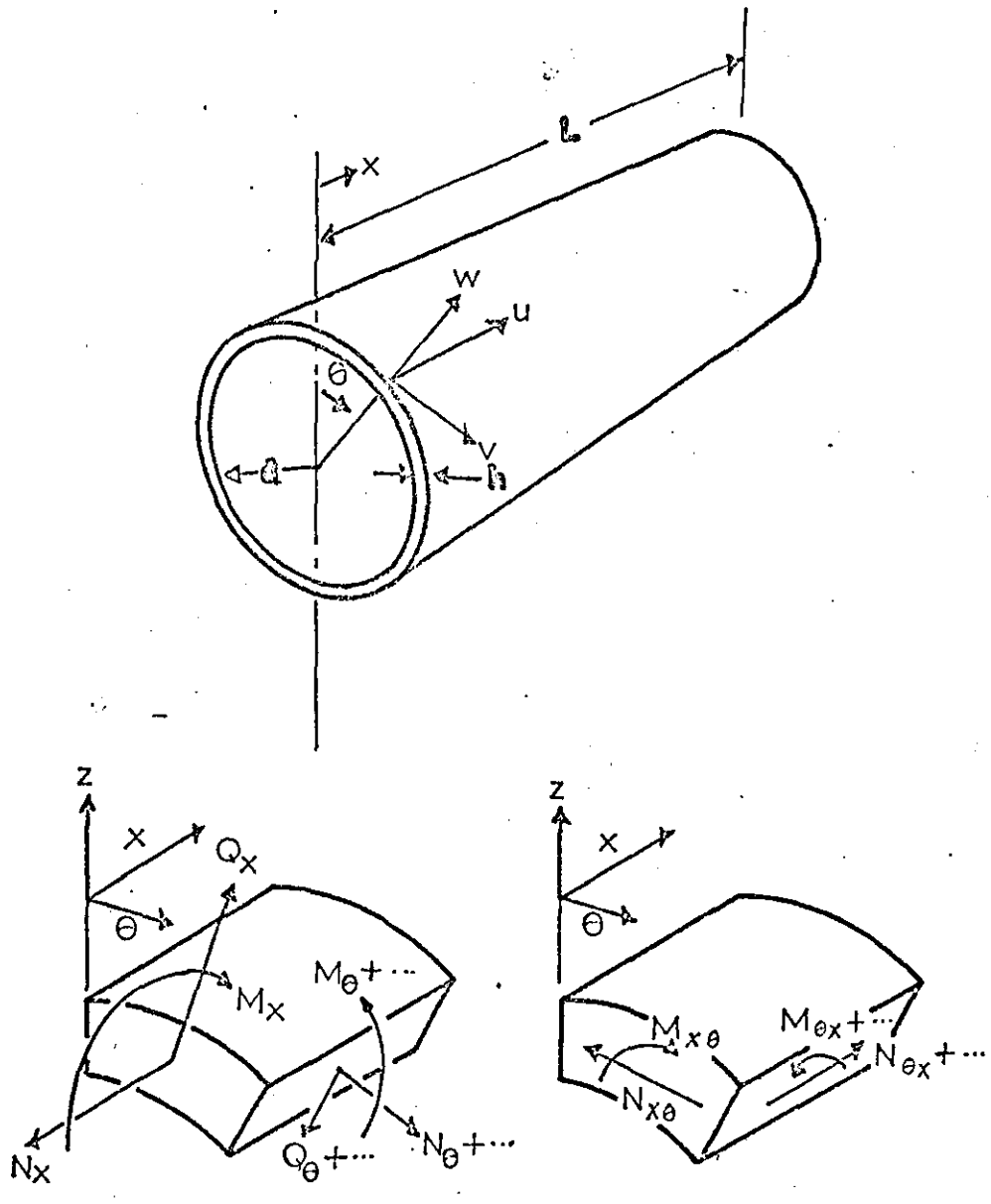

FIG. 1 COORDINATE SYSTEM AND SHELL ELEMENT

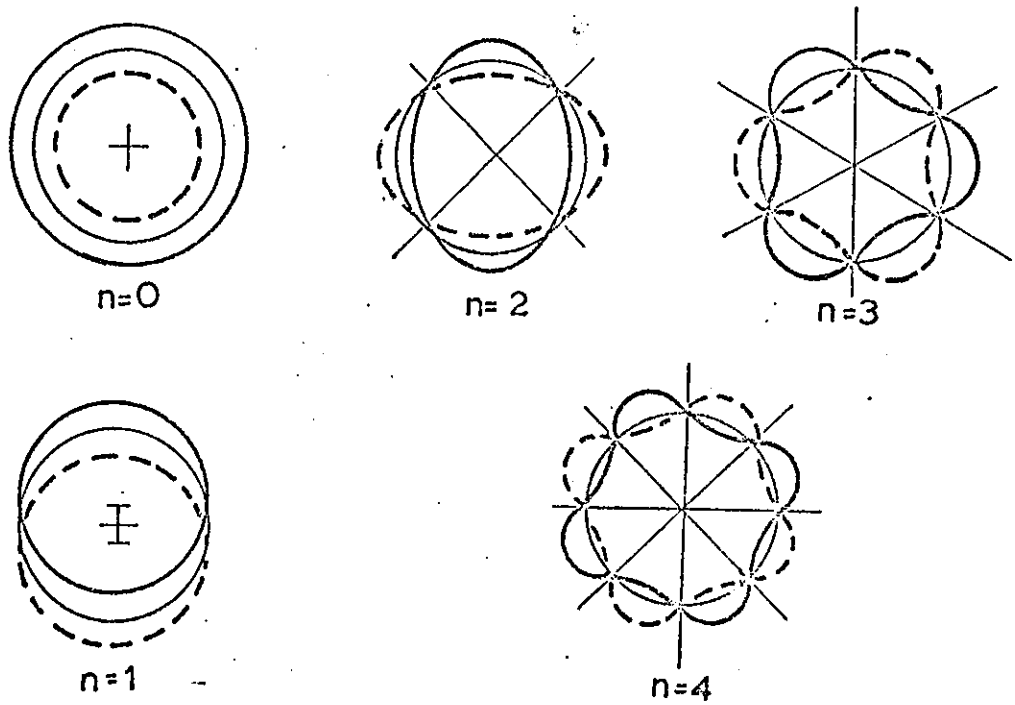

CIRCUMFERENTIAL NODAL PATTERN

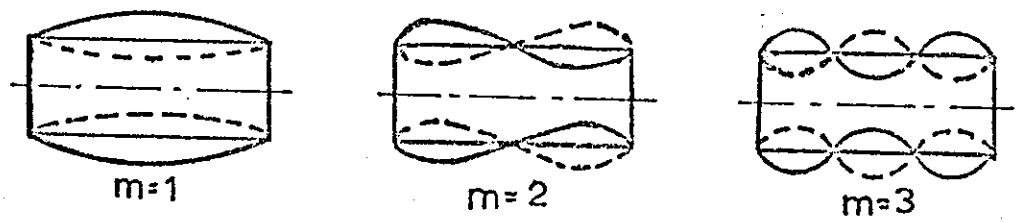

SIMPLY SUPPORTED

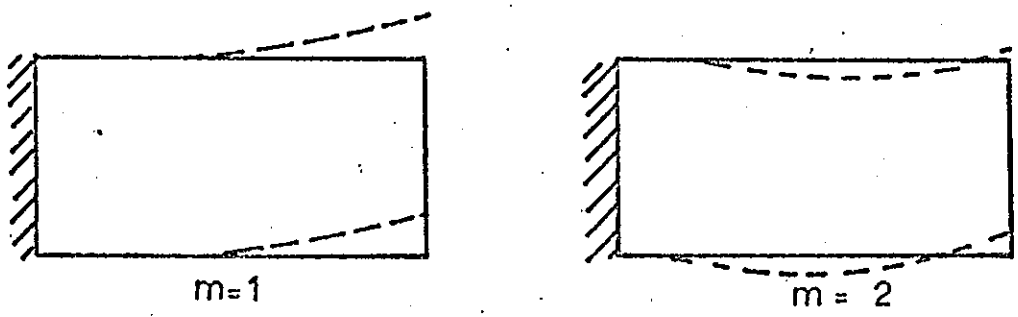

CLAMPED - FREE

AXIAL NODAL PATTERN

FIG. 2. NODAL PATTERNS

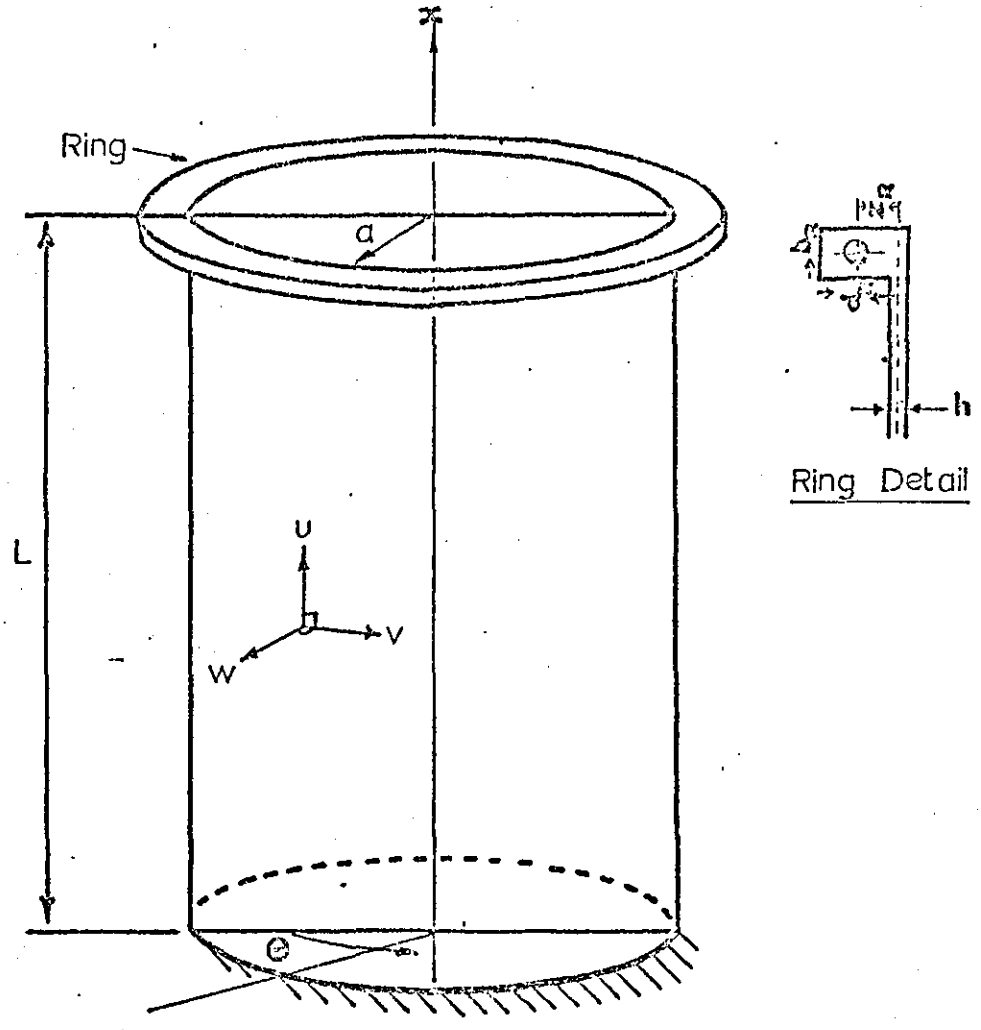

FIG.3 RING - STIFFENED, CYLINDRICAL SHELL CLAMPED AT BASE

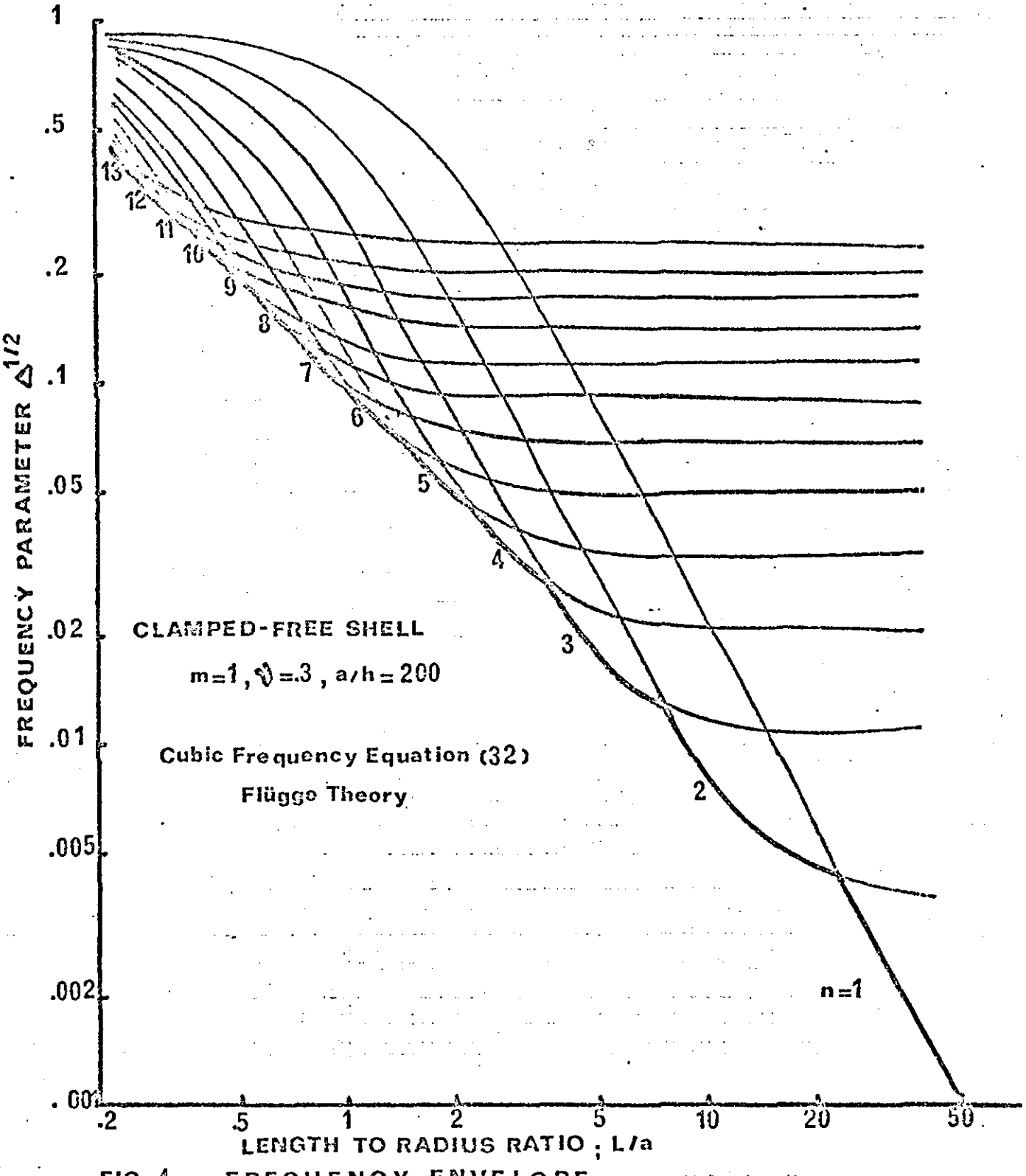

FIG:4 FREQUENCY ENVELOPE

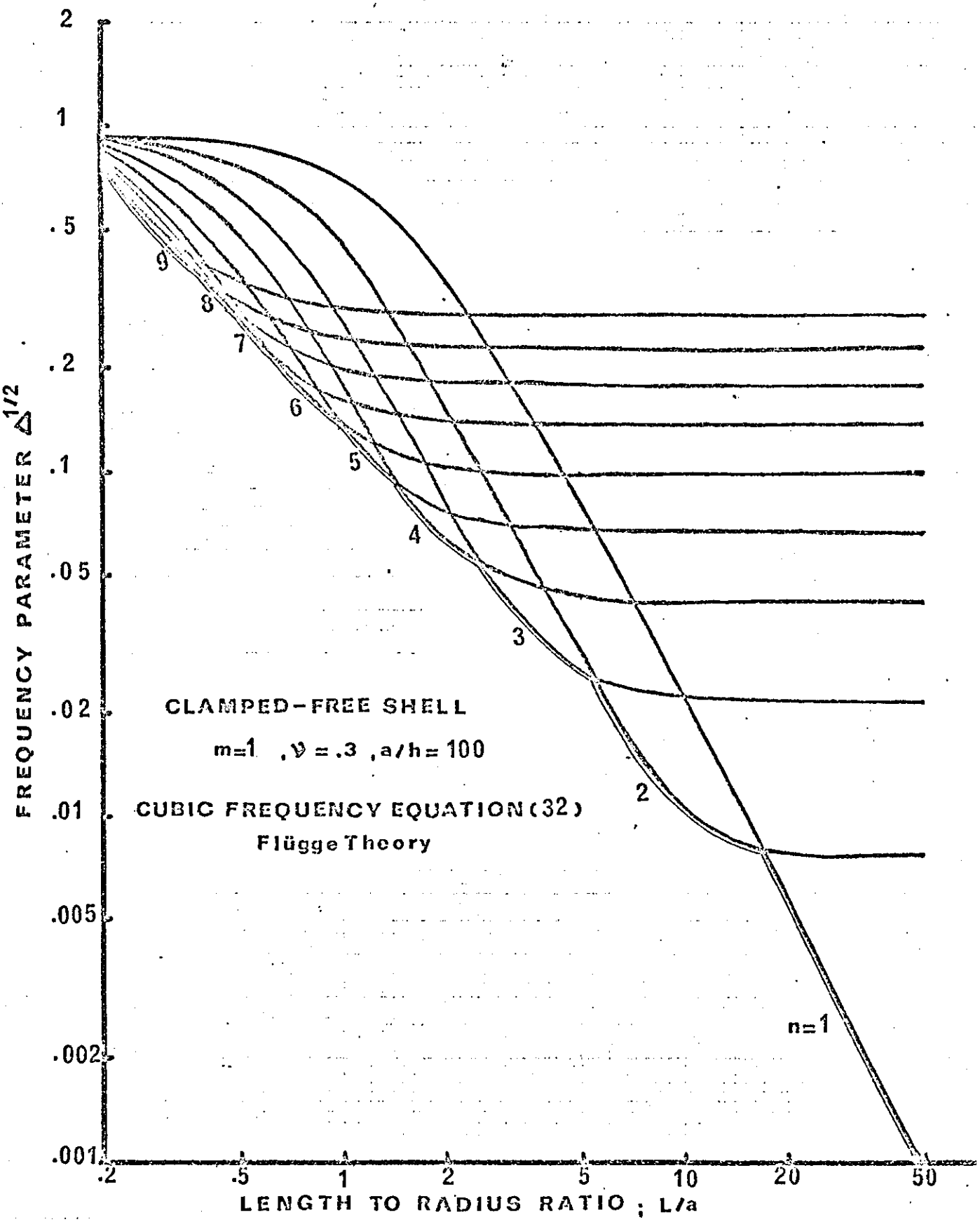

FIG:5 FREQUENCY ENVELOPE

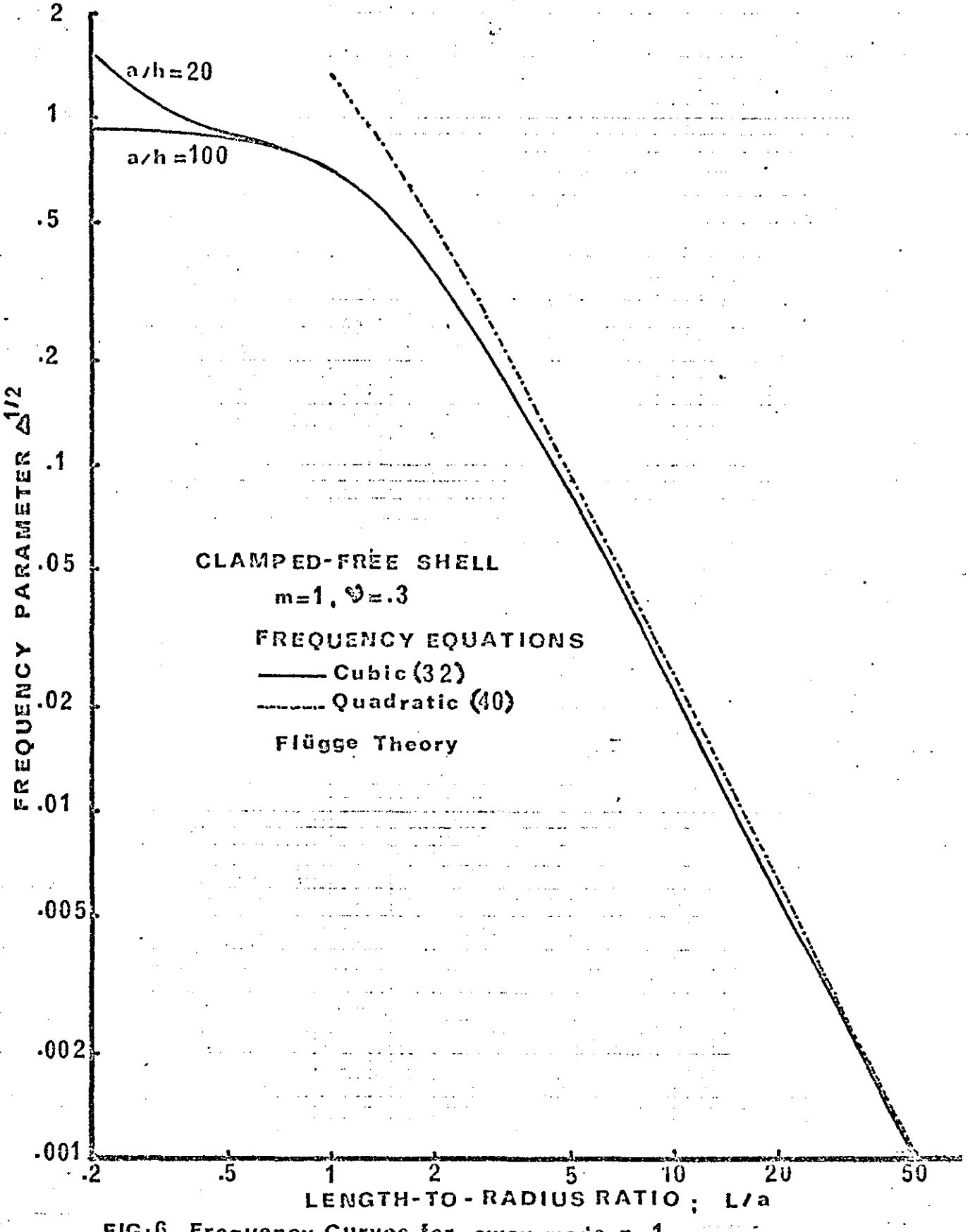

FIG:6 Frequency Curves for sway mode n=1

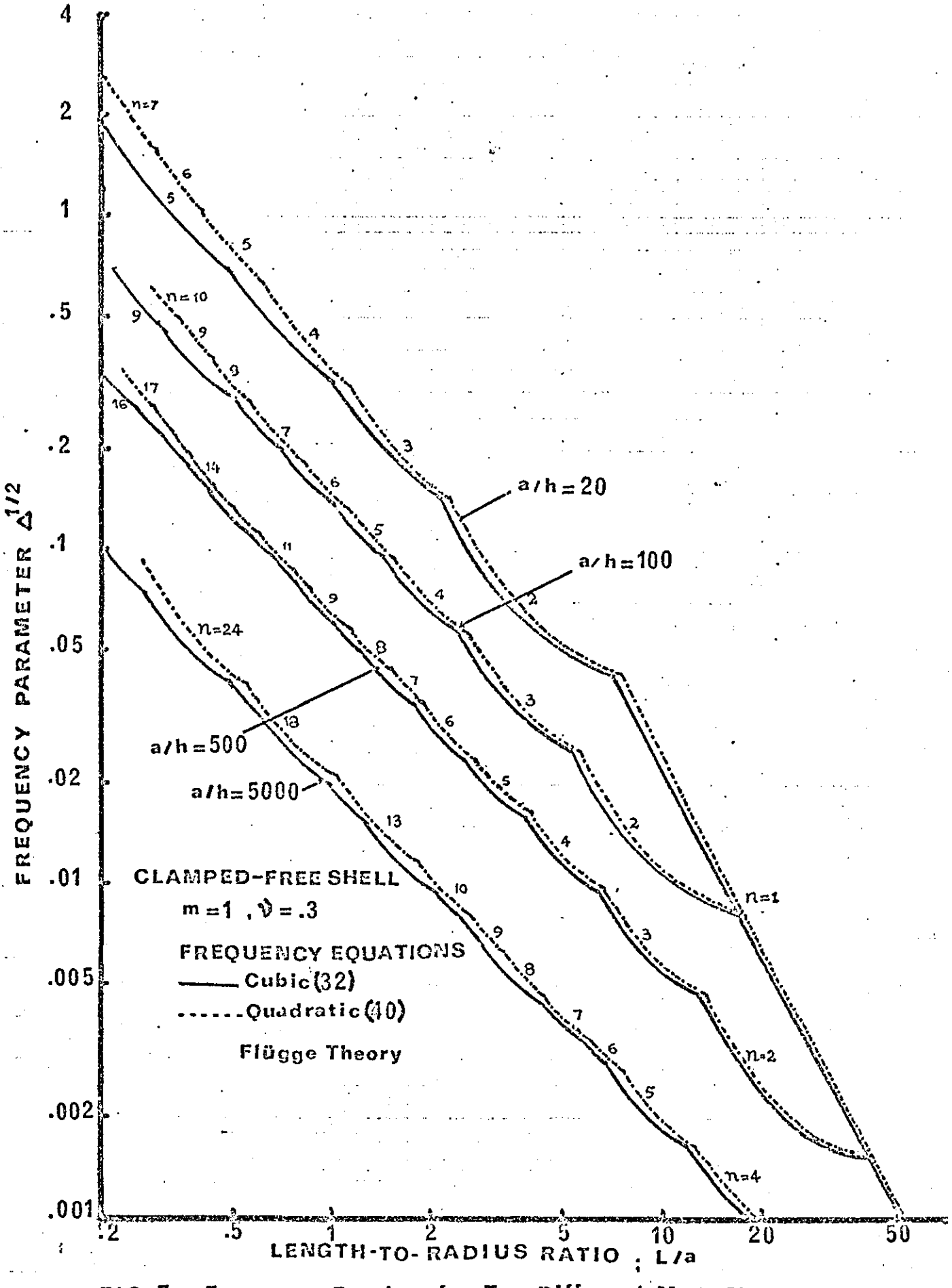

FIG: 7 Frequency Envelope for Two Different Mode Shapes

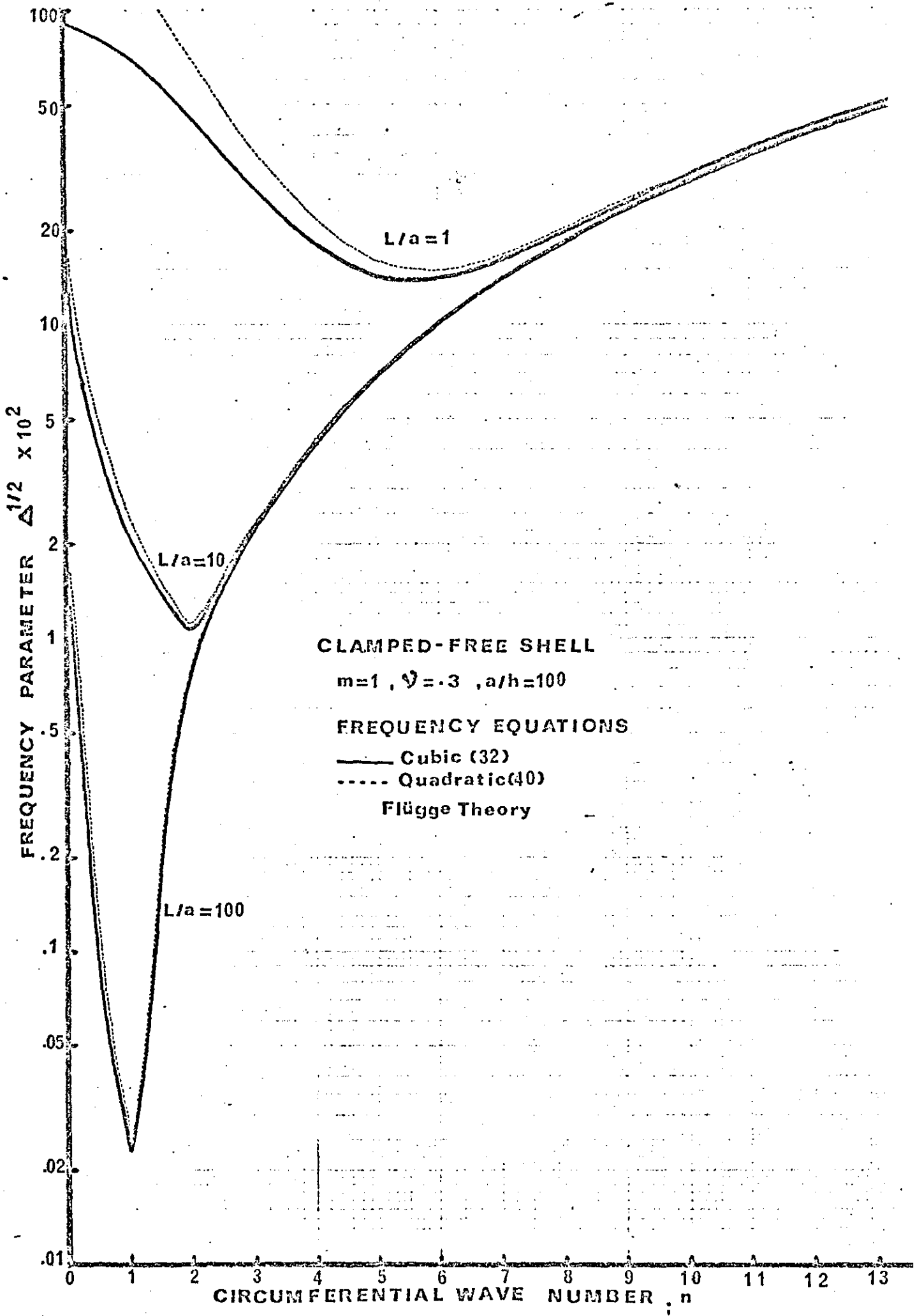

FIG: 8 Frequency Distribution for Two Different Modes for L/a= 1, 10, 100

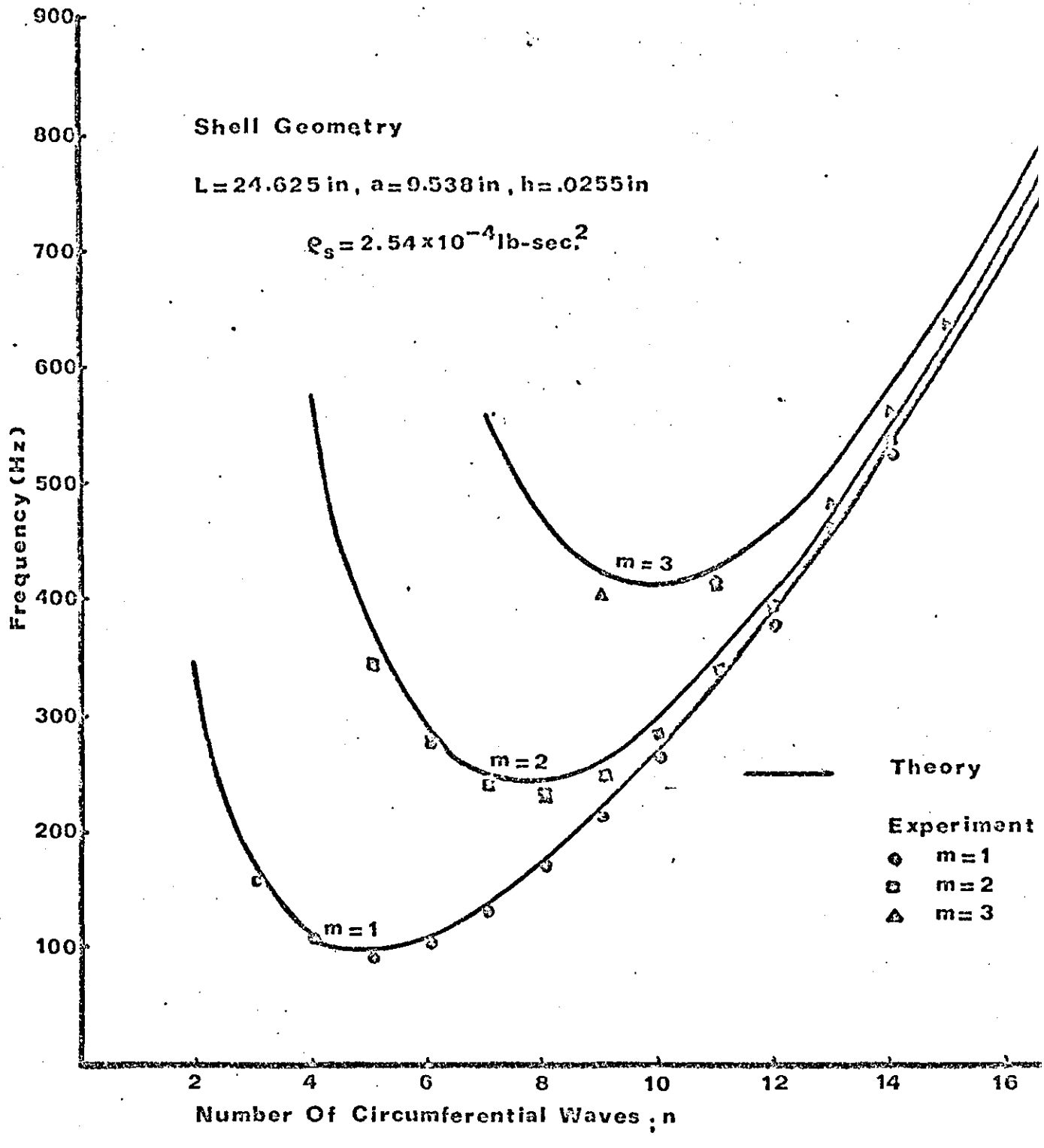

FIG. 9 Experimental and Analytical Frequencies of Clamped-Free Cylindrical Shell

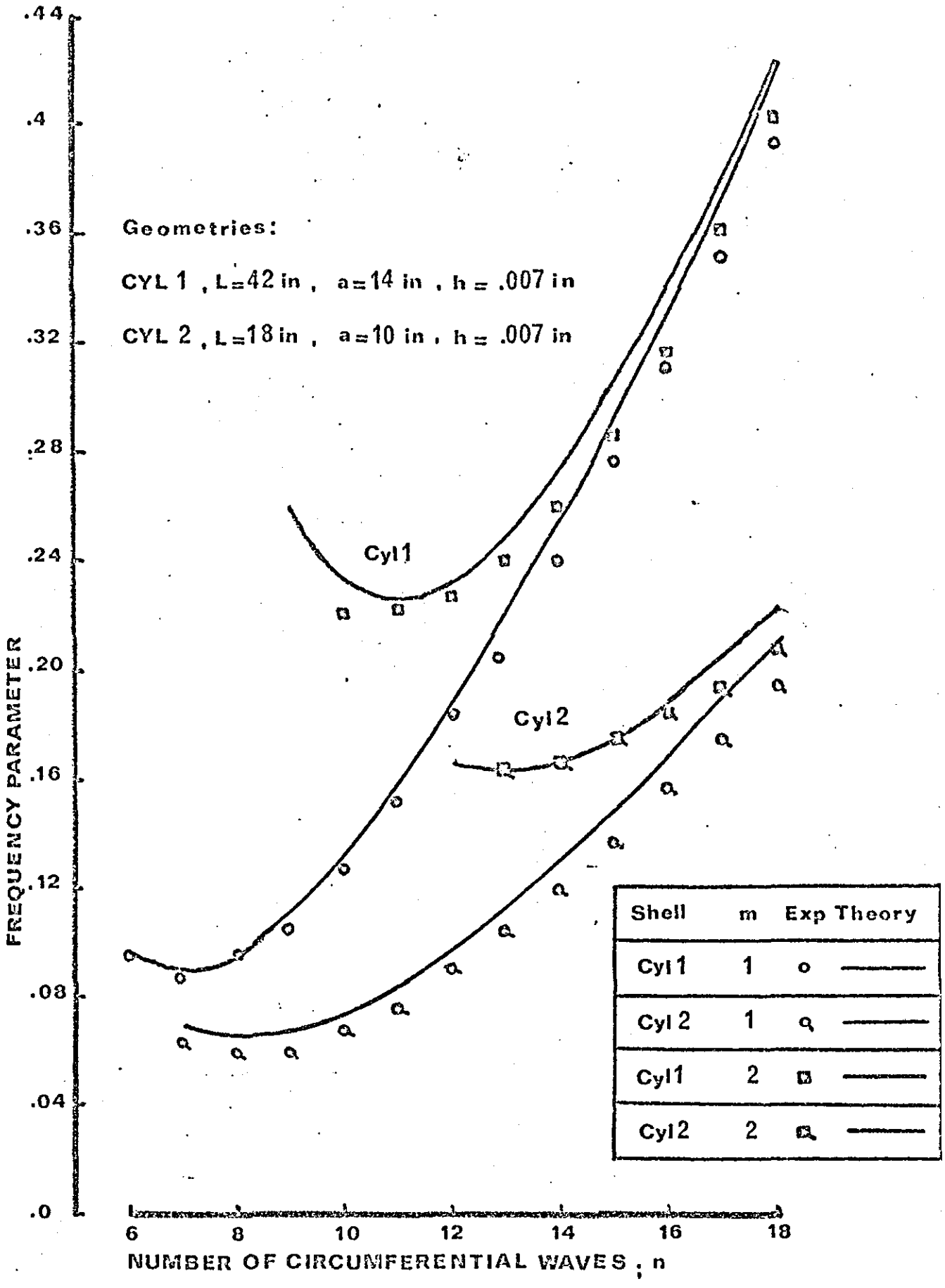

FIG.10 Experimental and Analytical Frequencies of Clamped-Free Shell

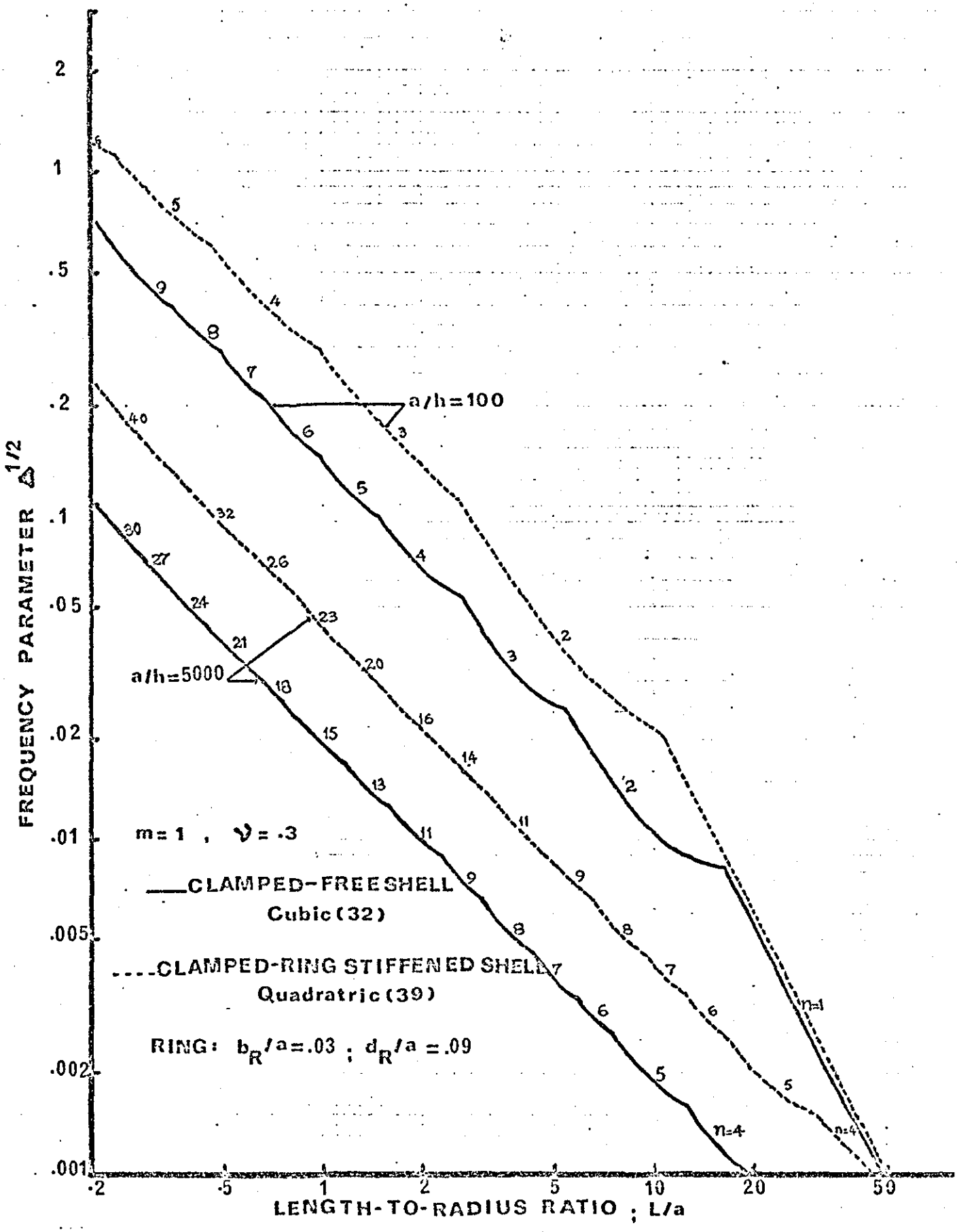

FIG:11 Effect of a Particular Ring at the Top

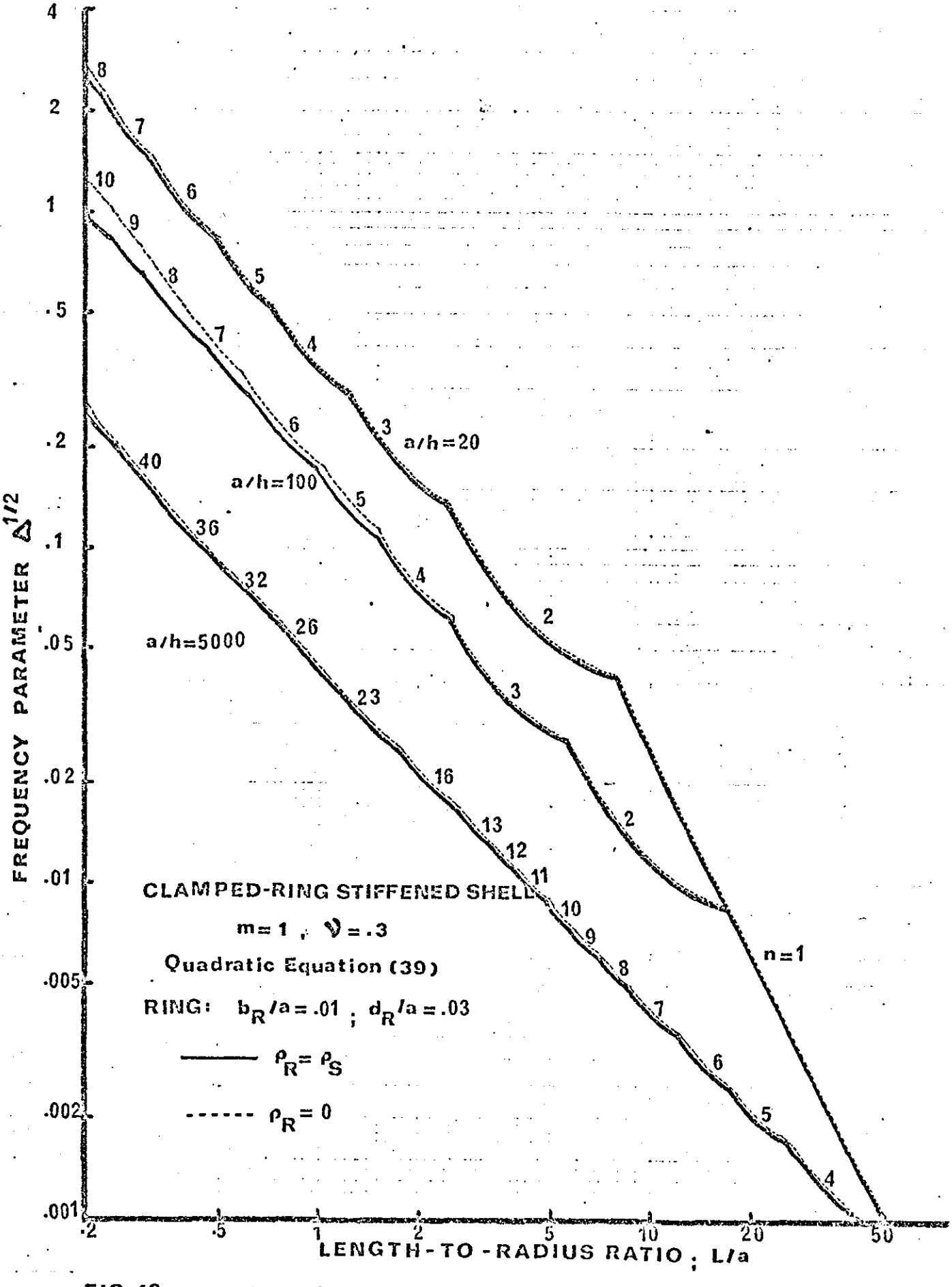

FIG: 12 Effect of Ring Mass on Frequency Envelope

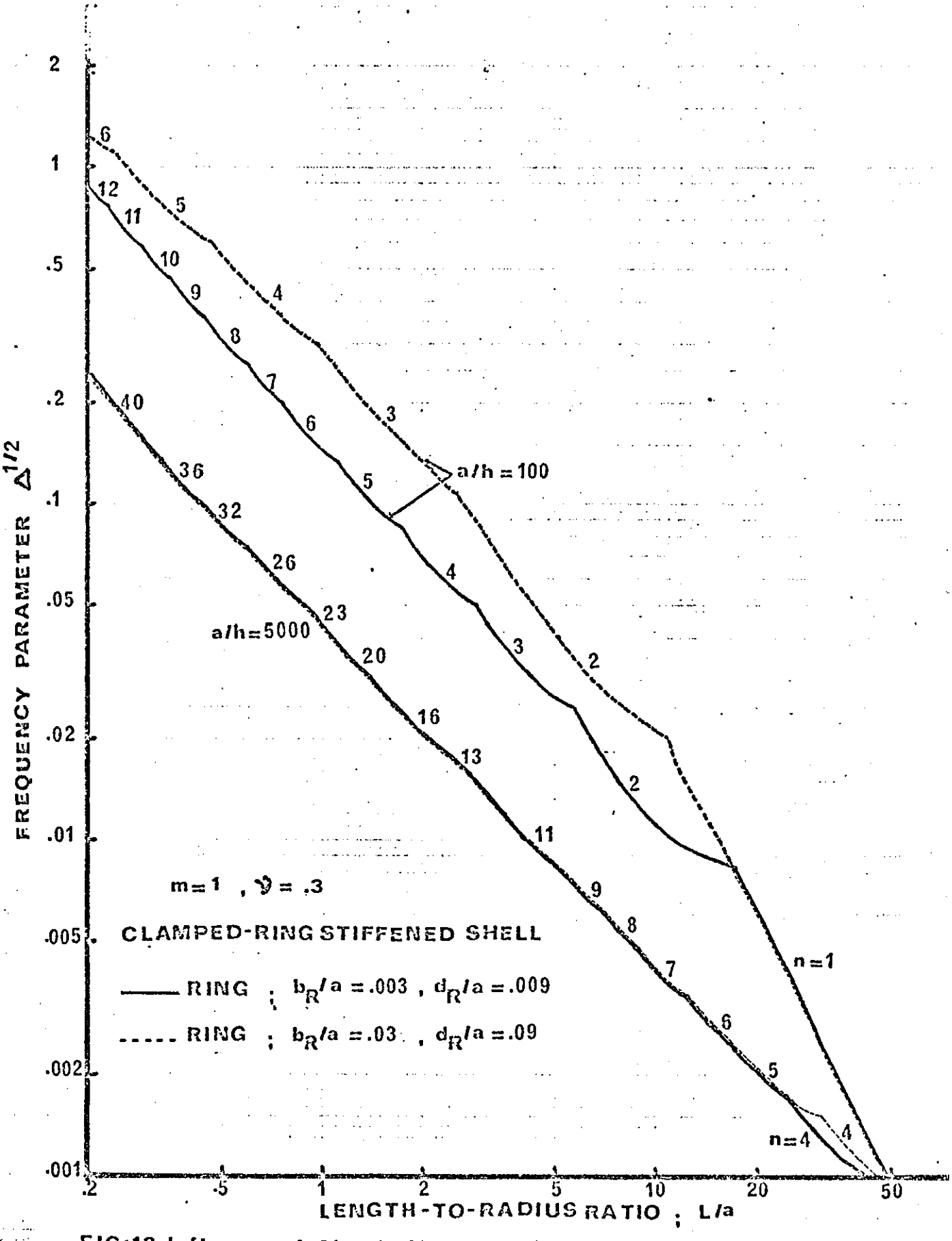

FIG:13 Influence of Ring Stiffness on Frequency Spectrum

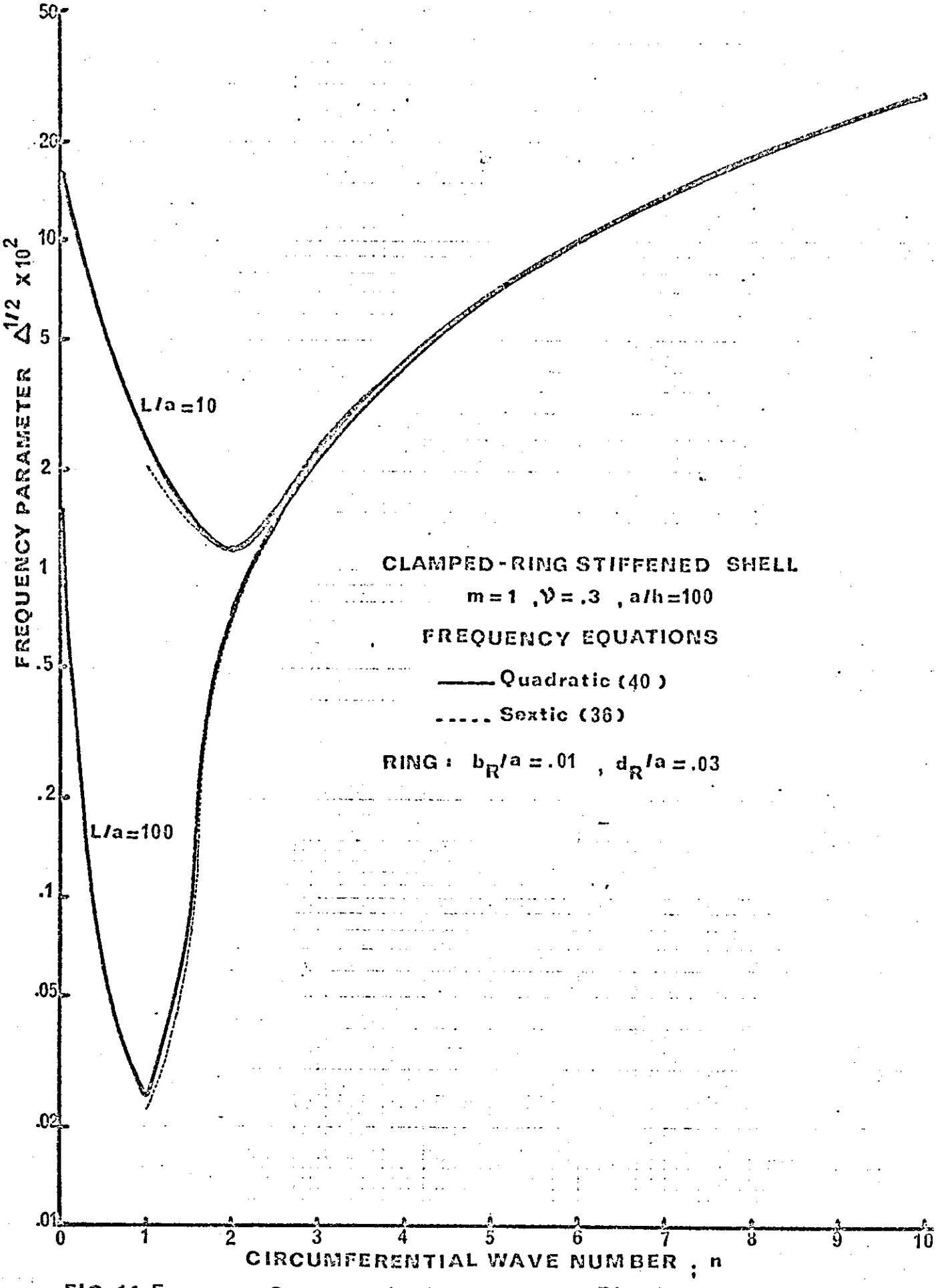

FIG: 14 Frequency Spectrum due to a Particular Ring for Two Mode Shapes

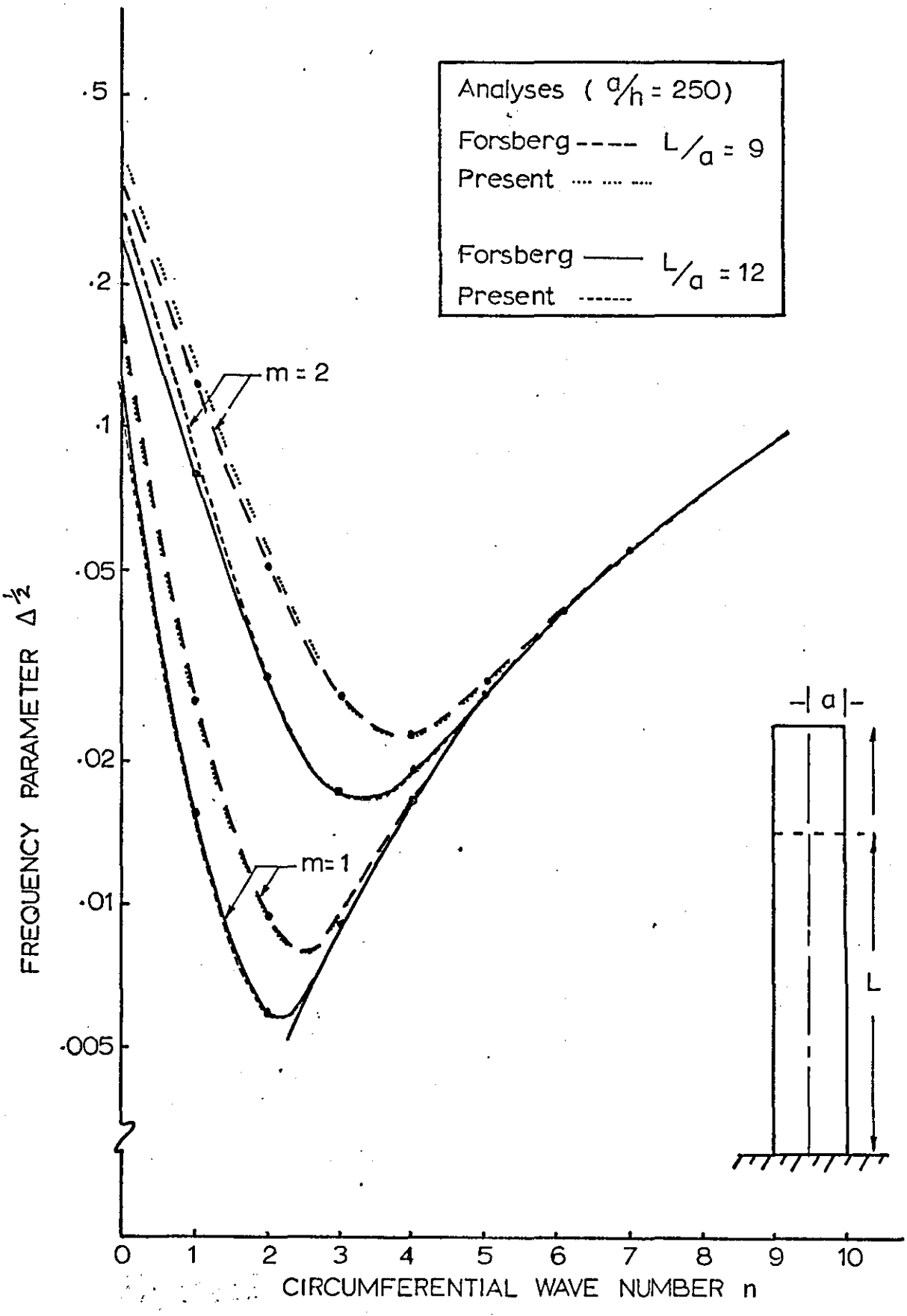
Analyses (a/h = 250)
Forsberg ---- L/a = 9
Present ....
Forsberg —— L/a = 12
Present ------
m = 2
m = 1
FREQUENCY PARAMETER Δ^½
·5
·2
·1
·05
·02
·01
·005
0 1 2 3 4 5 6 7 8 9 10
CIRCUMFERENTIAL WAVE NUMBER n
a
L

Figure 15

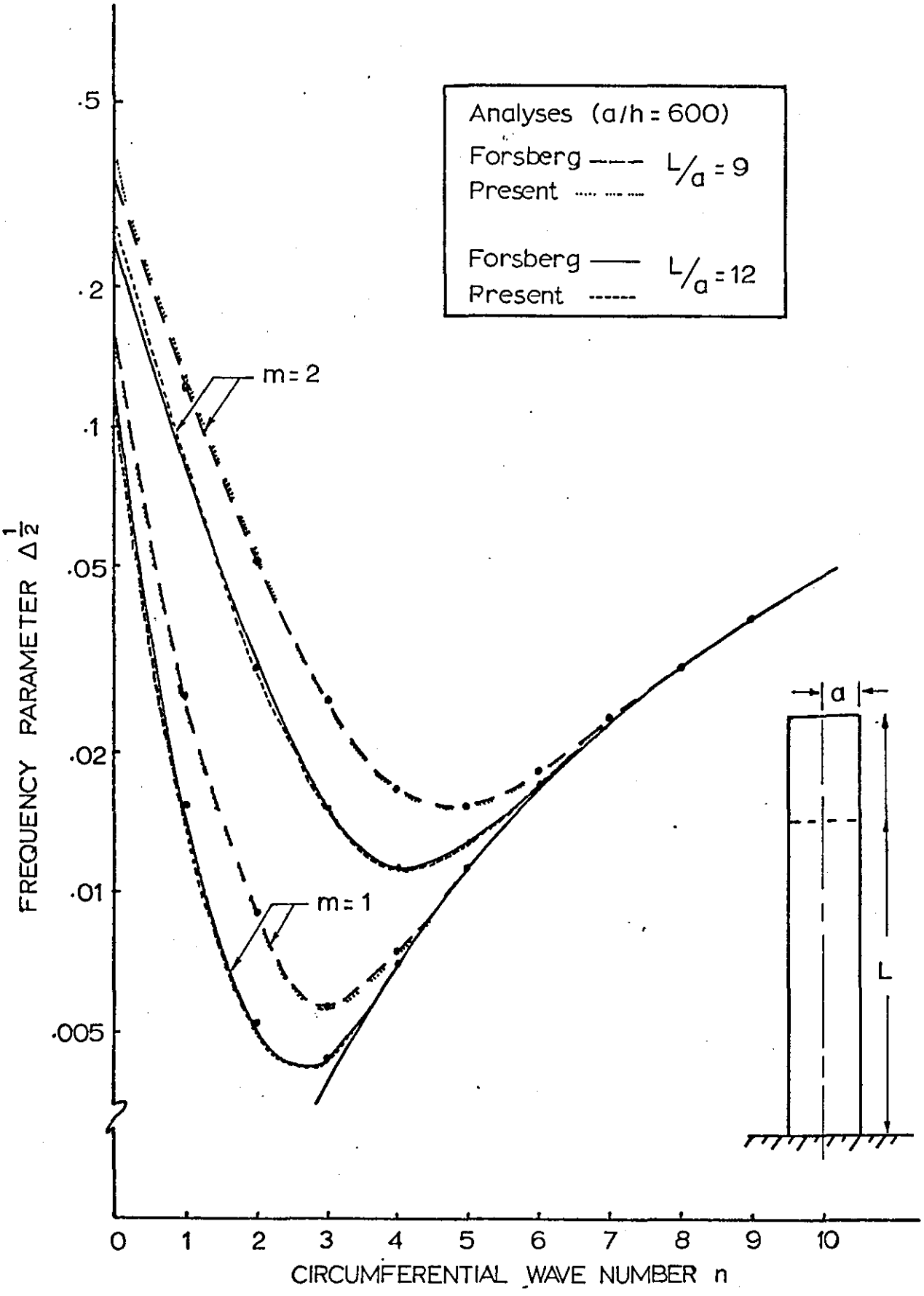
Analyses (a/h = 600)
Forsberg ---- L/a = 9
Present ....
Forsberg —— L/a = 12
Present ------
m = 2
m = 1
FREQUENCY PARAMETER $\Delta^{\frac{1}{2}}$
.5
.2
.1
.05
.02
.01
.005
0 1 2 3 4 5 6 7 8 9 10
CIRCUMFERENTIAL WAVE NUMBER n
a
L

Figure 16

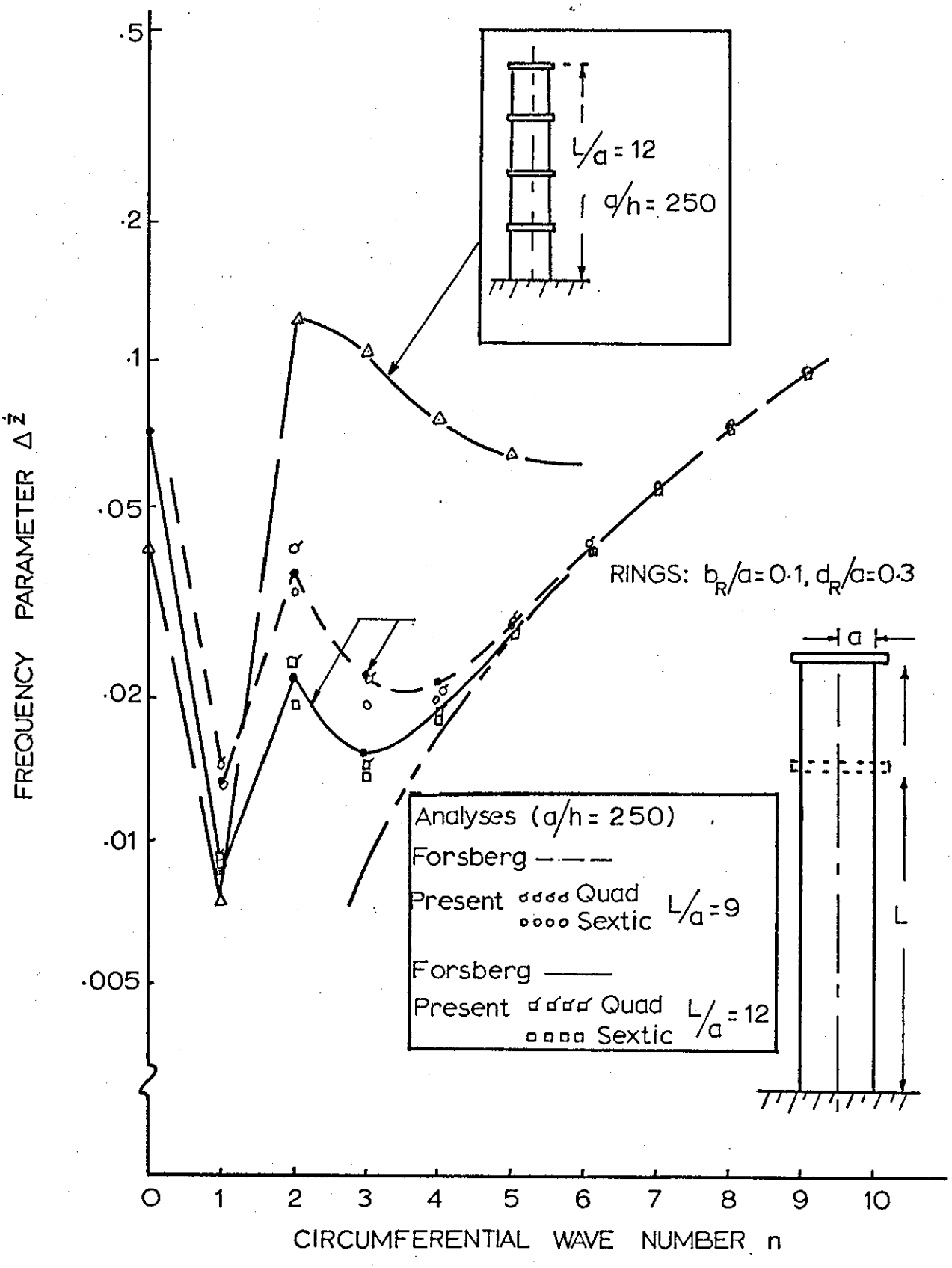
L/a = 12
a/h = 250
RINGS: $b_R/a = 0.1$, $d_R/a = 0.3$
Analyses (a/h = 250)
Forsberg
Present Quad
Sextic
L/a = 9
Forsberg
Present Quad
Sextic
L/a = 12
a
L
FREQUENCY PARAMETER $\Delta\bar{z}$
·5
·2
·1
·05
·02
·01
·005
0
1
2
3
4
5
6
7
8
9
10
CIRCUMFERENTIAL WAVE NUMBER n

Figure 17

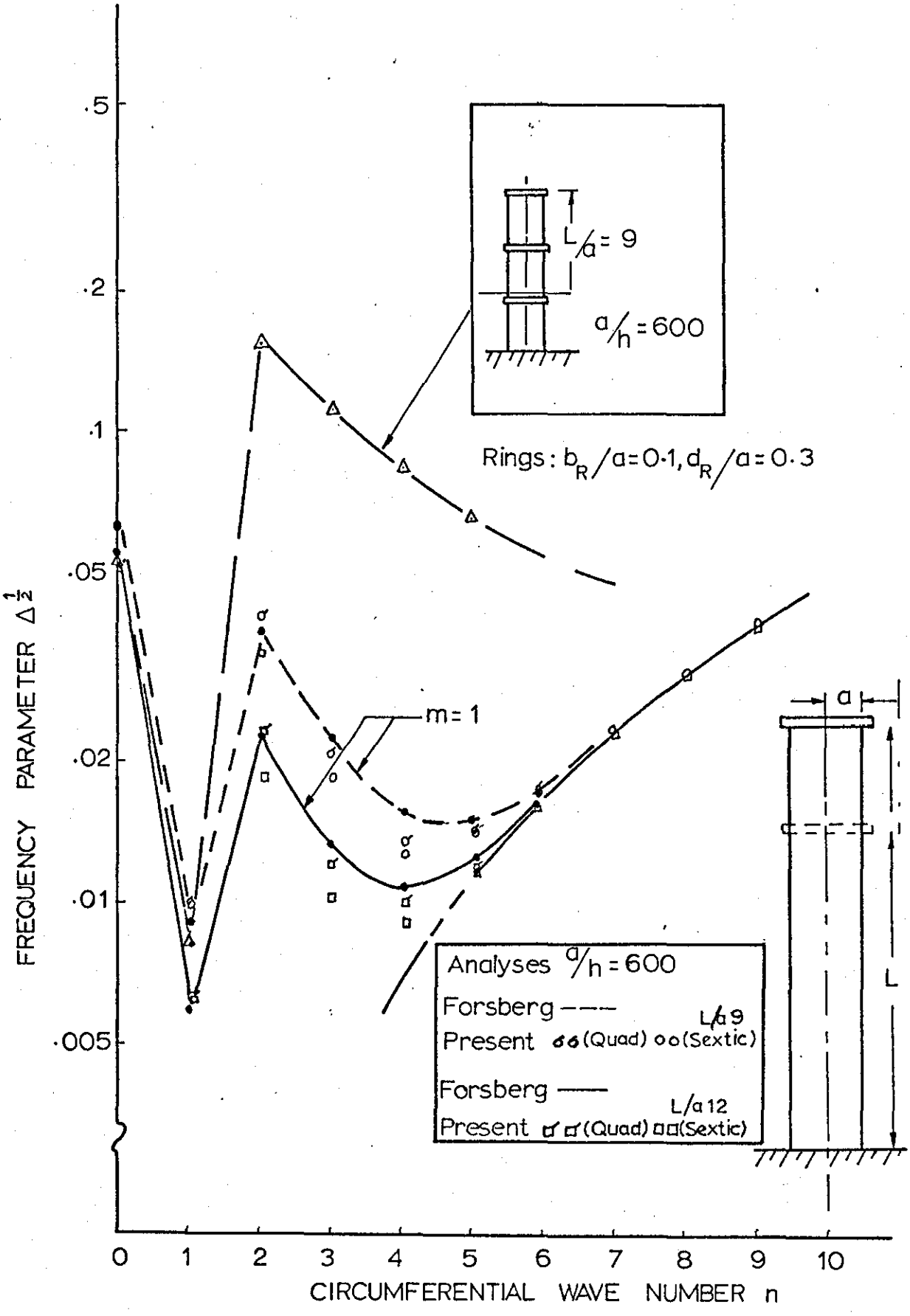
.5
.2
.1
.05
.02
.01
.005
FREQUENCY PARAMETER $\Delta^{\frac{1}{2}}$
L/a = 9
a/h = 600
Rings : $b_R/a = 0.1, d_R/a = 0.3$
m = 1
a
L
Analyses a/h = 600
Forsberg ——— L/a 9
Present ●● (Quad) ○○ (Sextic)
Forsberg —— L/a 12
Present ■■ (Quad) □□ (Sextic)
0 1 2 3 4 5 6 7 8 9 10
CIRCUMFERENTIAL WAVE NUMBER n

Figure 18.

WIND-INDUCED OSCILLATIONS OF CIRCULAR CYLINDRICAL SHELLS

PART B

AN EXPERIMENTAL INVESTIGATION

ABSTRACT

Present study discusses the wind induced oscillations of tall chimneys with the major concern being to study the vortex excited motion of tall circular cylindrical shell structures in either the swaying (bending) or the ovalling (breating) modes. The possible relationships between these modal natural frequencies and the frequency spectrum of the aerodynamic input (in this case the frequency of shedding of a pair of vortices) has been discussed.

A large number of model tests have been performed in the wind tunnel at Loughborough University of Technology, on the shells clamped at the base and free at the top. Model shells of different lengths and varying thickness and diameter have been taken. Also a mechanical shaker has been used as an excitation device. Measured frequencies are compared with those predicted by the relevant structural vibration analyses given in Part A of this study. In some cases the effect of a stiffening ring at the free end is assessed. An attempt has also been made to determine experimentally the structural damping characteristics for various modes of vibration in some cases. Also Fablon has been used to increase the structural damping, with some success, in a few cases.

CONTENTS

CONTENTS (contd)

LIST OF FIGURES

LIST OF FIGURES (contd)

LIST OF TABLES

NOTATION

a	radius to shell mid-surface
D	diameter to shell mid-surface
h, L	shell thickness and length
b_R, d_R	ring breadth and depth
m	number of axial "half waves"
n	number of circumferential waves
u, v, w	mid-surface displacement of the shell in the axial, circumferential, and radial direction
x, θ	axial and circumferential coordinates
E_s	Youngs modulus of the shell
M_x, $M_{x\theta}$)) N_x, $N_{x\theta}$, Q_x)	stress resultants
N	Strouhal frequency (Hz)
V	wind speed
S_N	Strouhal number
R_N	Reynolds number
r	integral value of critical relationship
g	measure of structural damping
X	measure of deflection (amplitude)
h_w	differences in heights of water levels in two manometer tubes
α	inclination of manometer tubes
ρ_s, ρ_A, ρ_w	densities of the shell, air, and water
ξ	critical damping ratio
ν	Poisson's ratio
ω	circular frequency
Ω	natural frequency of the shell in Hz

1. INTRODUCTION

The need to take winds into account in the design of civil engineering structures has long been recognised. But in the past decade a number of events in Britain have emphasised the destructive power of the wind. In February 1962 disastrous gales in Yorkshire caused widespread structural damage, particularly in the Sheffield area where nearly two thirds of the total dwellings were affected, some being damaged beyond repair. A similar catastrophe occurred in January 1968 in Glasgow causing widespread destruction. Also a subsequent gale in the Sheffield area in 1966 led to the collapse of Ferrybridge Cooling Towers. These have drawn attention to the limitations of the current knowledge on wind-induced instabilities. Even for such a simple structure as the circular cylindrical shell, the stability criteria are not completely defined for all types of wind loading.

In recent years there has been an increasing awareness of the need to allow for the static and dynamic effects of wind on the design of civil engineering and aerospace structures and there has been a useful cross-fertilisation of ideas and information feedback between these branches of engineering. This is particularly evident in the number and scope of major symposia, references [1, 2, 3] which have attracted meteorologists, architects, civil engineers, aerodynamicists and aerospace structural engineers.

The main concern of the present study is that class of dynamic problems resulting from excitation due to vortex shedding in case of circular cylindrical shell structures. This study was prompted by the following recent full scale ovalling experience:

In 1964 during a typhoon, ovalling oscillations were observed on a 150ft high and 10ft diameter chimney. The chimney material was mild steel of gauge $^{5}/_{16}$ in. thick. The nature of the oscillations as recorded on film was of an ovalling mode with n = 2 at a frequency of approximately 1.6 - 2.4 Hz. After some time the sole stiffening ring at the free end of the chimney broke

away from the basic shell whereupon the amplitude of the vibrations increased considerably prior to collapse.

It may be remarked that for a particular structure a study ofwind effects requires a prior knowledge of the maximum wind speeds at the proposed site for the structure. Since it would be unusual for this precise knowledge to be available it is necessary to infer it from meteorological records often taken a considerable distance away. The designer must also take account of local topography, prevailing wind directions, the variation of wind speed with the height, the presence of other adjacent structures etc., and most importantly, the degree of turbulence in the wind.

Because of uncertainties in these various parameters recourse is often had to wind-tunnel tests in which these parameters, especially wind profile and turbulence, and structural flexibility are all modelled. Some of such work is reported in references [1, 2 and 3]

The present report is a complementary study of that published in reference [4] and given in greater detail in Part A. The purpose of this study is to report comparisons of experimental frequencies and mode shapes with corresponding analytical results of reference [4] for clamped-free and clamped ring stiffened circular cylindrical shells.

The vortex shedding phenomenon and vortex induced oscillations are first discussed followed by a brief summary of the analytical procedure in [4]. This then is followed by details of the experimental investigations and comparisons of experimental and analytical results.

2. VORTEX SHEDDING PHENOMENON

2.1 VORTEX EXCITATION

The most common cause of oscillations of bluff shaped (e.g. cylindrical) bodies in a fluid flow is vortex shedding. A simple idealised physical explanation of the excitation due to vortices is as follows [5] [6].

As a vortex is shed, it induces a circulation round the cylinder in the opposite direction to that of the shed vortex, as shown in Figure 1. This temporarily increases the velocity on one part of the cylinder and decreases it on the other, both by an amount of v_1, and consequently a difference in the surface pressure on the cylinder is produced acting in a direction across that of the flow. As the vortex passes downstream, its effect on the cylinder is reduced and the resultant force decreases until another vortex is shed, from the other side of the cylinder, and a force is produced in the other direction. The cross flow force is therefore of the same frequency as that of the shedding of a pair of vortices.

If the cylinder is flexible and free to oscillate, then large amplitude motion may occur across the direction of the flow when the frequency of shedding of a pair of vortices (N) is in resonance with its natural frequency (Ω).

2.2 STROUHAL NUMBER vs REYNOLDS NUMBER

Research into vortex streets behind a circular cylinder dates from the late 15th Century. In 1878 early experiments by Strouhal led to the empirical correlation of the vortex shedding frequency N, the cylinder diameter D, and the stream velocity V through the non-dimensional Strouhal number

$$S_N = \frac{ND}{V} \qquad (1)$$

Many workers have discussed this parameter and its dependence on Reynolds number, and it appears that several distinct regions of Reynolds

number exist in which different phenomena occur. These various regions are not separated by clear boundaries but by transition zones which can be altered by individual experimental conditions. These regions are shown in Figure 2, as symmetric, regular, irregular and supercritical defining the nature of the vortex shedding phenomena.

It is with the irregular (sub-critical) and supercritical Reynolds Number range (i.e. $R_N > 300$) that this report is primarily concerned but the intervening transition zone around the critical Reynolds number ($2 \times 10^5 < R_N < 2 \times 10^6$) will also be discussed. Much of the data available on the aerodynamic Strouhal number over the above Reynolds number range is shown in Figure 2.

2.2.1 SUBCRITICAL REGIME

In the subcritical Reynolds number region ($300 < R_N < 2 \times 10^5$) the boundary layer is laminar, its separation from the surface is not appreciably affected by Reynolds number, and the Stouhal number in equation (1) remains at an almost constant value of 0.2 for an infinite aspect ratio circular cylinder.

Experiments have shown that one consequence of periodic vortex shedding has been the existence of a periodic force in a direction normal to the wind stream. The frequency of this force when the cylinder is stationary is given by a value of $S_N \approx 0.2$ in equation (1) but it appears that for an oscillating cylinder there are certain ranges of wind speed for which the cylinder oscillations themsevles control the frequency. Thus Parkinson has shown (Paper 18 - Ref. 2) that onset of oscillations can occur (if the structural damping is sufficiently small) when the Strouhal frequency equals the natural frequency of the cylinder and the instability which persists over a range of wind speed (which also depends on the structural damping) will do so with a frequency dominated by the natural frequency (Ω) and not by the Strouhal frequency (N) corresponding to the particular wind speed.

The assumed 1 to 1 relationship between successive bending oscillations at the natural frequency and the vortex shedding is given in Figure 3(a) but

Figure 3(b) presents alternatively a 3 to 1 relationship which could result in a lower critical wind speed. There is no experimental evidence for this known to the author although, as mentioned in (iii) below, higher harmonics of the Strouhal frequency are likely to be present which might produce an apparently lower critical wind speed than would correspond to a value of $S_N = 0.2$.

As well as lateral bending oscillations, it is possible, with lightly damped plain cantilevers, for significant vibrations to develop in the direction of the flow. These have been reported to occur at a frequency twice that of the lateral oscillations and this suggests that the periodic forces associated with vortex shedding can have a significant streamwise component. This may be explained as follows (reference [6]):

The force on a cylinder may be resolved into a mean (or time averaged) drag force in the direction of the flow and a periodically fluctuating force which does not act precisely across the direction of the flow but has drag and side force components (Figure 1). The fluctuating drag attains a maximum value every time an individual vortex is shed and hence has the same frequency as the shedding of single vortices. The crossflow force attains a maximum in one direction each time a vortex is shed from the other side, and therefore has the same frequency as the shedding of a pair of vortices, as shown in Figure 1(b). Thus the fluctuating drag force has twice the frequency of the fluctuating side force. The largest amplitudes in flow direction occur when $N = \frac{1}{2}\ \Omega$.

From the available data for the sub-critical regime it is clear that the cylinder response to fluid dynamic forces from vortex shedding is not strictly speaking a resonance effect since the cylinder motion alters the flow field significantly. The main conclusions for sub-critical flow are summarised in paper 37 of reference [2] .

(i) cylinder motions increase the circulatory strength of developing vortices,

(ii) cylinder motions increase the two-dimensionality of the flow field,

(iii) the dynamic lift contains higher harmonics of the Strouhal frequency,

(iv) striking flow field modulations can occur when the ratio of the shell natural frequency to Strouhal frequency is between 0.8 and 1.1 but not close to unity.

2.2.2 SUPERCRITICAL REGIME

Unfortunately most practical structures of interest operate at Reynolds numbers up to and into the supercritical regime and the data available for this region and the transition zone which precedes it have been rather inconclusive.

According to some research workers they have found a marked rise in S_N above $R_N = 2 \times 10^5$ such that a value of $S_N = 0.46$ occurred at $R_N = 1.5 \times 10^6$ whereas others have shown completely contradictory results with values of $S_N < 0.2$. Typical results are given in Figure 2 taken from reference [7] where it is asserted that it is questionable whether periodicity if vortex shedding still exists above $R_N = 2 \times 10^5$ and that only a wide frequency band turbulence occurs. The evidence presented in Figure 2 certainly indicates no discrete vortex shedding for $2 \times 10^5 < R_N < 1.5 \times 10^6$ but for $1.5 \times 10^6 < R_N < 3 \times 10^6$ one might deduce that there is progressive decrease in S_N from 0.46 to 0.2. This would mean that a structure of bending frequency Ω could experience a corresponding progressive increase in V_{cr} (since $V_{cr} = \Omega D/S_N$) with V and a continual condition of resonance of increasing severity, due primarily to the consequent increase in dynamic pressure. This condition of increasing amplitude with speed and no pronounced single critical speed has been quoted elsewhere as evidence for the absence of a discrete vortex shedding frequency but from the above argument that is not necessarily proven.

It is of interest that data has been presented by Chen [7] in Figure 2 for a value of $S_N \simeq 0.2$ in the supercritical region although he

proceeds to discount it based on his own experimental results.

The results of Fung [8] and Roshko [9] for a rigid cylinder have shown no discrete frequency in the broad turbulence spectrum for the transition range of Reynolds numbers although each spectrum in this range has a peak at a value of S_N which decreases in this range from 0.17 to 0.05. These values imply a low effective forcing frequency in a broad frequency band and if significant vibrations are to occur as a result the dynamic pressures must be sufficiently great and the structural damping sufficiently low and the possibility referred to earlier might then apply with the effective Strouhal frequency lower than the natural frequency (i.e. $N = \frac{1}{3}\Omega$). Roshko has also shown that a discrete frequency peak can occur for $R_N > 3.5 \times 10^6$ corresponding to $S_N = 0.267$.

It is believed that the probable main causes for the disagreements between various research workers are the differences in end effects and other three-dimensional effects and the fact that many of the cylinders tested have been rigid.

When the cylinder is not held rigidly but can interact with the flow it would appear that the correlation length can increase markedly when the phase of the vortex shedding is locked into synchronism along the entire cylinder by the cylinder motion itself.

The results of some recent experiments at N.P.L. reference [10] showed that the presence of a free end can have significant effects as the flow is entrained over the free end of the cylinder to pass down the leeward face thereby causing a thickening of the wake and a consequent decrease in the local vortex shedding frequency. This gives a wider spectral peak to the overall oscillatory forces. The lower vortex shedding frequency yields a value of $S_N \triangleq .16$.

3. VORTEX-INDUCED OSCILLATIONS

Two types of wind-induced oscillations of chimneys have been experienced in practice viz "sway" or cantilever type and "ovalling" (or more appropriately "breathing" in case $n > 2$). These can both be caused by periodic shedding of discrete vortices from the shell.

3.1 SWAYING OSCILLATIONS

The wind forces on a cylinder may be resolved into a mean drag force in the direction of the flow and a periodically fluctuating force which does not act precisely across the direction of the flow but has drag and side force components (Figure 1). The fluctuating drag attains a maximum value every time an individual vortex is shed and thus has the same frequency as the shedding of single vortices. The crossflow force attains a maximum in one direction each time a vortex is shed from the other side, and therefore has the same frequency as the shedding of a pair of vortices, as shown in the lower diagram in figure 1. Thus the fluctuating drag force has twice the periodic frequency of the fluctuating side force. Thus the streamwise vibrations are clearly caused by the stream-component of the vortex shedding periodic force at a frequency twice the lateral component.

The swaying oscillation of the chimney as a cantilever beam occurs primarily in a direction transverse to that of the wind and at the natural frequency in bending of the structure, although under certain conditions it is possible with lightly damped, plain, cylindrical cantilevers for significant vibrations to develop in the direction of flow. Experiments have shown that the onset of transverse bending oscillations can occur at a wind speed (V) at which the frequency (N) of the shedding of a pair of vortices, as determined by the expression $S_N = ND/V \simeq .2$ equals the natural frequency in bending (Ω) of the cantilever i.e. when $V \simeq 5\,\Omega\,D$. The instability persists for a range of wind speeds dependent on the amount of structural damping. The assumed 1 to 1 relationship between successive

bending oscillations and vortex shedding is given by Figure 3(a) but it should be noted that Figure 3(b) presents a possible alternative whereby there is a 3 to 1 relationship between the bending and vortex shedding frequencies resulting in a lower critical wind speed.

3.2 OVALLING OSCILLATIONS

Ovalling oscillations have also been experienced on various chimneys as reported by Scruton (Paper 24 of Ref. [1]); Johns and Allwood (Paper 28 of Ref. [3]). From such results it has been suggested by several workers that the ovalling occurs at a wind speed such that a 2 to 1 relationship exists between the ovalling natural frequency and the vortex shedding frequency, see Fig. 4(a). However, this assumption has been questioned in paper 28 of Ref. [3] and Fig. 4(b) shows that a 4 to 1 relationship is also possible, if the axes of ovalling do in fact remain orthogonal with the wind direction. Figs. 4(c), (d) show that a 1 to 1 or 3 to 1 relationship is possible if the axes of ovalling mode are oriented at 45^{o} to the wind direction. Thus instead of the previous 2 to 1 relationship Fig. 4 shows a possible 1 to 1, 2 to 1, 3 to 1 or 4 to 1 relationship and even higher relationships are possible from the same argument. If r is the value of this critical relationship and $S_N = 0.2$ or 0.16 the critical wind speed is given by either

$$V \simeq 5\ \Omega D/r \qquad \text{or} \qquad V \simeq 6\ \Omega\ D/r \qquad (2)$$

where r = 1, 2, 3, 4,...., signifying progressively lower critical ovalling wind speeds. The lowest actual critical wind speed would depend upon the structural damping present and on some parameter such as the ratio of aerodynamic and structural stiffness. The results for the full scale chimney described in paper 28 of Ref. [3] indicate a value of r = 1 as being most likely rather than the value of r = 2 reported earlier.

Figs. 4(c) and (d) are based on the possibility that the axes of ovalling mode are <u>not</u> orthogonal with the wind direction but are aligned with the axes of resultant periodic surface pressure distribution which are not necessarily orthogonal to the wind.

Evidence for this latter possibility is given by the fact that significant streamwise swaying oscillations are possible at a frequency twice that of the lateral oscillations Ref. [6] and by the form of the measured pressure distribution shown in Paper 28 of Ref. [3] which is seen to have a resultant close to a line 135^{o} from the stagnation line.

As will be discussed later the tests in the wind tunnel on model stacks confirm the possibilty of various critical relationships as well as the orientation of the axes of the ovalling from the wind direction.

4. WIND-TUNNEL TESTS

Wind tunnel studies have been made at Loughborough University of Technology on model stacks of different geometries to study the frequency pattern critical wind speeds, the critical mode and its orientation to the wind direction to determine the degree of correlation with theoretical predictions.

4.1 DESCRIPTION OF THE WIND TUNNEL

The tunnel is of open jet working section 42 in. long by 34 in. wide. Its maximum output in the effective range is a wind velocity of 102 ft. per sec. at atmospheric pressure. The photograph of the test section can be seen in the Figure 5.

4.2 CONSTRUCTION OF THE RIG AND MODELS

A circular steel plate, with provision to take thin shells of diameter 4.8 in., 8in., 12in., was made. To ensure stability this was attached to a fixed steel base as shown in photograph in Figure 5. Removable thick steel rings were made to fix the bottom end of the shells of different diameters.

To start with, the idea of attempting machining circular cylindrical shells from tubular stock material, was conceived. This method had the advantage of avoiding any seam discontinuity or joint in the shell. The disadvantages that led to the abandonment of this idea,, are that it is restricted to relatively small diameters; is very difficult to hold an acceptable tolerance on the wall thickness dimensions for thin shells, and above all it is quite expensive.

Subsequently, a successful attempt was made in forming circular cylindrical shells from flat rolled sheet stock. The initial sheet stock can be obtained with very good tolerance on the thickness dimension. This sheet is then rolled into desired form and joined by one or two seams along a generatrix of the shell. The size or the diameter of the shell is not restricted as in case of machined shell. Complete shell models are relatively inexpensive. There are some discontinuity effects at each seam (as discussed later) but these are considered to be minimal. Some non-circularity effects are also present. Constructional technique is pictured in Fig. 14.

4.3 INSTRUMENTATION

The detection and identification of vibratory modes in thin shells has been a problem for experimentalists for years. The contact type sensors very frequently influence the modal preference and for mobile probes can cause modal rotation. Surface strain measuring techniques have been affected by the large amplitude of vibrations which resulted in the breakage of the ordinary strain gauges. Special strain gauges were used to detect the signal of the oscillating chimney model in the tunnel.

The electronic equipment used in the test is shown in Figure 5. A schematic representation of this type of instrumentation, as used in the present investigation is shown in Figure 6.

The strain gauge output goes through a strain gauge bridge and operational amplifier, connected with a d.c. power supply unit (20 volts), and goes as input into the wave analyser and a double beam CRO. Wave analyser is used to measure the correct frequency in Hertz.

Since there was no direct scale to measure the wind velocity, the equipment shown in Figure 7 was used for this purpose. The pitot-static tube shown in Figure 5, with its end facing into the wind is connected with the manometer. The differential pressure in inches of water is noted here and the formula

$$\tfrac{1}{2} \rho_A V^2 = \rho_w g h_w \sin \alpha \qquad (3)$$

where

ρ_A is air density
V is wind velocity
ρ_w is density of water
g is acceleration due to gravity
h_w is difference in the height of water level in two tubes
α is angle of inclination of manometer tubes.

If h_w is in inches and $\rho_A = .00238$ slugs/ft^3, $\rho_w = 1.94$ slugs/ft^3, $g = 32.2$ ft/sec^2, $\alpha = 30^0$ the formula (3) reduces to:

$$V = \sqrt{2184\, h_w} \text{ ft/sec} \qquad (4)$$

The control box on the right is provided to switch the wind tunnel on and off and to control the wind speed. The maximum wind speed which can be achieved in this tunnel is 70 miles/hour or 102 ft/sec.

4.4 GENERAL TEST PROCEDURE

The general test procedure was as follows:

1. The wind speed was slowly increased until a maximum oscillatory signal was obtained from a strain gauge.
2. Since the circumferential mode number n is of the order of 1 to 4 in the case of tall shells, it was determined by visual observation.
3. The model frequency was determined by using the wave analyser
4. Wind speed was determined by noting the differential pressure in inches of water and using formula (4)
5. Wind speed was again increased to find the other modes.

5. MODEL EXCITATION BY SHAKER

5.1 RIG DESCRIPTION

To start with the experimental rig shown in Figures 8 and 9 was designed. It has 3 thick steel rings of diameters 12", 8", 4.8" fixed to the wooden base which can take shells of respective diameters. The motion sensing device is mounted on the screwed rod supported by the assembly of four vertical rods fitted at the centre of the rig. The circumferential and vertical traverse is made possible by the two wheels shown in Figure 9 which are handled manually. The model stack is mounted on this rig with its lower end clamped onto the base ring with the help of another 3" wide steel ring which can be tightened as required to ensure a clamped end.

5.2 EXCITATION SYSTEM

The energy input device to the shell was originally an acoustic exciter since this type is non-contacting which was thought to have advantage. This was later replaced by an electromechanical shaker (seen sitting in Figure 9). The shaker was not attached to the shell but allowed to rest against it. In this configuration it was found that a more uniform vibration pattern was produced with all the antinodes vibrating at equal amplitude. The shaker is powered by an oscillator and amplifier. The oscillator is a precision decade oscillator (shown in Figure 10, Muirhead-Wigan type D-890-A Decade Oscillator) which can be varied in 0.1 Hz steps making the detection of the resonances more accurate. The amplifier (see Figure 10) used has a 50 watt output which directly powers the shaker.

5.3 RESONANCE DETECTION SYSTEM

In this case several motion sensing devices were tried and abandoned for one reason or the other. A few are stated as follows:

For shell which is not circular the instrumentation system if non-contacting will have a variable gap circumferentially which implies tedious calibration problems. If the non-circularity is pronounced an

instrument to be traversed circumferentially has to have its minimum gap where it most closely approaches the shell with a consequent large gap elsewhere. Apart from calibration problems - this large gap may cause non-linearity and considerable weakening of the signal.

Thus the capacitance device suffers from its size or its small linear range, the pressure transducer responds too well to the acoustic excitation system initially used and thereby makes it difficult to distinguish the shell vibration modes. The mechanical (contacting) excitation system has removed this last problem and so the pressure transducer was developed and used.

A further alternative scheme considered and tried without success was the Doppler radar device, but this also suffered from the shell's non-circularity and has been abandoned.

For the present system the equipment used is shown in the Figure 10 and a schematic representation of this resonance detection system and excitation system is shown in Figure 11. The inside of the shell is scanned with a microphone (Acos MIC 43-3) mounted in a perspec holder. This microphone was used finally in preference to any other because of its small size, cheapness and availability. The inlet to the microphone of signals due to the shell wall vibration is via a one inch long, $^1/8$ inch diameter bore steel tube. This tube is to confine to a smaller area of the portion of the shell being monitored. The electric output from the microphone is fed to the input of a double beam CRO and a wave analyser (see Figure 10) via a screened cable. The wave analyser filters the input at the excitation frequency and by careful tuning the exact vibration frequency can be determined. The instrument is fitted with a pair of output terminals which monitor the filtered signal. The output goes through an amplifier to a chart recorder which gives the number of circumferential waves when the shell is scanned by travelling the microphone circumferentially.

The attempt has been made to make all tests as definitive and sophisticated as possible, e.g. to perfect the instrumentation system so as

to measure circumferential and axial modes of vibration both under mechanical vibration and wind excitation. The observed results of the tests have been compared with the predicted results in later sections

5.4 GENERAL TEST PROCEDURE

In this case also the general test procedure was as follows:

1) The oscillator frequency was slowly increased until a maximum signal was obtained from the microphone.
2) Longitudinal wave number, m, was obtained by traversing microphone vertically with the help of the wheel shown in the right of Figure 9.
3) Number of circumferential waves, n, in the case when it is small can actually be counted just by viewing the top of the vibrating model stack. In the case when n is large the circumferential scanning is done by the microphone and the value of n is counted on the chart recorder. Alternatively voltage readings on the wave analyser scale can be taken while scanning circumferentially. Nodes and antinodes correspond to minimum and maximum scale readings, but one has to be very careful in this case because due to shell irregularities when the signal is very weak the difference between two readings (i.e. maximum and minimum) is so small that it may be overlooked.
4) The model frequency is determined by proper tuning of the wave analyser.
5) The measure of inherent structural damping is also obtained experimentally by using the wave analyser which will be discussed later.
6) The degree of clamping afforded by the base rings (Figure 13) was checked several times during the test as it was known that less than a fully constrained base might give spurious results.

6. COMPARISON OF EXPERIMENTAL AND ANALYTICAL RESULTS:

Table 1 shows the geometrical and structural properties of the models tested in the wind tunnel and by excitation with an electrodynamic shaker. A notation for the cylinders tested in the wind tunnel is recognised by putting letter 'T' before the number whereas for the shells tested with the electrodynamic shaker the letter 'S' precedes the number of the shell. Most of the models tested were made out of aluminium alloy because of availability. Two model steel stacks were also tested, one in the wind tunnel and the other by exciting with electromechanical shaker. In the following sections discussion is given on the values of the frequency parameters and mode shapes for different models.

6.1 MODEL SHELL EXCITATION BY SHAKER: RESULTS

As described in section 5 the model stacks were mounted on the rig shown in figures 8 and 9 and excited by an electrodynamic shaker powered by an oscillator and amplifier. The frequencies corresponding to different mode shapes, i.e. axial wave number m and circumferential wave number n have been determined and they are correlated with the corresponding results predicted by the present theory reference [4] . The first three fundamental axial modes i.e. m = 1, 2, 3 have been taken and associated with each of these are various values of circumferential wave number n, i.e. n = 0 (axisymmetric mode), n = 1 (swaying mode), n = 2 (ovalling mode) and n >2 (breathing modes). The calculated values of the frequencies are given for m = 1, 2, 3 and n varying from 0 to 10 for each m. The measured frequencies are given wherever possible. Experimental structural damping has also been measured. The procedure for the same is as follows:

6.1.1. MEASUREMENT OF EXPERIMENTAL STRUCTURAL DAMPING:

The structural damping of the shell is measured as shown in the diagram given here. The relative deflection X_{max} and frequency Ω are measured on the wave analyser with scales shown on the left and right respectively. The wave analyser is seen sitting on the top of double beam CRO in figure 10. Then the frequency is reduced to Ω_1, such that the net deflection now becomes $\frac{1}{\sqrt{2}} \times X_{max}$. In the same way the frequency then is increased from Ω to Ω_2 to give net deflection equal to $\frac{1}{\sqrt{2}} \times X_{max}$. Then if $\Omega_2 - \Omega_1 = \Delta\Omega$, the measure of structural damping,

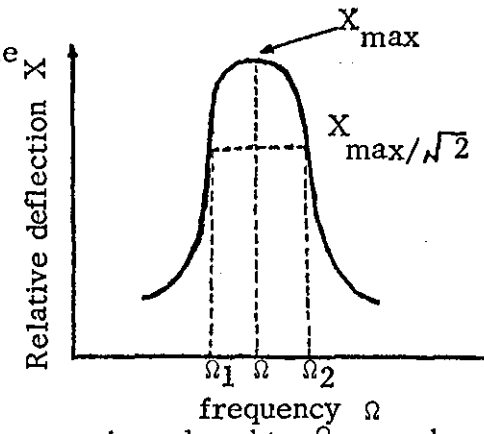

$$g = \Delta\Omega / \Omega \qquad (5)$$

This can also be given in terms of critical damping ratio $\xi = g/2$. In the tables it is given in terms of percentage i.e. g x 100.

6.1.2 MODEL SHELL ANALYSIS

Model shell SI is considered in table 2. The calculated analytical frequency is compared with the measured frequency. Measured frequencies are the ones which could be found by exciting the shell. The agreement seems to be quite good. The maximum difference in the calculated and measured frequencies is within 10%. The axisymmetric mode could not be excited because of its high frequency; neither could the sway mode i.e. bending oscillations. For higher values of n, the frequencies corresponding to axial wave numbers m = 1, 2, 3 interfere with each other and distinction becomes almost impossible. It was observed that for lower frequencies corresponding to n = 2, 3, 4 the amplitude was significantly big but for higher values of n the amplitude was small as expected. The structural damping for all the cases corresponding to various m's and n's

is fairly uniform and its value (in terms of g) lies between 2% to 2.5% as seen in table 2. Fig. 15 shows results for various modal frequencies.

An attempt was made to increase the structural damping of this shell by spraying a 0.005 in. thick coat of self applied polyvinyl plastic coating Vy coat CA 90. The corresponding results for this shell are given in table 2 marked with asterisks. It is seen that these results tend more to decrease the frequencies than to increase the structural damping coefficients. In other words this added "damping" probably does more harm than good by decreasing the frequency with a negligible increase in the structural damping. The decrease in frequency is caused probably by the added mass of the polyvinyl coat. To quote the advantages of this process, it was observed (which is obvious in table 2) that some interference between the various modes was stopped and it was possible to find a few more frequencies corresponding to higher values of n and m = 3 which were not possible for the original shell. Since the coating was black the reflections from the surface showed quite beautifully the number of axial and circumferential waves which could then be counted by looking at the shell.

Table 3 shows the comparison of analytical and experimental frequencies of model shell SII. This is the shell which is shown in photographs in figures 8, 9 and 12. In this case it was possible to get quite a number of frequencies experimentally. The comparison here is very good. The maximum difference is about 2%. In some cases the measured frequency is a little higher than the predicted one but the trend is fairly consistent. For m = 1, the frequencies corresponding to n = 2 - 6 could be traced, for m = 2 those corresponding to n = 3 - 7 and for m = 3 corresponding to n = 4 - 9 could be traced. Fig. 16 shows results for various modal frequencies.

The circumferential nodal pattern for this shell is seen in the photographs of figures 17 and 18. Figure 17 shows the number of circumferential waves to be 3 (or 6 half waves) whereas figure 18 show n = 4 (or 8 circumferential halfwaves). Deflections are quite substantial as seen in these pictures and they decrease with n. The good agreement between theory and

experiment as is evident in table 3 over the entire test ranges of m and n value is perhaps due to the fact that shell SII was very well constructed and probably much better than shell SI. In this case the interference between any two modal frequencies was not appreciable as in case of shell SI and that is the reason why quite a few frequencies could be traced. These tests as in every other case were repeated three times and experimentally observed frequencies were identical in all the cases. It was essential to ensure that the base of the model is perfectly clamped to ensure axial constraint which is a very important boundary condition affecting the frequency.

Table 4 is the table of values of frequencies and structural damping for the model shell SIII. As is seen on the table 4, not many frequencies were traceable but the agreement otherwise appears to be satisfactory. The difference in the analytical and measured values varies from 5 to 10 percent. It is seen that the agreement becomes less good for the higher modes.

This shell was also sprayed with polyvinyl coat (Vy coat CA90) for the purpose of increasing structural damping. The layer was 0.01 in. thick. Again it was found as in the case of model SI that this process decreases frequency as much as 8% in some cases but the structural damping is not very significantly increased. The coating also reduces the amplitude of vibration and due to this fact not many frequencies were traceable as is obvious in table 4.

Shell model SIV is analysed in table 5. The agreement between the predicted and measured values seems to be reasonable. The calculated minimum frequency for the first fundamental axial mode (m = 1) corresponding to n = 2 is nearly 8% higher than the observed frequency. Otherwise, for all m i.e. m = 1, 2, 3 and associated n values the agreement is fairly satisfactory, the difference being only of the order of 5%. It was observed that as we increase the number of circumferential waves, n the mode preferred is that due to higher axial wave number e.g. for m = 1, 2 and n = 4, the amplitude was bigger for m = 2 than m = 1. Of course this is a

case when two modal frequencies are not very much different from each other.

Model SV, which is made up of .028 in. thick steel, can be compared to the similar aluminium model SIII where the thickness was .030 in. The frequencies are more or less the same because the ratio ρ/E is nearly the same in both the cases, as seen in table 6.

Here also the agreement is reasonable. The minimum frequency for m = 1 corresponding to n = 2 gives the worst agreement. The measured and analytical values differ by about 12%. The modes higher than n = 5 could not be detected in the present system.

Based on the detailed results presented in these tables, it is possible to gain a more general insight into the vibration characteristics of clamped-free cylindrical shells. Frequencies corresponding to the axisymmetric case are generally very high in all cases. The swaying (n = 1) frequency is also high and it was not possible to excite this with the help of the electrodynamic shaker. Ovalling frequency (n = 2) for m = 1 is minimum for all shells except SI where the frequency associated with n = 3 is minimum. For the higher axial modes i.e. m = 2, 3 the number of circumferential waves n corresponding to the minimum frequency increases. For example for shell SI the minimum frequencies for the three axial modes m = 1, 2 3 correspond to the number of circumferential waves n = 3, 4,5 respectively and for shell SV for m = 1, 2, 3 minimum frequency corresponds to n = 2, 3, 4 respectively.

6.2 MODEL TESTS IN THE WIND-TUNNEL

6.2.1 GENERAL

The most direct and reliable assessment of the wind-induced oscillations of tall chimney stacks is to be derived from model tests in wind tunnels. However it is seldom that a wind tunnel test can be devised in which all the relevant parameters can be correctly represented and this results in the uncertainties in the interpretation of the test results.

Some of the models used are oscillatory replicas of the full scale stacks with structural and dynamic properties correctly scaled so as to correspond to the full scale in the wind. In addition to model properties, the properties associated with the wind (Reynolds number, shear and turbulence) should also correctly be represented in the tunnel airstream. These similarity requirements are too severe for all to be observed in practice and necessary relaxations introduce uncertainties in the results.

Nevertheless, model tests do provide useful indications, and while not always providing reliable quantitative predictions, they allow development work on the prevention of wind-induced oscillations with reasonable surety that a design which does not exhibit any form of instability in the wind tunnel will be satisfactory in the full scale.

6.2.2 WIND TUNNEL TESTS: MODEL ANALYSIS

Wind tunnel model studies have been made in the Loughborough University Open Jet Wind-tunnel. The geometrical and structural properties of these shells are given in table 1. The description of the tunnel and its associated equipment is given in the section 4.

Based on the theoretical vibration results the models were designed to be excited in various modes according to equation (2).

Model Stack TI (L/a = 8.3) was designed to be excited by the wind in the modes n = 2 and n = 3 because the frequencies for these two modes are approximately the same. It was observed oscillating in the mixed mode (n = 2, 3) with considerable amplitude as given in table 7 . A value of $r \approx 3$ was obtained (cf. equation 2).

Stack TII (L/a = 15) was designed only to vibrate in the ovalling mode (n = 2). As seen in table 8 the frequency of oscillation is very close to that predicted and a value of $r \approx 3$ was again obtained in this case. This ovalling mode persisted with increase in wind speed and it was not possible in this wind tunnel speed range to excite any other mode.

Stack TIII (L/a = 25) was designed in such a way that the swaying frequency and ovalling frequency were very close to each other

and it was expected that they might be excited simultaneously but table 9 shows that ovalling commenced first at a wind speed of 39 fps with a value of $r \approx 3$. Afterwards at a wind speed of 59 fps and value of $r \approx 2$ the swaying mode (n = 1) is excited. At a wind speed of 64.5 fps the n = 3 mode was excited with an approximate value of $r \approx 5$.

It is seen that the measured frequencies in the case of ovalling and breathing (n = 3) agree well with those predicted; the difference being of the order of 4-5 percent. The swaying mode predicted frequency is nearly equal to the measured value. Also the seam position affected the preferred mode orientation though not its frequency. This was apparent when after 3 tests the shell developed a crack near the seam due to fatigue and started ovalling with axes at 45° to the wind. The amplitude grew much larger and the frequency was reduced. This was true for the n = 3 case also.

The model stack TIV, when in the tunnel, behaved in a very interesting manner. The shell started ovalling at a wind speed of 33.2 fps with axes of oscillation being 45° to the wind direction as shown in the photograph of figure 19. Table 10 analyses the behaviour of this model in the wind. As is obvious the first ovalling commenced at a value of $r \approx 3$ confirmed by figure 3(d). This was also observed by Johns and Allwood in paper no. 28 of reference [3] . The justification they gave was that the predicted orientation given in figures 3(c), (d), is suggested by some measurements taken at N.P.L., of the unsteady pressures acting on a circular cylinder during vortex shedding. These show that the effective centre of pressure of the circumferential distribution acts on the leeward face of the cylinder close to a line 135° from the stagnation line.

But as the wind speed was increased a gradual change in the direction of axes was observed. At a wind speed of about 66 fps the change was complete and the axes of oscillation were orthogonal to the wind direction as is evident from the photograph in figure 20. In this case the value of $r \approx 2$ is obtained as predicted in figure 3(a) when the axes are orthogonal.

In this case as seen in figure 20 the amplitude of oscillation was considerably big. This perhaps caused the observed reduction in frequency by about 2 Hz from the previous case when ovalling axes were at 45^{o} to the wind. This was also observed by D.A. Evensen [11] while dealing with the effect of non-linearity on the vibrations of infinitely long cylindrical shells. He remarks that in the case of both inextensional and extensional vibrations the vibration frequency should decrease with amplitude.

The reduction in frequency may also be attributed to the following factor. In the 3rd test the shell started tearing down its length parallel to and near the seam. The split was about 6" - 8". This is evident in the photograph of figure 20 by a corner in the right if one faces the wind. After splitting the shell started ovalling with axes orthogonal to the wind at a comparatively lower windspeed of 60 fps and frequency 41 Hz. Part reduction in frequency may be due to the fact that the torn shell was less stiff. It can be remarked at this stage that the frequency reduction was probably due to the combined effects of non-linearity due to large amplitudes in the vibrations and of flexibility due to vertical split.

At a wind speed of about 85 fps the swaying was observed but the amplitude was not very big. Swaying also commenced but not very clearly inbetween the two stages of ovalling described above. It is seen from the table 10 that the predicted and measured frequency compare quite well. The difference being of the order of 4 to 6 percent.

To account for the effect of structural damping on the wind induced vibrations an attempt was made to increase the damping of model stack TIV by spraying on a .005" thick coat of polyvinyl (Vy coat CA 90). During the tunnel test this coated stack started ovalling with axes at 45^{o} to the wind at a slightly increased wind speed of 40 fps and reduced frequency of 40.8 Hz as compared to the plain stack TIV where the corresponding wind speed and frequency were 35 fps and 43 Hz respectively. At a wind speed of about 51 fps the amplitude grew quite big (about $\frac{3}{4}$") and the frequency came down to 40.4 Hz. At a wind speed of 65 fps the ovalling amplitude became

quite small. As the wind speed was increased the shell began to oscillate in the sway mode (n = 1) with a fairly big amplitude of about .8 in. contrary to its counterpart shell TIV which had then begun to oval again with axes orthogonal to the wind at a speed of about 66 fps. The sway frequency of this coated shell was measured as 31.6 Hz as compared to 33 Hz of the plain shell. The amplitude of swaying grew quite large with increases in wind speed to 75 fps. At a wind speed of about 85 fps the amplitude started to decrease and the shell virtually stopped swaying at a wind speed of about 92 fps. The shell was almost flattened on the windward side at a wind speed of 99 fps due to the high static pressure there.

Summing up one can see that the coating has not been very effective in stopping the ovalling or swaying or even in bringing down the amplitude of the vibrations for that matter. However it has changed the way in which the shell behaved in the wind compared to the plain shell.

In the second attempt to damp this shell .005" thick white Fablon was stuck over this pvc coated shell. This model then was mounted in the tunnel. As the wind speed was increased this shell did not oval (n = 2) at all and at a wind speed of about 78 fps swaying oscillations (n = 1) were observed with very much decreased amplitude of about .25 in. compared to .8 in. for the pvc coated shell. At the top speed of the tunnel of about 100 fps the shell windward region distorted about 0.5 in. from a circular cross-section to an elliptic one.

The natural frequency (ovalling) was found for this shell by storing its transient response on to a storage oscilloscope. This frequency was found to be $\approx$38.1 Hz as compared to 40.8 Hz of pvc coated and 43 Hz of plain shell TIV.

In summing up it can be said that this fablon wrapped shell has completely eliminated the ovalling (n = 2) mode. Fablon has only added to the inertia and damping of the system but not to the stiffness, which can be inferred from the reduced natural frequency of 38.1 Hz. This has also decreased the amplitude of the swaying oscillations by about 75 percent.

The increased damping may be due to the viscous adhesive on the Fablon because painting with pvc did not make much difference, either in stopping the ovalling or in reducing the amplitude of the oscillations.

Table 11 gives the results of the tunnel tests compared with predicted results for the model stack TV. It was designed to oscillate in the modes n = 2 and 3. At the wind speed of 40.5 fps the shell oscillated in a breathing mode with n = 3 and at a wind speed of 56 fps the amplitude for this mode dies out. As the wind speed was increased the shell started ovalling at 60 fps wind. It was observed that $r \approx 5$ (reference equation (2)) in both these cases.

Model stack TVI analysed in table 12 was designed so as to have ovalling (n = 2) and breathing with n = 3 frequencies nearly the same, as can be seen from the predicted frequencies. It was expected that the shell would oscillate with mixed modes i.e. n = 2 and n = 3 at the same time. But in the test the breathing (n = 3) commenced first at about one fifth of the predicted critical wind speed (i.e. at $r \approx 5$). The wind speed was 38 fps. As the wind speed was increased the shell was trying to vibrate with n = 2 and n = 3 at the same time and at 59 fps the stack ovalled at the value of $r \approx 3$. As is obvious in table 12 the predicted and measured frequencies are very close to each other the difference being of the order of 2 to 3%.

The effect of seam was also observed on this shell. This shell had two seams 180° apart. The above test was carried out when the two seams were in the wind direction. In a second test seams were placed 90° to the wind direction. This change in position did not affect the frequencies but there was a slight increase in critical wind speeds e.g. from 38 to 44 for n = 3 mode and from 59 to 65 for n = 2 mode. This may be remarked that although ovalling (n=2) frequency was lower than the n = 3 mode the n = 3 mode was excited first and the n = 2 mode next.

Table 13 examines model stack TVII in the wind tunnel. The model was designed to oscillate first with the n = 2 mode and then with the n = 3 mode. At a wind speed of about 30 fps the shell started ovalling.

Ovalling persisted with increasing wind speed and the amplitude of the oscillation grew bigger and was maximum at a wind speed of about 36.4 fps causing a slight drop in frequency (from 23.2 to 22 Hz) due to a non-linearity effect as in reference [11] . A value of $r \approx 3$ applies in this case. As the wind speed is increased the amplitude of ovalling decreases and at a wind speed of about 52 fps the n = 3 mode appears and the amplitude grew big reaching a maximum at a wind speed of about 60 fps causing again a drop in frequency of about 1 Hz. The shell was nearly flattened on the windward face and the strain gauge was broken at this point. In the case of ovalling the seam appeared to force a node at itself though not a preferred position.

Model shell TVIII which is discussed in table 14 was designed to oscillate at various circumferential modes n = 2, 3, 4. At a wind speed of about 25 fps and $r \approx 5$ the mode n = 3 was excited. At an increased wind speed of about 35 fps the shell started ovalling though the amplitude was not very big. The ovalling axes were orthogonal to the wind direction with $r \approx 4$ approximately.

At a wind speed of about 38 fps the shell was oscillating with n = 4 and a value of $r \approx 5$. Increasing wind speed caused a sudden change. At 45 fps wind the shell reverted back to a n = 3 mode, $r \approx 3$, with amplitude considerably large. The frequency of oscillation was decreased from 22.4 to 19 Hz due perhaps to a non-linearity effect. The shell was nearly flattened at the windward face as the speed was increased. The predicted frequencies were very close to measured values as seen in the table 14. The maximum difference was of the order of 8%.

The steel shell TIX, counterpart if the Al-shell TV is examined in table 15. This behaved quite differently. The oscillations in the n = 3 mode occurred at a considerably higher speed of 72 fps ($r \simeq 3$) instead of 40 fps ($r \approx 5$) for the Al-shell. This then persisted for higher wind speeds and at 81 fps the amplitude grew bigger and there was a drop in frequency from 58 to 56 Hz. The ovalling mode could never be excited on this shell unlike the case of the Al-shell TV. This was perhaps due to differences in material

properties, especially the inherent structural damping. The frequency measured was very close to predicted frequency as seen in table 15.

To study the effect of an elastic ring at the top end of the shell a ring of dimensions b_R = .125 and d_R = .125 was stuck on the top of the shell TIII. This resulted in eliminating ovalling oscillations. The swaying occurred at a slightly reduced frequency (49 Hz from 50 Hz) at a slightly higher wind speed of about 65 fps than the shell TIII. The breathing oscillations (n = 3) were observed at a wind speed of 72.5 fps instead of 64.5 fps and the frequency is increased from 119 Hz to 124.6 Hz. Thus as predicted by putting an elastic ring lowers sway frequency because of the inertia of ring being predominant for the sway mode. But the frequency for breathing oscillations (n = 3) is increased because of predominant ring stiffness.

6.2.3. WIND EFFECTS ON SHORT SHELLS

An attempt was made to measure the frequencies excited by wind of short shells typical of storage tanks. Some tests were being performed on such shells under another research programme to examine their static stability in the wind. It was found that before buckling the shell oscillated with a very small amplitude of vibration. The frequencies of these shells were measured by strain gauge output as in case of the other models tested. However the output was recorded on magnetic tape and analysed to give the frequencies. For example two such shells are analysed below:

Geometry of the first model was L = 15 in., a = 7.5 in. and h = 0.01 in. At a wind speed of about 58 fps the measured frequency was 102 Hz whereas the corresponding calculated minimum frequency for this shell geometry was 108 Hz for n = 7. The value of r is approximately of the order of 12 - 14 ". Another frequency excited was 115 Hz at a wind speed of 74 fps and the corresponding calculated frequency was 120 Hz for n = 8. The value of r is then either 10 or 12. As is evident calculated values are only about 5% higher than measured ones.

The second shell tested had a geometry defined by L = 18 in.

a = 7.5 in. and h = 0.01 in. This was excited at a wind speed of nearly 80 fps and at a frequency of 90 Hz. The calculated minimum frequency in this case was 89 Hz for n = 6 which is very close to the measured value. The value of r is then either 7 or 9 (approximately). At a wind speed of 85 fps the frequency recorded was 94 Hz as compared to 95 Hz by calculations for n = 7. The value of r is about 7 or 9 in this case also.

The above examples show that the present vibration theory is suitable for predicting the frequencies for tall stacks and also for short shells representative of storage tanks. However the significance of the parameter r in the latter case is questionable and it may be argued that the vibrations experienced on the short shells were due to either free stream turbulence or unsteady pressures generated near to the free end of the short shell. It is noteworthy though that the excited frequency did appear to increase linearly with increase in wind speed suggesting a form of Strouhal Number relationship. Since these results for wind-excited oscillations are thus inconclusive the only conclusion to be fairly drawn is that the present vibration theory applies to shells of $L/a > 2$.

6.3 PREVENTING INSTABILITY BY STRUCTURAL MEANS

In a previous section it was shown how a fablon coated model stack reacted to the wind. This in fact resulted in completely cutting down the ovalling and very significantly reducing the amplitudes in swaying oscillations.

In general it may be remarked that if the critical wind speed in the lowest mode of oscillations can be increased above the wind speed likely to be encountered during the lifetime of the chimney stack, large amplitudes of oscillations will not occur. A design wind speed based on a short term gust speed may be an over-estimate of the maximum speed that a structure will respond to, since it takes a few cycles of oscillations for the amplitude to build up. Another way of increasing critical wind speed is to increase the frequency of stack by stiffening it with the help of many intermediate rings. The effect of such stiffening may be seen theoretically in the figures 17 and 18

of reference [4]. But increase in the ovalling (n = 2) and some breathing ($n \geq 3$) frequencies is very significant as can be seen in these figures.

It should be noted, however, that increasing the mass of the structure may not always be beneficial if it is subjected to vortex instability. Because inertia effect reduces the natural frequencies and consequently the critical wind speeds, thus making it possible that addition of mass may reduce the critical speed in a certain mode from a level outside the design wind speed range to a level within it.

There are several methods by which the structural damping may be increased. Active mechanical dampers produce a force on the structure that opposes the aerodynamic force. A sensing device fitted to the structure activates the mechanical force. Such a system is likely to be complex and to need continual maintenance.

There are several types of simple passive dampers, which absorb energy rather than produce an opposing force. Tuned and direct viscous and friction dampers have been employed and are notable for durability and cheapness. An interesting system consists of a chain, covered with rubber sleeve and suspended with freedom to impact against a vertical channel. This is fitted near an antinode of vibration of structure to have maximum effect.

The addition of guys to a free standing structure may not only increase the natural frequencies but will usually increase the structural damping.

It is often possible to design structures from the outset to have a high structural damping. The addition of gunnite lining, for example, to a steel stack increases its structural damping. In general, concrete, and particularly brick structures, have a higher structural damping than steel structures, and riveted or bolted construction has more damping than welded.

The helical strake device has been applied successfully to many stacks. The most effective system consists of three thin, rectangular strakes with a pitch of one revolution in 5 D and height of 0.10 D to 0.13 D. It is usually sufficient to strake only the top one third of a stack to prevent

instability in the fundamental mode. It should be noted that fitting of a small external duct to the outside of a straked stack may impair the efficiency of the system. The addition of strakes sufficiently increases the drag of the cylinder at Reynolds number above the critical. Strakes have also been used to reduce the oscillations due to enhancement of vortex instability caused by buffet.

An alternative to the strake is provided by the fitting of a shroud. This consists of a perforated cylindrical shell separated from the cylinder surface by a gap. A gap width of 0.12 D and an open area ratio of between 20 and 36% have been shown to be effective. Shrouds, like strakes, need only be fitted at anti-nodes of the vibration mode.

The devices were tried and have been patented by N.P.L. and more about them can be found in references [10, 12] .

7. CONCLUSIONS

The study covers the wind-tunnel studies and shaker excited vibration tests on model circular stacks. The test results are compared with analytical results calculated by using variational technique in Part A. The shell models were made of Al-alloy and a couple also out of steel. The structural damping of the model stacks has been measured experimentally. The attempt has been to increase the structural damping by spraying a thin coat of polyvynil paint on the model and also by using .005" fablon wrapped round the shell.

From the observations of this study following conclusions appear to be valid:

1. Good agreement between theoretical and test frequencies has been observed.
2. It has been observed from model tests that for swaying and particularly ovalling and breathing oscillations the measured critical wind speed is lower than predicted wind speed, $V = 5\,\Omega\,D$ for full scale. In fact it is $V = 5\,\Omega D/r, r = 1, 2, 3, \ldots$. It may be due to incompleteness in similarity requirements, such as structural damping, material difference, in the model tests and full scale experience.
3. A change in the direction of axes of oscillation to the wind can occur as the wind speed is increased. In case of ovalling it has been observed for a particular shell that first axes are at 45° to the wind at a value of $r \approx 3$ and then they change direction orthogonal to the wind at $r \approx 2$.
4. An increase in amplitude causes a slight reduction in frequency because perhaps of non-linearity effects.
5. The structural damping is not a function of mode shapes and was observed to be nearly the same for Al and steel stacks for measured range. Fablon coated model appeared to be significantly damped because it eliminated ovalling and reduced the amplitude in swaying by about 90% with a slight reduction in natural frequency due, perhaps, to the added mass.

6. Al elastic ring at the top controls ovalling (n = 2) but breathing oscillations (n = 3) did occur at a slightly raised wind speed and natural frequency.

7. It was found by the test performed later that there was only a very small increase in the structural damping of the shell due to fablon but perhaps enough to stop ovalling and reduce amplitude of oscillation for other modes (n = 1, 3 etc.). It may, however, be remarked that the method of measuring the structural damping was not sensitive enough and an error of $\pm$ 30% is possible to be incurred.

REFERENCES

1. Anon — Wind Effects on Buildings and Structures, Symposium No. 16, N.P.L., Teddington, England (Published by H.M.S.O.), June 1963.
2. Anon — Wind Effects on Buildings and Stru ctures, International Research Seminar, N.R.C., Ottawa, Canada (Published by Univ. of Toronto), September 1967.
3. Johns, D.J., Scruton, C. Ballantyne, A., (Editors) WindEffects on Buildings and Structures Sympposium at Loughborough, England (Published by Univ. of Loughborough), April 1968.
4. Sharma, C.B., and Johns, D.J. Vibration Characteristics of a Clamped-Ring Stiffened Cylindrical Shell. Report TT 7001, Loughborough University of Technology, Jan. 1970.
5. Johns, D.J., Wind-Excited Behaviour of Cylindrical Structures: - Its Relevance to Aerospace Design; Paper No. 25, AGARD CP No. 48, September 1969.
6. Wootton, L.R., Sainsbury, R.N., Warner, M.H., and Cooper, D.H. The Flow Induced Oscillation of Piles , N.P.L. Aero Special Report 025, January 1969.
7. Chen, Y.N. Vibration excited by Wakes on Circular Cylinders at Supercritical Reynolds Numbers. Sulzer Technical Review - Research Number, pp. 70-77, 1966.
8. Fung, Y.C. Fluctuating Lift and Drag Acting on a Cylinder in a Flow at Supercritical Reynolds numbers. J. Aero/Space Sci. pp. 801-814, Nov. 1960.
9. Roshko, A. Experiments on the Flow Past a Circular Cylinder at a very high Reynolds Number, J. Fluid Mech., Vol. 10, Pt. 3, pp. 345-356, May 1961.
10. Wootton, L.R., The Oscillation of Model Circular Stacks due to Vortex Shedding at Reynolds Numbers from 10^5 to 3×10^6, N.P.L. Aero Report 1267, June 1968.

11. Evensen, D.A. Non-linear Vibrations of an Infinitely Long Cylindrical Shell. AIAAJ., Vol 6., No. 7, July 1968.

12. Wootton, L.R., and Scruton, C., Aerodynamic Stability , Paper 5, A CIRIA Seminar on "The Modern Design of Wind-Sensitive structures" 18th June, 1970.

TABLE 1. Geometrical and Structural Properties of the Models Tested

Cylinder Notation	Length (L) in	Radius (a) in	Thickness (h) in	Youngs Modulus (E) psi	Poisson's Ratio (ν)	Mass density ρ lb-sec^2/in^4	Material
+SI	72	6	0.010	10^7	0.3	2.59×10^{-4}	Al
SII	69	6	0.023	10^7	0.3	2.59×10^{-4}	Al
SIII	69	6	0.030	10^7	0.3	2.59×10^{-4}	Al
SIV	69	6	0.036	10^7	0.3	2.59×10^{-4}	Al
SV	69	6	0.028	3×10^7	0.3	7.37×10^{-4}	Steel
*TI	20	2.4	0.01	10^7	0.3	2.59×10^{-4}	Al
TII	36	2.4	0.01	10^7	0.3	2.59×10^{-4}	Al
TIII	60	2.4	0.01	10^7	0.3	2.59×10^{-4}	Al
TIV	71	2.4	0.01	10^7	0.3	2.59×10^{-4}	Al
TV	36	4	0.01	10^7	0.3	2.59×10^{-4}	Al
TVI	46	4	0.01	10^7	0.3	2.59×10^{-4}	Al
TVII	71	4	0.01	10^7	0.3	2.59×10^{-4}	Al
TVIII	70	6	0.01	10^7	0.3	2.59×10^{-4}	Al
TIX	36	4	0.01	3×10^7	0.3	7.37×10^{-4}	Steel

+ Letter 'S' preceding the no. indicates that electromechanical shaker is used as excitation device.

* Letter 'T' indicates the models tested in the L.U.T. Wind-Tunnel.

TABLE 2. Calculated and Measured Frequencies (Hz) of Clamped-Free Shell (Model, SI)

m	1			2			3		
n	Calculated frequency Hz	Measured frequency Hz	Structural Damping g x 100	Calculated frequency Hz	Measured frequency Hz	Structural Damping g x 100	Calculated frequency Hz	Measured frequency Hz	Structural Damping g x 100
0	579	-	-	1530	-	-	2360	-	-
1	84.3	-	-	470	-	-	1120	-	-
2	28.1	26.3	2.28	164	-	-	446	-	-
3	23.7	21.0	2.1	80.9	76.8, 72.7*	2.36, 2.38*	222	-	-
4	38.9	37.3, 36.6*	2.4, 2.46*	59.5	56.9*	2.46*	135	-	-
5	62.0	60.6	2.0	68.8	69.2, 61.3*	2.4, 2.44*	105	99.8, 92.6*	2.5, 2.5*
6	90.7	86.9, 84.8*	2.2, 2.4*	93.3	91, 86*	2.4, 2.6*	109	105.3, 100*	2.5, 2.6*
7	125	121.2, 113.7*	2.5, 2.5*	126	-	-	133	125.8*	2.5*
8	164	160.4	2.3	165	-	-	169	157.1*	2.6*
9	209	-	-	209	-	-	211	-	-
10	258	-	-	260	-	-	261	-	-

* These values correspond to the shell SI coated with Vy coat CA 90.

TABLE 3. Calculated and Measured Frequencies (Hz) of Clamped-Free Shell (Model, SII)

m	1			2			3		
n	Calculated frequency Hz	Measured frequency Hz	Structural Damping g x 100	Calculated frequency Hz	Measured frequency Hz	Structural Damping g x 100	Calculated frequency Hz	Measured frequency Hz	Structural Damping g x 100
0	604	-	-	1600	-	-	2460	-	-
1	91.6	-	-	507	-	-	1200	-	-
2	33.8	31.6	2.26	179	-	-	483	-	-
3	48.0	46.4	2.37	97.2	95.0	2.32	244	-	-
4	88.3	86.0	2.5	102	100.1	2.1	167	163.8	2.42
5	142	144.0	2.27	147	147.8	2.22	171	170.4	2.19
6	208	208.5	2.26	210.7	208.6	2.21	221	217.8	2.17
7	287	-	-	288	284.0	2.27	294	294.6	2.27
8	377	-	-	379	-	-	382	389.0	2.0
9	480	-	-	481	-	-	484	492.0	2.24
10	594	-	-	595	-	-	598	-	-

TABLE 4. Calculated and Measured Frequencies (Hz) of Clamped-Free Shell (Model, SIII)

m	1			2			3		
n	Calculated frequency Hz	Measured frequency Hz	Structural Damping g x 100	Calculated frequency Hz	Measured frequency Hz	Structural Damping g x 100	Calculated frequency Hz	Measured frequency Hz	Structural Damping g x 100
0	604	-	-	1600	-	-	2460	-	-
1	91.6	-	-	507	-	-	1200	-	-
2	36.5	33.6, 30.5*	2.12, 2.5*	179	-	-	483	-	-
3	61.5	59.1, 55*	2.06, 2.3*	105	101.4, 92*	2.36, 2.5*	248	239.0	2.3
4	115	110.6	2.3	126	119.6,114.6*	2.1, 2.3*	184	173.0, 170*	2.3, 2.44*
5	185	-	-	190	183.0	2.3	210	192.5,190.3*	2.28,2.36*
6	272	-	-	274	-	-	283	267.8	2.32
7	374	-	-	376	-	-	381	-	-
8	492	-	-	494	-	-	497	-	-
9	626	-	-	627	-	-	630	-	-
10	775	-	-	777	-	-	780	-	-

* These values correspond to shell SIII with .01 in. thick coat of Vy coat CA 90.

TABLE 5. Calculated and Measured Frequencies (Hz) of Clamped-Free Shell (Model, SIV)

m	1			2			3		
n	Calculated frequency Hz	Measured frequency Hz	Structural Damping g x 100	Calculated frequency Hz	Measured frequency Hz	Structural Damping g x 100	Calculated frequency Hz	Measured frequency Hz	Structural Damping g x 100
0	604	-	-	1600	-	-	2460	-	-
1	91.6	-	-	507	-	-	1200	-	-
2	39.1	36.0	2.3	180	-	-	484	-	-
3	73.2	69.7	2.3	112	107	2.24	251	-	-
4	138	132.5	2.27	148	140.6	2.35	200	187.6	2.33
5	222	-	-	226	217.5	2.36	245	240.8	2.41
6	326	-	-	329	-	-	337	328	2.13
7	449	-	-	451	-	-	456	-	-
8	590	-	-	592	-	-	596	-	-
9	751	-	-	753	-	-	756	-	-
10	930	-	-	932	-	-	935	-	-

TABLE 6. Calculated and Measured Frequencies (Hz) of Clamped-Free Shell (Model, SV)

m	1			2			3		
n	Calculated frequency Hz	Measured frequency Hz	Structural Damping g x 100	Calculated frequency Hz	Measured frequency Hz	Structural Damping g x 100	Calculated frequency Hz	Measured frequency Hz	Structural Damping g x 100
0	622	-	-	1640	-	-	2540	-	-
1	94.3	-	-	522	-	-	1230	-	-
2	36.7	32.3	2.4	184	-	-	498	-	-
3	59.3	54.2	2.4	106	100.8	2.3	254	-	-
4	111	100.1	2.39	123	113.9	2.46	184	176.9	2.38
5	178	167.5	2.27	183	179.6	2.4	205	186.1	2.42
6	261	-	-	264	-	-	273	-	-
7	359	-	-	361	-	-	367	-	-
8	473	-	-	474	-	-	478	-	-
9	601	-	-	603	-	-	606	-	-
10	745	-	-	746	-	-	749	-	-

TABLE 7. Wind Tunnel Tests on Model Stack T I. (L/a = 8.3 , a/h = 240)

Circum - ferential Wave number n	Predicted Freq. Ω (Hz)	Critical V = 5 ΩD fps	Critical V = 6 ΩD fps	Measured Frequency (Hz)	Measured Wind Speed fps	Remarks
1	410.4	820.8	984.0			This shell, fairly short was designed in such a way on the basis of theoretical predictions that the minimum frequencies corresponding to n = 2, 3 are nearly identical, while testing the shell appeared to oscillate at two modes at the same time. As can be seen from the table from predicted critical wind speeds and measured wind speed the value of r in equation (2) is nearly 3.
2	142.1	284.2	342.0	138, 137	110	
3	140.6	281.2	337.0	137, 138	110	
4	242.2	484.4	582.0			
5	387.3	774.6	930.0			
6	567.0	1133.8	1609.0			
7	779.7	1559.4	1870.0			
8	1025	2051	2460.0			
9	1304	2608	3130.0			
10	1615	3230	3875.0			

TABLE 8 . Wind Tunnel Tests on Model Stack T II (L/a = 15, a/h = 240)

Circum-ferential Wave number n	Predicted Freq. Ω (Hz)	Critical V = 5ΩD fps	Critical V = 6ΩD fps	Measured Frequency (Hz)	Measured Wind Speed fps	Remarks
1	136.0	272.0	326.4			This shell was designed to excite only n = 2 mode in the L.U.T. wind tunnel. All other frequencies are quite distinct from each other. As can be seen in the table the only excited mode was n = 2 and here also one can see by comparison that the predicted critical wind speed is nearly 3 times the measured wind speed thus r ≃ 3. Though the shell started oscillating at a wind speed of 40 f.p.s. as seen on the oscilloscope the maximum deflection was achieved at a wind speed of 49 f.p.s.
2	62.0	124.0	148.8	60.2	49.0	
3	126.3	252.6	303.1			
4	239.0	478.0	573.6			
5	386.0	772.0	926.4			
6	566.0	1132.0	1358.4			
7	779.0	1558.0	1869.6			
8	1025.0	2049.0	2460.0			
9	1303.0	2606.0	3127.2			
10	1614.0	3229.0	3873.6			

TABLE 9 . Wind Tunnel Tests on Model Stack T III (L/a = 25, a/h = 240)

Circum-ferential Wave number n	Predicted Freq. Ω (Hz)	Critical V = 5ΩD fps	Critical V = 6ΩD fps	Measured Frequency (Hz)	Measured Wind Speed fps	Remarks
1	49.5	99.0	118.8	50	59.2	This shell was designed to be excited in 3 modes n = 1, 2, 3, which it does as is evident here.
2	46.8	93.5	112.3	45	39.0	
3	124.7	249.3	299.3	119	64.5	Here the values of r are different for different n. For n = 1, r ≃ 2, for n = 2, r ≈ 3 and for n = 3, r ≈ 5. The seam was put at different directions to the wind and it was found that although this does not affect the frequency it does affect the preferred mode i.e. the angle which axes of vibration make with wind direction. This is because during the 4th test there developed a vertical crack 4" long just near the seam. The ovalling axes became 45° to the wind direction which appeared to be the preferred mode orientation. Also frequencies were reduced slightly after this - for n = 2, it reduced to 44 from 45 and for n = 3 from 119 to 116.
4	238.6	477.2	572.6			
5	385.7	771.5	925.7			
6	565.8	1131.6	1358.0			
7	778.7	1557.4	1869.0			
8	1024.4	2048.8	2458.6			
9	1303.0	2606.0	3127.2			
10	1614.2	3228.4	3874.1			

TABLE 10. Wind Tunnel Tests on Model Stack TIV. ($L/a \simeq 29.6$, $a/h = 240$)

Circumferential Wave number n	Predicted Freq. Ω (Hz)	Critical $V = 5\,\Omega D$ fps	Critical $V = 6\,\Omega D$ fps	Measured Frequency (Hz)	Measured Wind Speed fps
1	35.4	70.8	85.0	33	75.2
2	45.4	90.9	109.0	43, 41*	34.6, 66.1*
3	124.5	249.0	299.0		
4	238.5	477.0	572.4		
5	385.7	771.4	925.7		
6	565.8	1131.5	1358.0		
7	778.7	1557.3	1869.0		
8	1024.4	2048.8	2458.6		
9	1303.0	2605.0	3127.2		
10	1614.2	3228.3	3874.1		

Remarks

Tests on this shell brought out quite a few interesting features. The shell started ovalling (n = 2) at a wind speed of 33.2 fps with axes of oscillation being at 45° to wind direction seen in figure 19. As the wind speed was increased there was a gradual change in direction of axes of oscillation. Finally at a wind speed of about 66 fps the change was complete and axes of ovalling were orthogonal to the wind as seen in figure 20. In between these two stages there was also swaying (n = 1).

As can be seen at 1st stage $r \simeq 3$ and at the second stage $r \simeq 2$ with a bigger amplitude and reduced frequency of 41 Hz from 43 at the first stage. In the 3rd test the shell started tearing off down the length near the seam. The split was about 6"-8". Afterwards shell vibrated more freely and with frequency and critical wind speeds slightly reduced.

* Ovalling with axes orthogonal to wind direction at higher windspeed.

TABLE 11. Wind Tunnel Tests on Model Stack TV. ($L/a \simeq 9$, $a/h = 400$)

Circum-ferential Wave number n	Predicted Freq. Ω (Hz)	Critical $V = 5\Omega D$ fps	Critical $V = 6\Omega D$ fps	Measured Frequency (Hz)	Measured Wind Speed fps	Remarks
1	220.7	735.6	882.8			This shell was designed to be excited in wind for n = 2, 3 modes. At the wind speed of 40.5 fps it was oscillating with n = 3 and at wind speed of 56 fps it was stopped and at wind speed of 60 fps it started oscillating with n = 2 mode i.e. ovalling. It is evident that the value of $r \simeq 5$ in both the cases as given by equation (2).
2	74.0	246.7	296.0	77.0	60.0	
3	56.6	188.6	226.4	54.0	40.5	
4	88.4	294.5	353.6			
5	139.7	465.7	558.8			
6	204.2	680.5	816.8			
7	280.7	935.6	1122.8			
8	369.1	1230.4	1476.4			
9	469.4	1564.5	1877.6			
10	581.4	1938.0	2325.6			

TABLE 12. Wind Tunnel Tests on Model Stack TVI (L/a = 11.5, a/h = 400)

Circum-ferential Wave number n	Predicted Freq. Ω (Hz)	Critical V = 5 ΩD fps	Critical V = 6 ΩD fps	Measured Frequency (Hz)	Measured Wind Speed fps	Remarks
1	137.3	457.8	549.2			Based on theoretical predictions this shell was designed to be excited with n = 2 and n = 3 modes at the same time. In fact it first started oscillating with n = 3 at about one-fifth of critical windspeed, i.e. with r≈5. As the windspeed was increased the shell was trying to vibrate with n = 2 and n = 3 at the same time. At a wind speed of about 59 fps shell was ovalling with r≈3. For this test the two seams were in the wind direction.
2	47.2	157.2	188.8	46.0	59.2	
3	49.6	165.3	198.4	48.0	38.0	
4	86.7	289.5	346.8			
5	139.2	464.1	556.8			
6	204.0	679.7	816.0			In the second test when the seams were at 90° to the wind the frequency was not affected but the critical speed was raised slightly, e.g. from 38 to 44 for n = 3 and from 59 to 65 for n = 2.
7	280.5	935.1	1122.0			
8	369.0	1230.0	1476.0			
9	469.2	1564.0	1876.8			
10	581.2	1937.6	2324.8			Although the ovalling (n = 2) frequency was lower than the frequency for n = 3 the n = 3 mode was excited first and n = 2 mode next.

TABLE 13. Wind Tunnel Tests on Model Stack TVII (L/a = 17.75, a/h = 400)

Circum-ferential Wave number n	Predicted Freq. Ω (Hz)	Critical V = 5 ΩD fps	Critical V = 6 ΩD fps	Measured Frequency (Hz)	Measured Wind Speed fps	Remarks
1	58.5	195.1	234.0			This shell was designed to oscillate with n = 2 and then n = 3. As can be seen it ovals at a wind speed of 30.4 fps and like all other shells this mode persists with increasing wind speed and at a wind speed of about 36.4 fps when the amplitude is maximum frequency appears to drop (from 23.2 Hz to 22 Hz). In this case r≈3. Seam appeared to force a node there though not preferred. With increase in wind speed the n = 3 mode appears at a windspeed of about 52 fps. At a wind speed of about 60 fps amplitude grows very big for n = 3 and frequency drops from 43 Hz to 42 Hz. The shell was flattened on the windward face and strain gauge broke at this point.
2	24.5	81.7	98.0	23.2, 22*	30.4, 36.4*	
3	45.7	152.3	182.8	43, 42*	52.25, 60.1*	
4	86.1	286.9	344.4			
5	139.0	463.1	556.0			
6	203.7	679.1	814.8			
7	280.4	934.6	1121.6			
8	368.8	1239.4	1475.2			
9	469.1	1563.6	1876.4			
10	581.2	1937.2	2324.8			

TABLE 14. Wind Tunnel Tests on Model Stack TVIII (L/a = 11.67, a/h = 600)

Circum-ferential Wave number n	Predicted Freq. Ω (Hz)	Critical V = 5ΩD fps	Critical V = 6ΩD fps	Measured Frequency (Hz)	Measured Wind Speed fps	Remarks
1	89.0	445.1	534.0			This shell was designed to oscillate in 3 different modes n = 2, 3,4 in the wind tunnel. At a wind speed of about 25 fps shell oscillated with n = 3. At a wind speed of about 33 fps mode n = 3 stopped and n = 2 was excited at a wind speed of about 35 fps though the amplitude was not very big. The ovalling axes were orthogonal to wind and r≈4 in this case. As the wind speed was increased the shell started oscillating with n = 4 at a wind speed of about 38 fps. At a wind speed of about 45 fps the shell again reverted back to the n = 3 mode. This time the frequency was reduced from 22.4 Hz to 19 Hz and the amplitude was much bigger than in the previous n = 3 case. The shell was almost collapsed at the windward face.
2	29.6	148.1	177.6	29.0	35.2	
3	24.2	120.8	145.2	22.4, 19*	25.6, 45.5*	
4	39.0	195.1	234.0	36.0	37.7	
5	62.0	310.0	372.0			
6	90.7	453.3	544.2			
7	124.7	623.4	748.2			
8	164.0	820.0	984.0			
9	208.5	1042.7	1251.0			
10	258.3	1291.7	1548.0			

TABLE 15. Wind Tunnel Tests on Model Stack T IX (L/a = 9, a/h = 400)

Circumferential Wave number n	Predicted Freq. Ω (Hz)	Critical V = 5 ΩD fps	Critical V = 6 ΩD fps	Measured Frequency (Hz)	Measured Wind Speed fps	Remarks
1	227.2	757.4	908.8			This steel shell behaved in the wind tunnel quite differently from its aluminium counterpart shell T V. This started oscillating at a much higher speed of 72 fps in the n = 3 mode and frequency 58 Hz. This persisted for higher wind speeds and at a wind speed of about 81 fps the amplitude grew bigger and the frequency reduced from 58 Hz to 56 Hz. Ovalling was not seen here at all in the given speed range contrary to its Al-counter part shell T V.
2	76.2	254.0	304.8			
3	58.2	194.2	232.8	58, 56*	72, 81*	
4	91.0	303.3	364.0			
5	144.0	479.5	576.0			
6	210.2	700.7	840.8			
7	289.0	963.3	1156.0			
8	380.0	1266.8	1520.0			
9	483.2	1610.8	1932.8			
10	598.6	1995.4	2394.4			

Figure 1

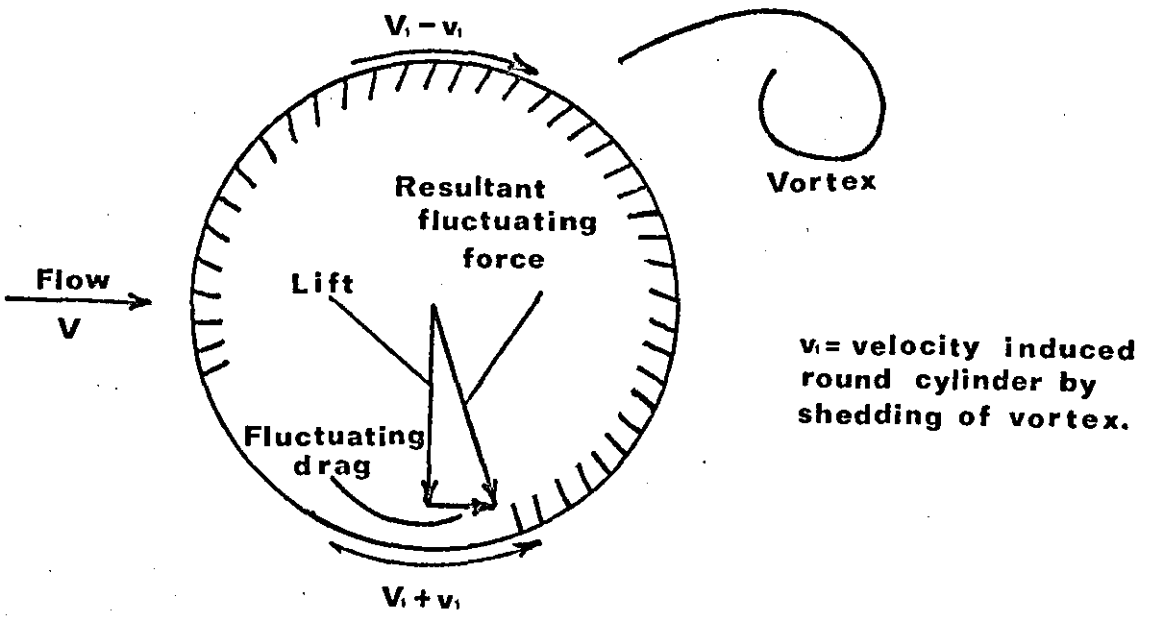

The derivation of the vortex-induced fluctuating force.

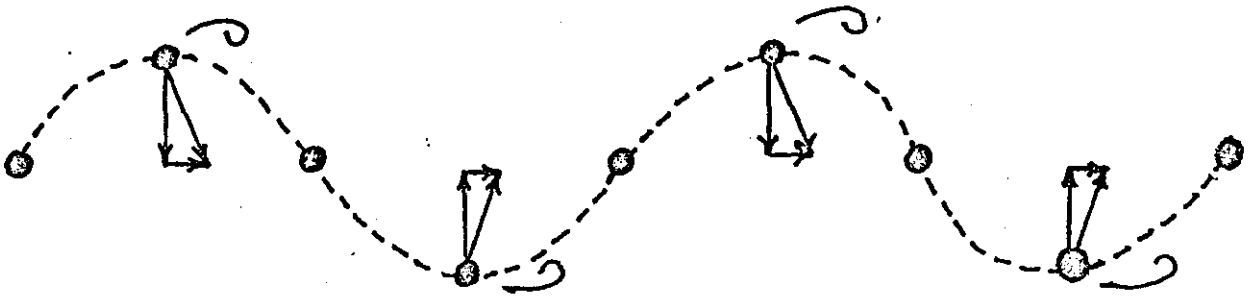

The motion of a cylinder free to oscillate across the direction of the flow when the velocity is such that $N=\Omega$. The fluctuating drag has twice the frequency of the fluctuating side (lift) force.

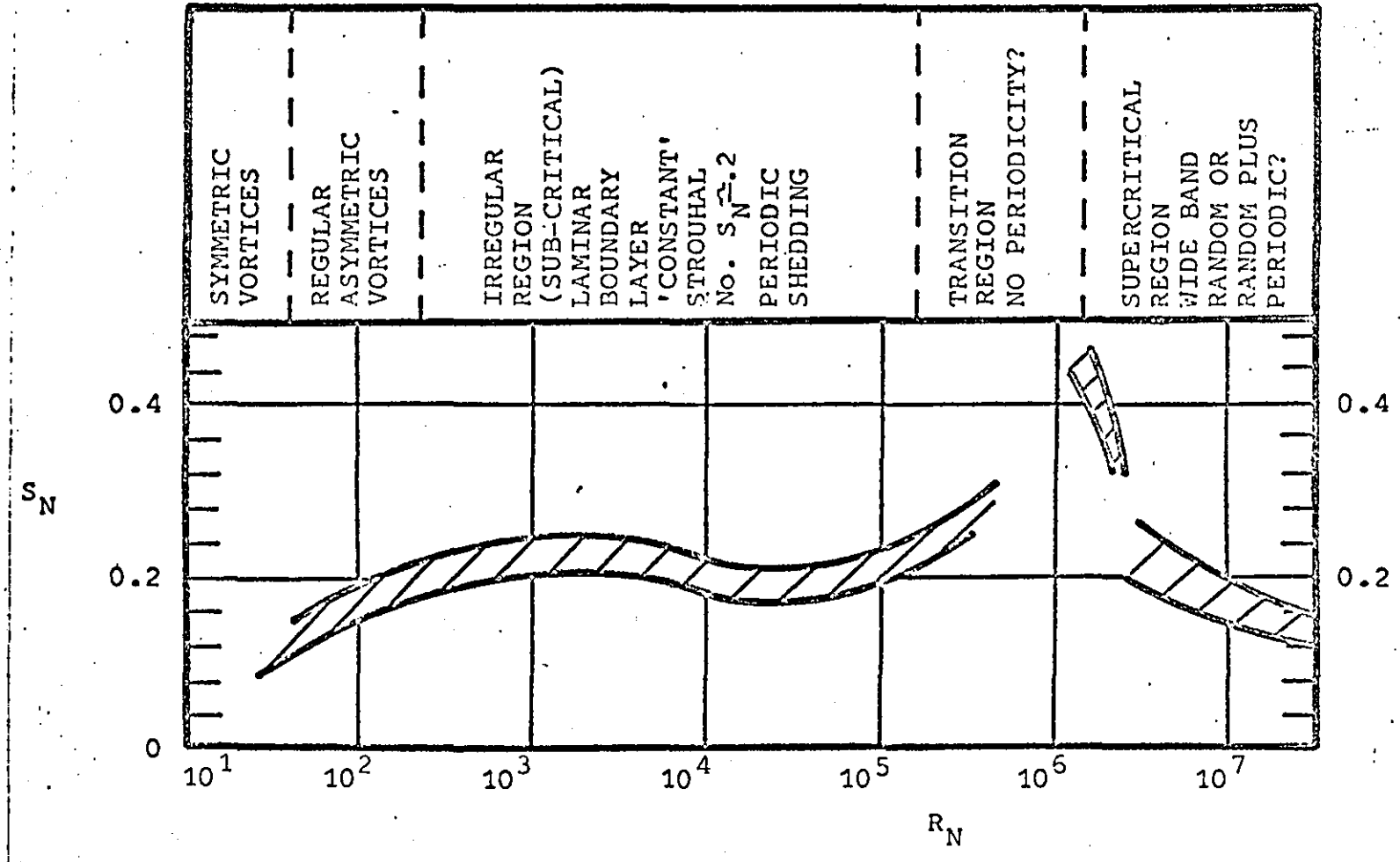

FIG 2 VORTEX SHEDDING FREQUENCIES FOR VARIOUS REYNOLDS Nos. (DATA FROM REFS 15-18)

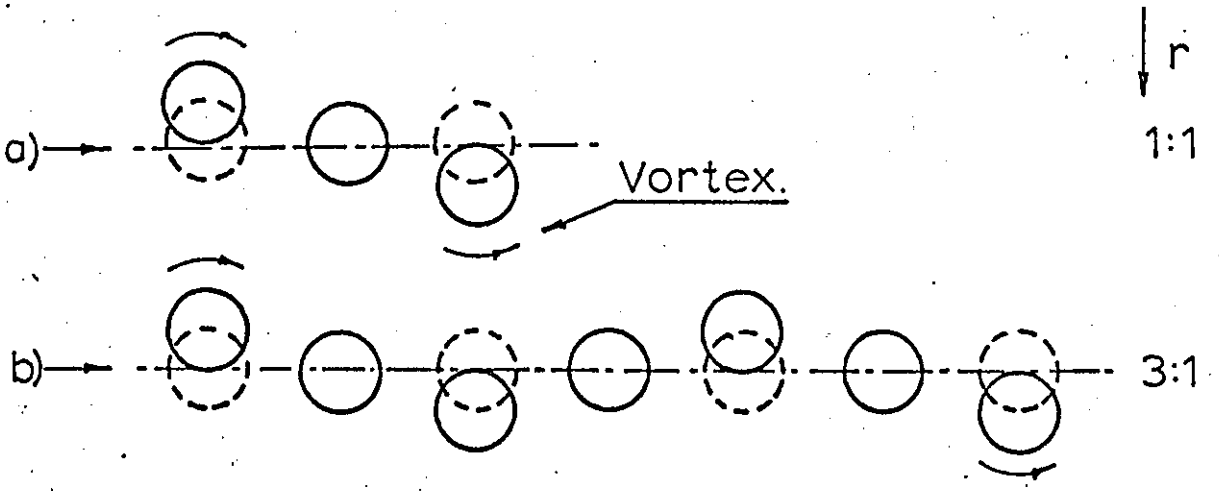

FIG.3 ALTERNATIVE RELATIONSHIPS BETWEEN BENDING OSCILLATIONS & VORTEX SHEDDING.

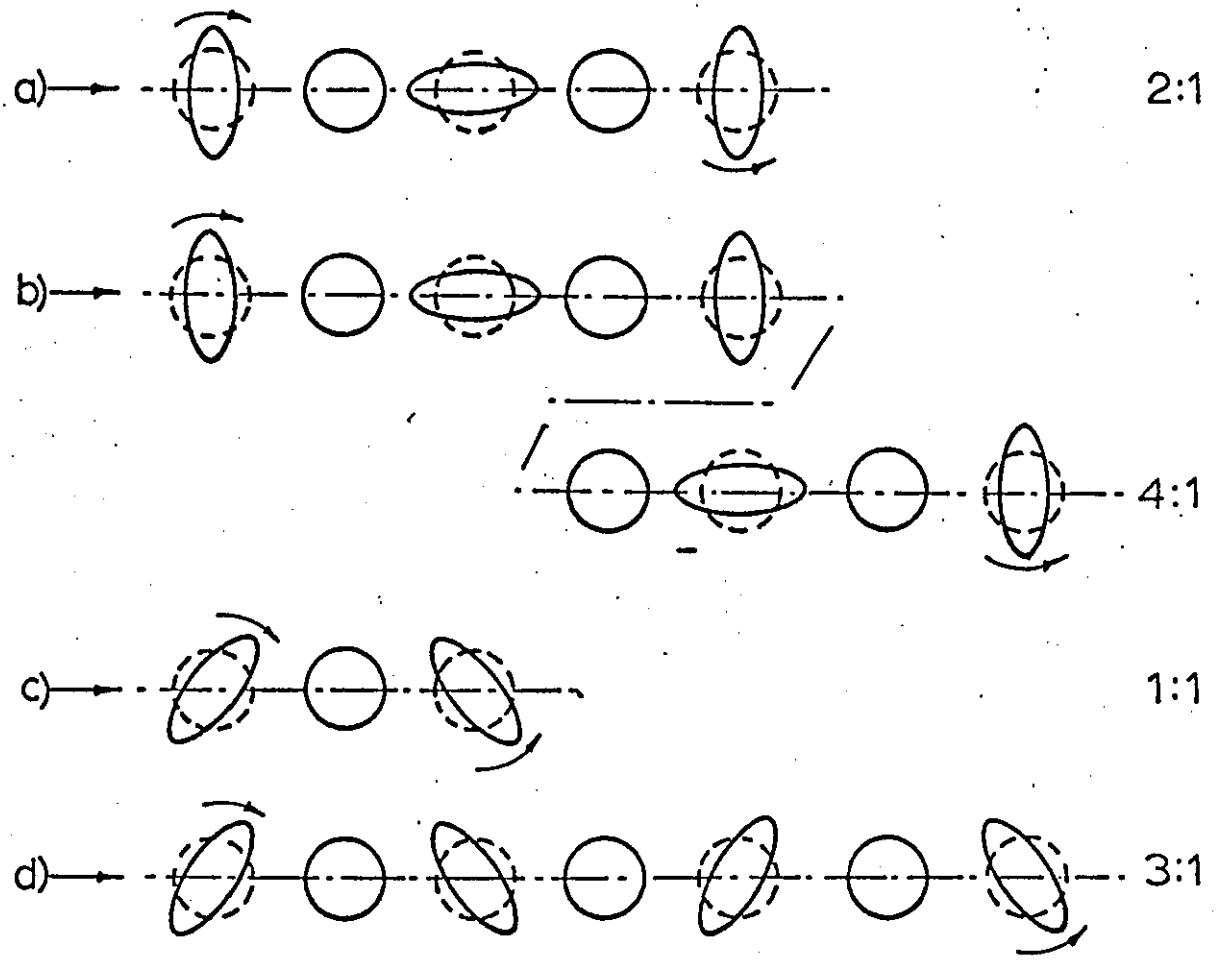

FIG.4. ALTERNATIVE RELATIONSHIPS BETWEEN OVALLING OSCILLATIONS & VORTEX SHEDDING.

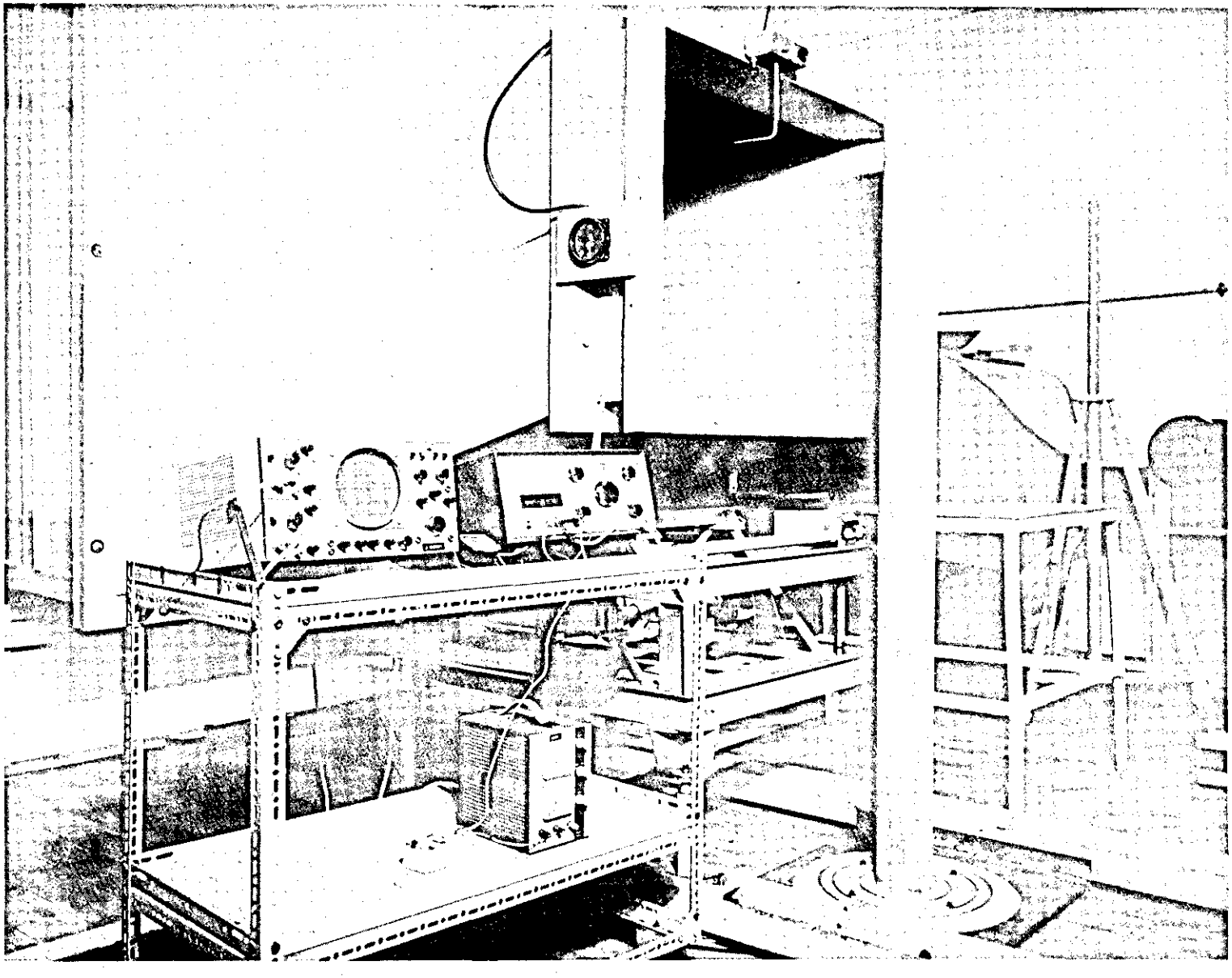

FIG. 5 A Pictorial View of a Model Stack in the Wind Tunnel & Instrumentation

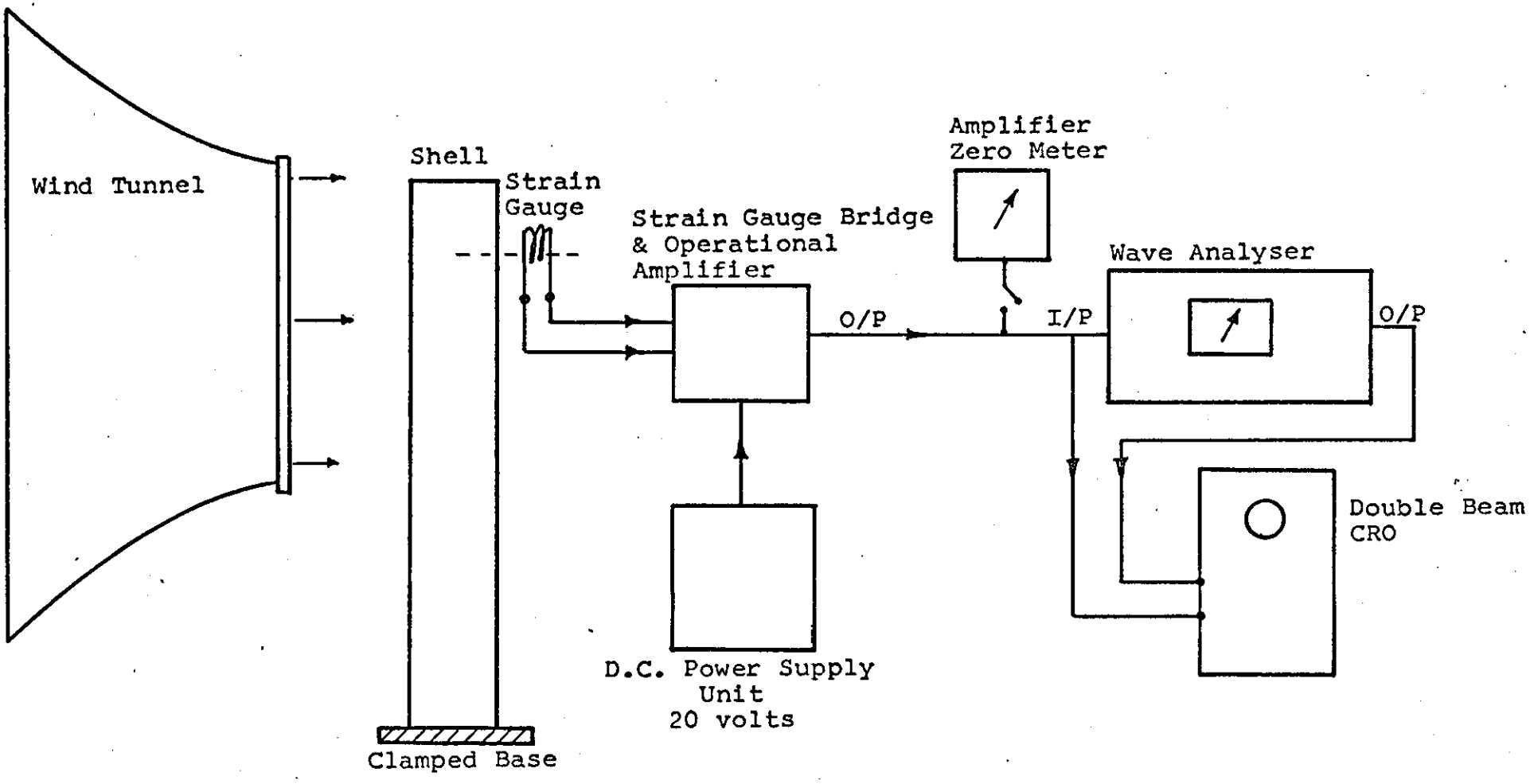

FIG. 6 WIND-TUNNEL TEST INSTRUMENTATION BLOCK DIAGRAM

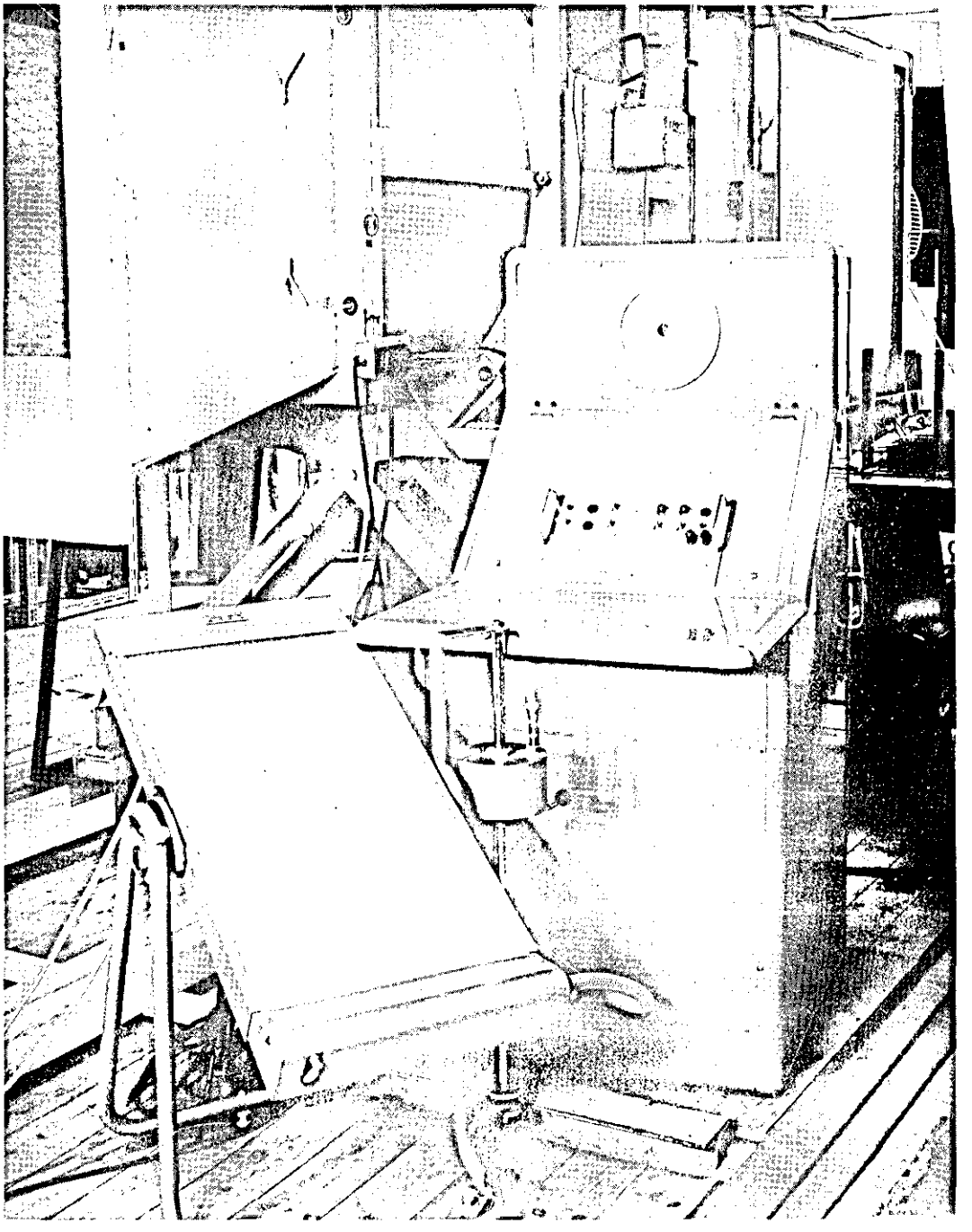

FIG.7 Wind speed measuring device

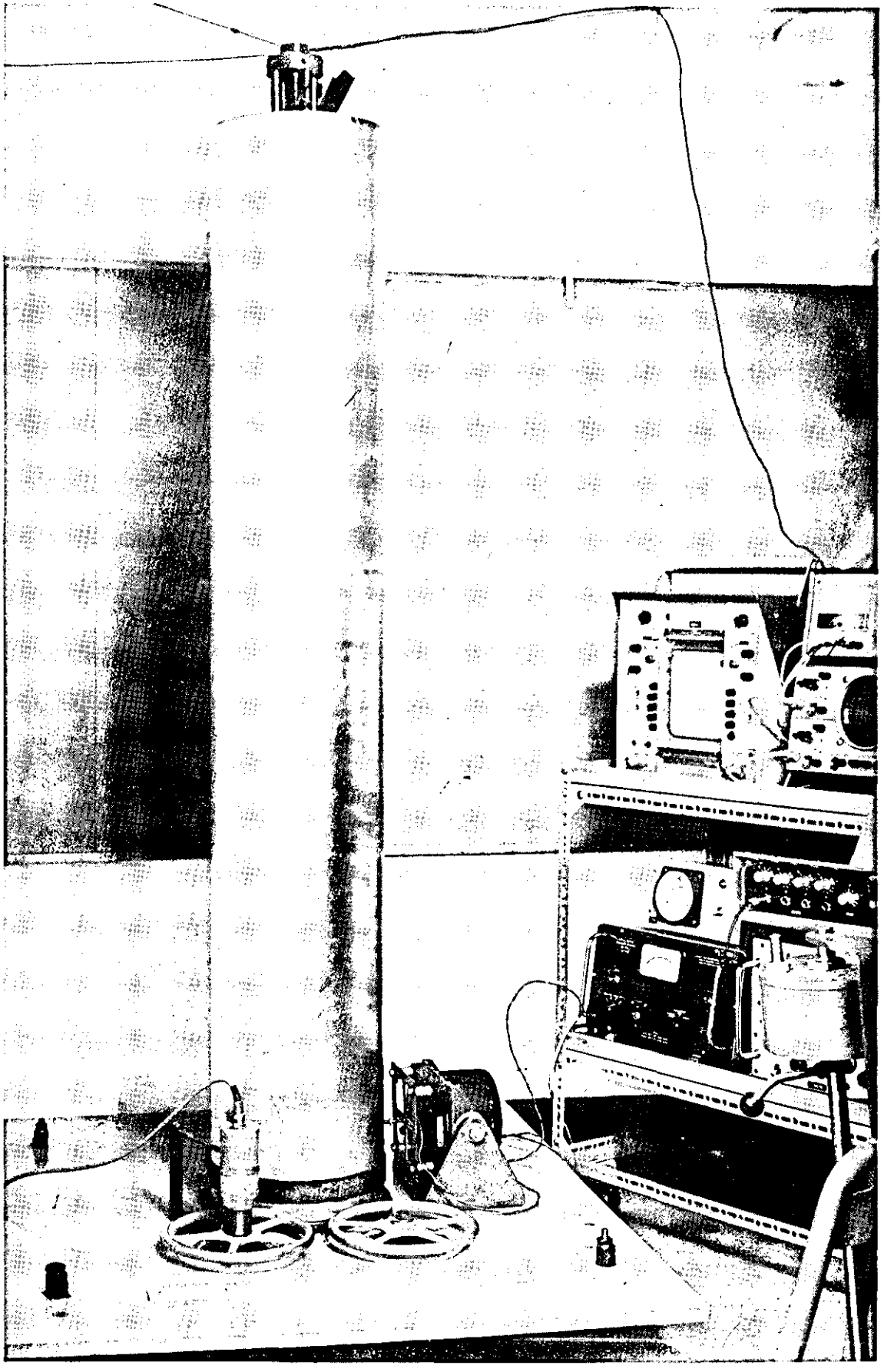

FIG. 8 A model stack mounted on the shaker rig

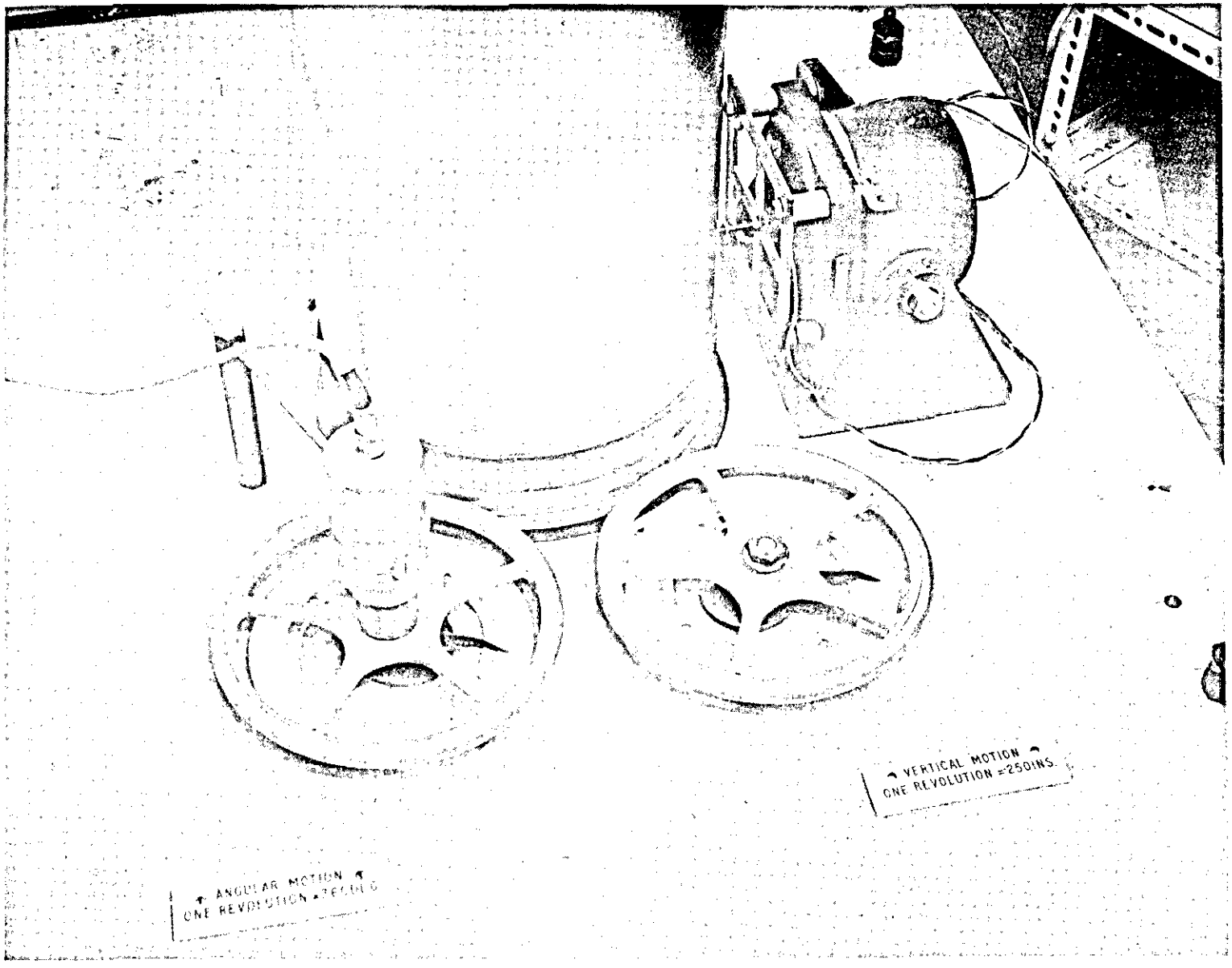

FIG.9 Shaker Installation & Vertical & Angular Moving Devices for the Microphone

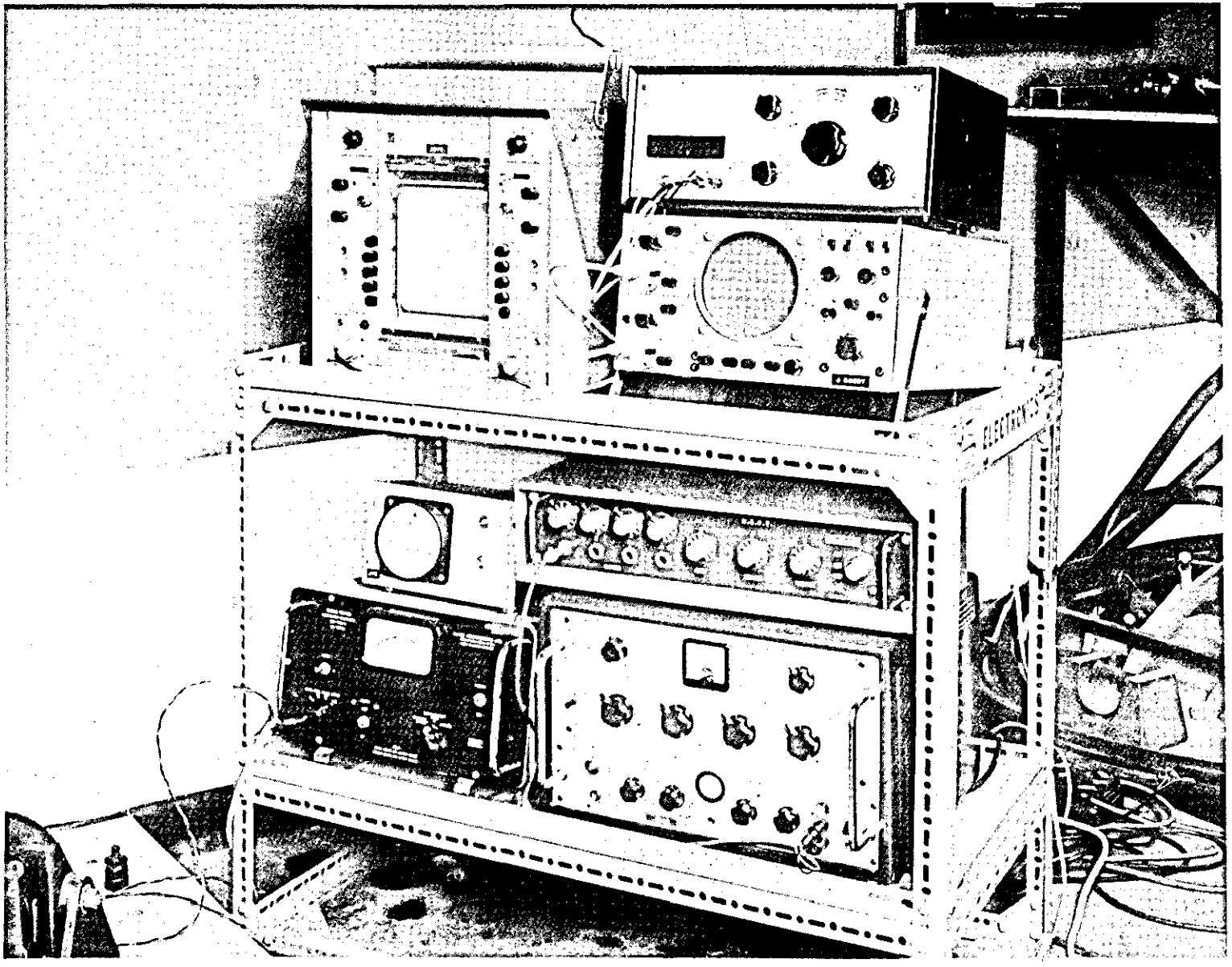

FIG.10 PHOTOGRAPH OF INSTRUMENTATION FOR THE SHAKER RIG

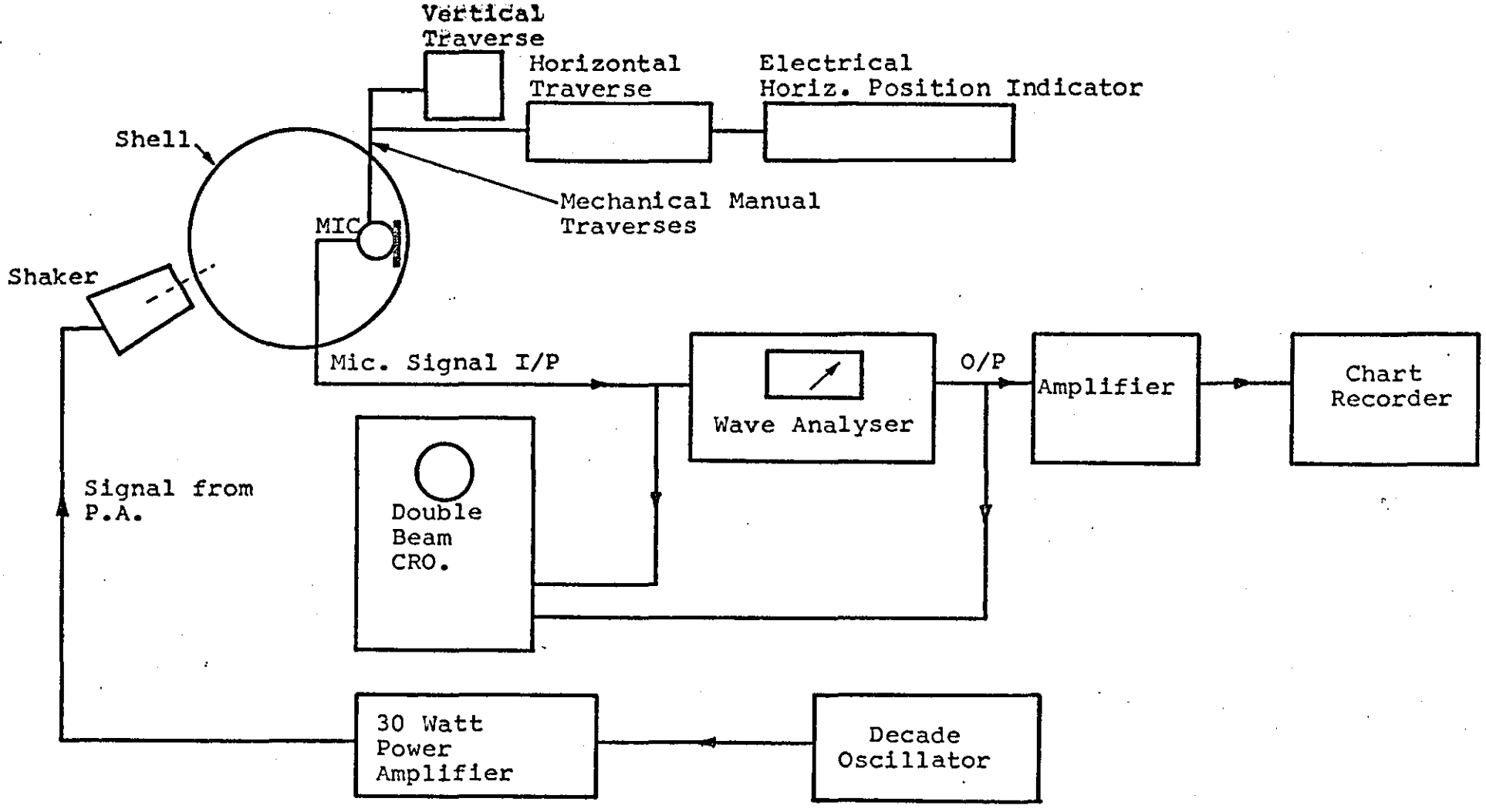

FIG. 11 INSTRUMENTATION BLOCK DIAGRAM FOR THE SHAKER RIG

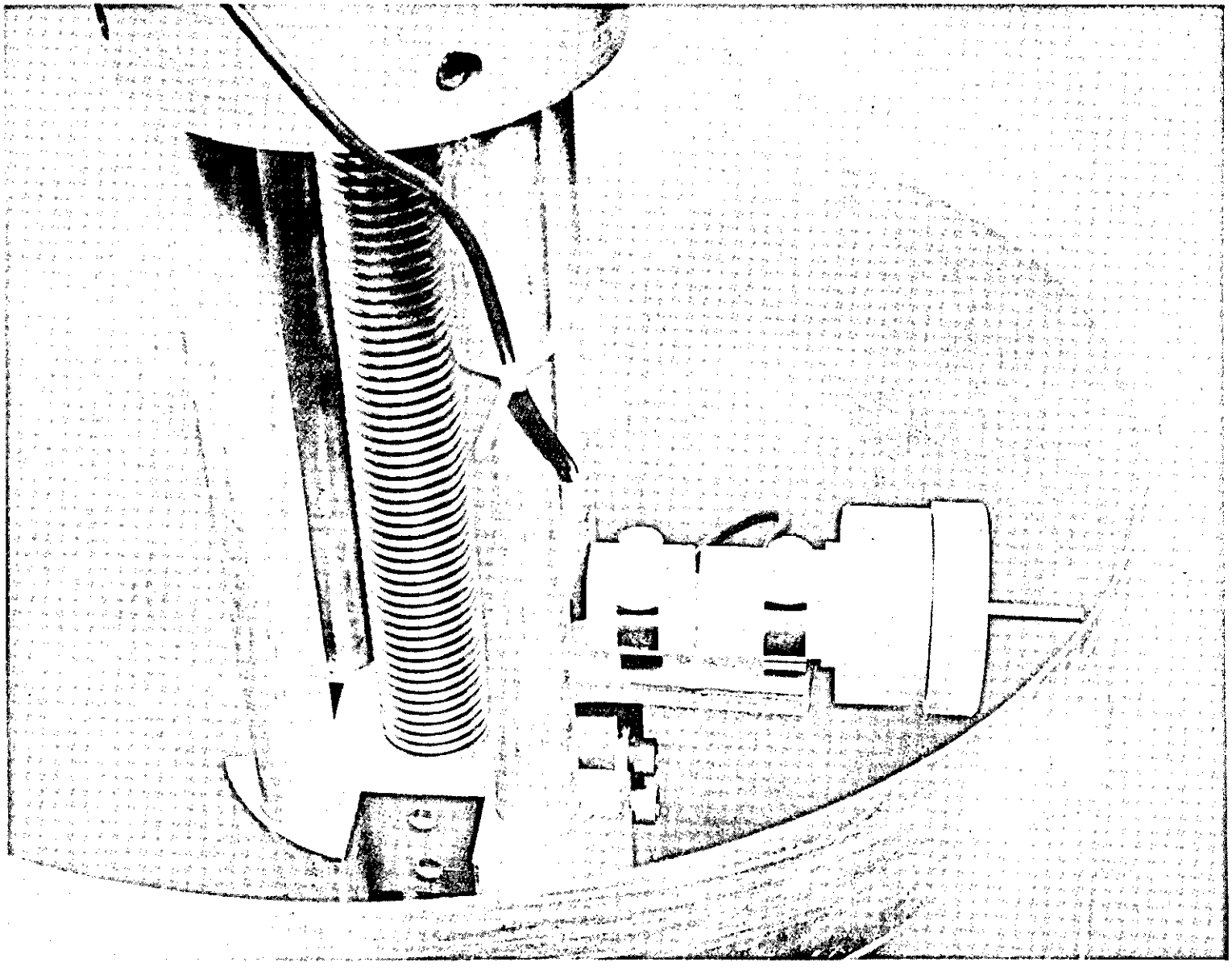

FIG.12 MICROPHONE INSTALLATION ON THE SHAKER RIG

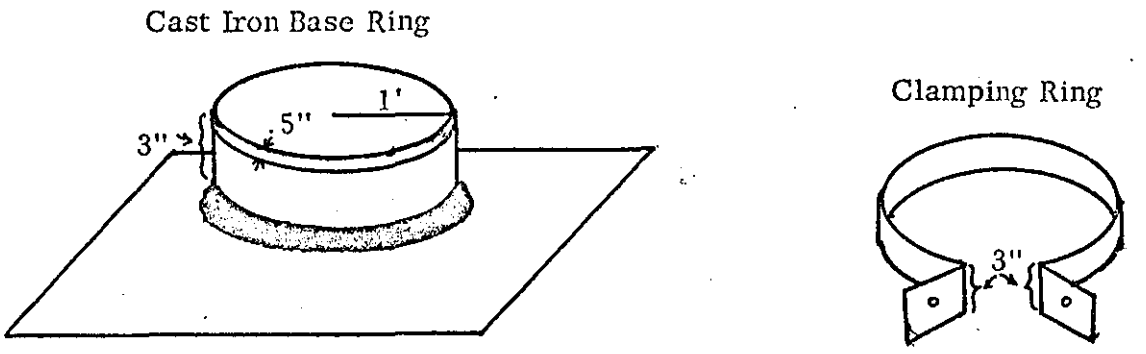

FIG. 13. Sketch showing dimensions of base ring and root clamping.

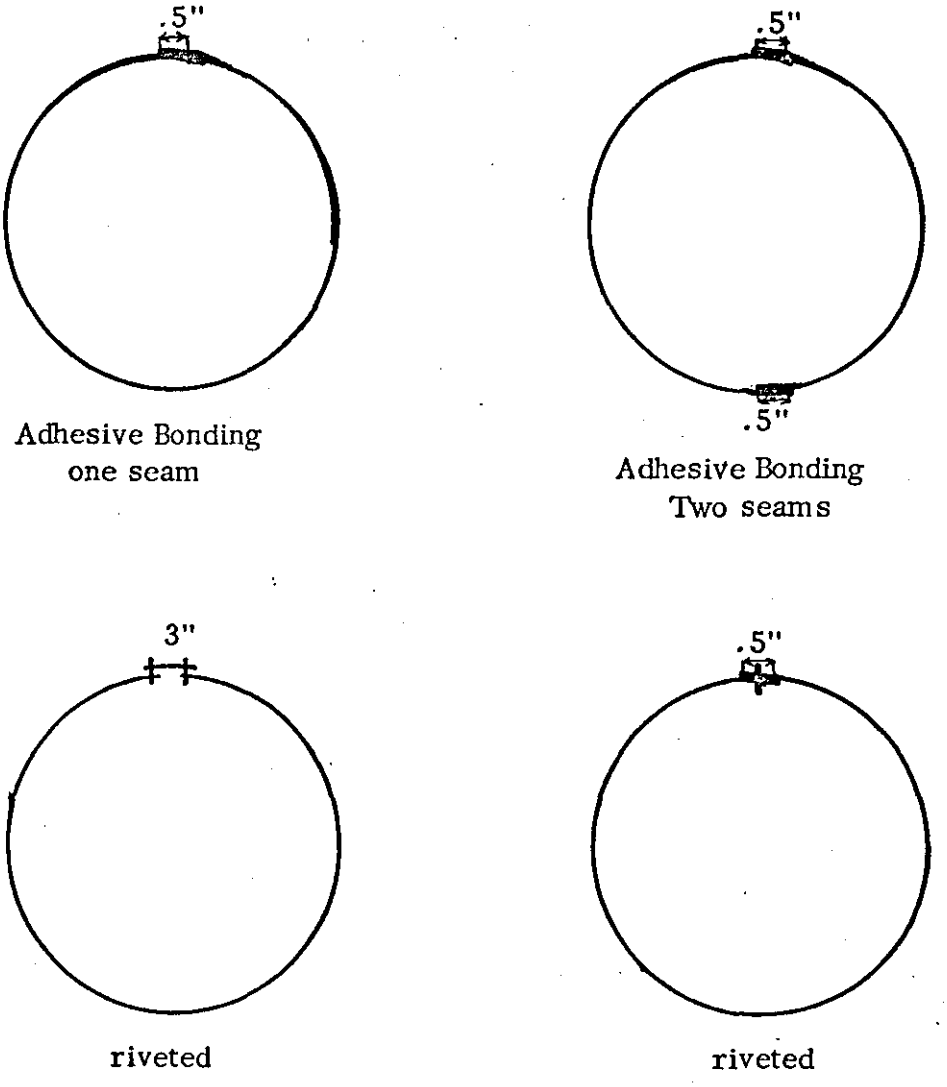

FIG. 14 Constructional Techniques for Shells:
One or more joints type of shells.

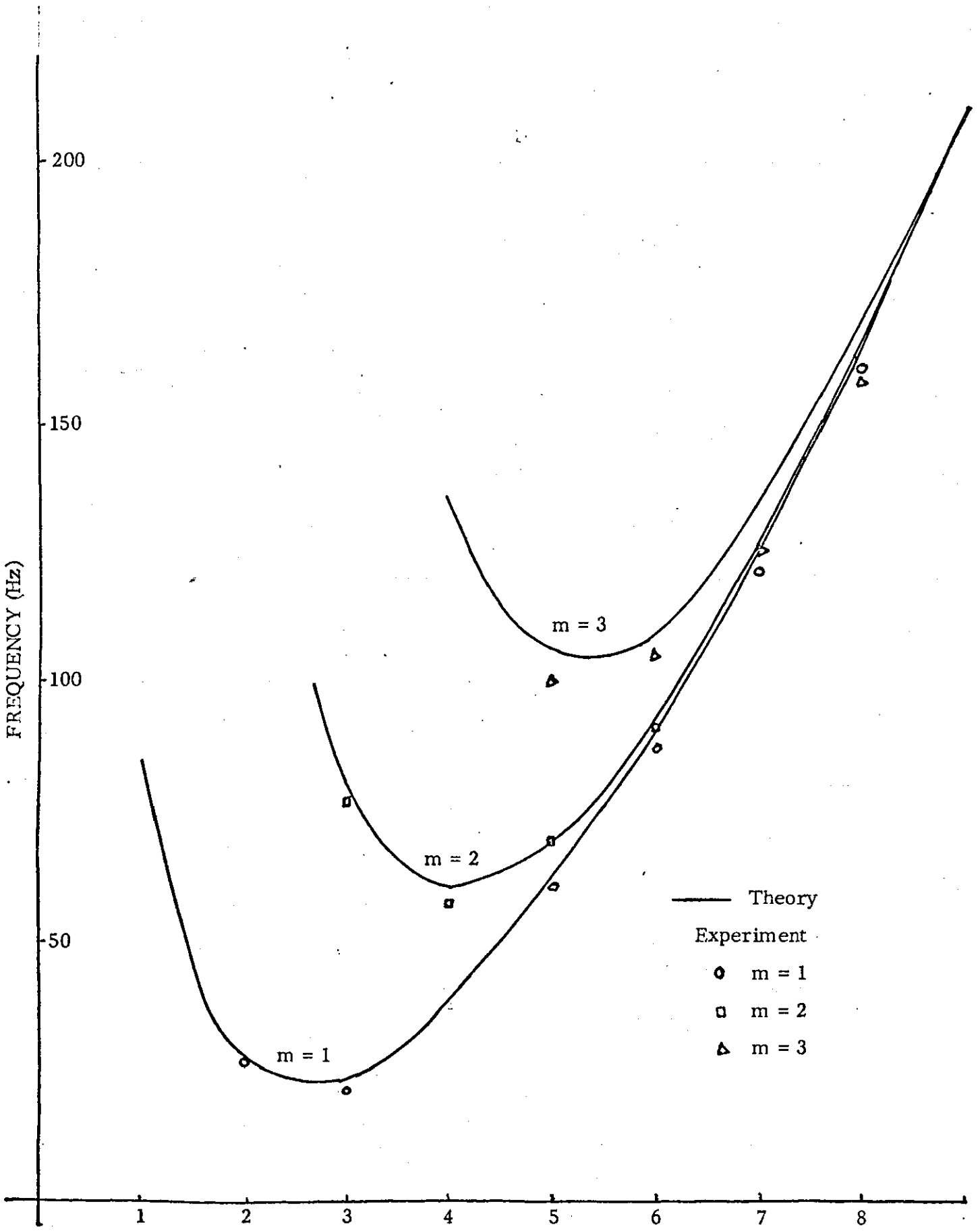

FIG. 15 EXPERIMENTAL AND ANALYTICAL FREQUENCIES OF CLAMPED-FREE SHELL (MODEL SI)

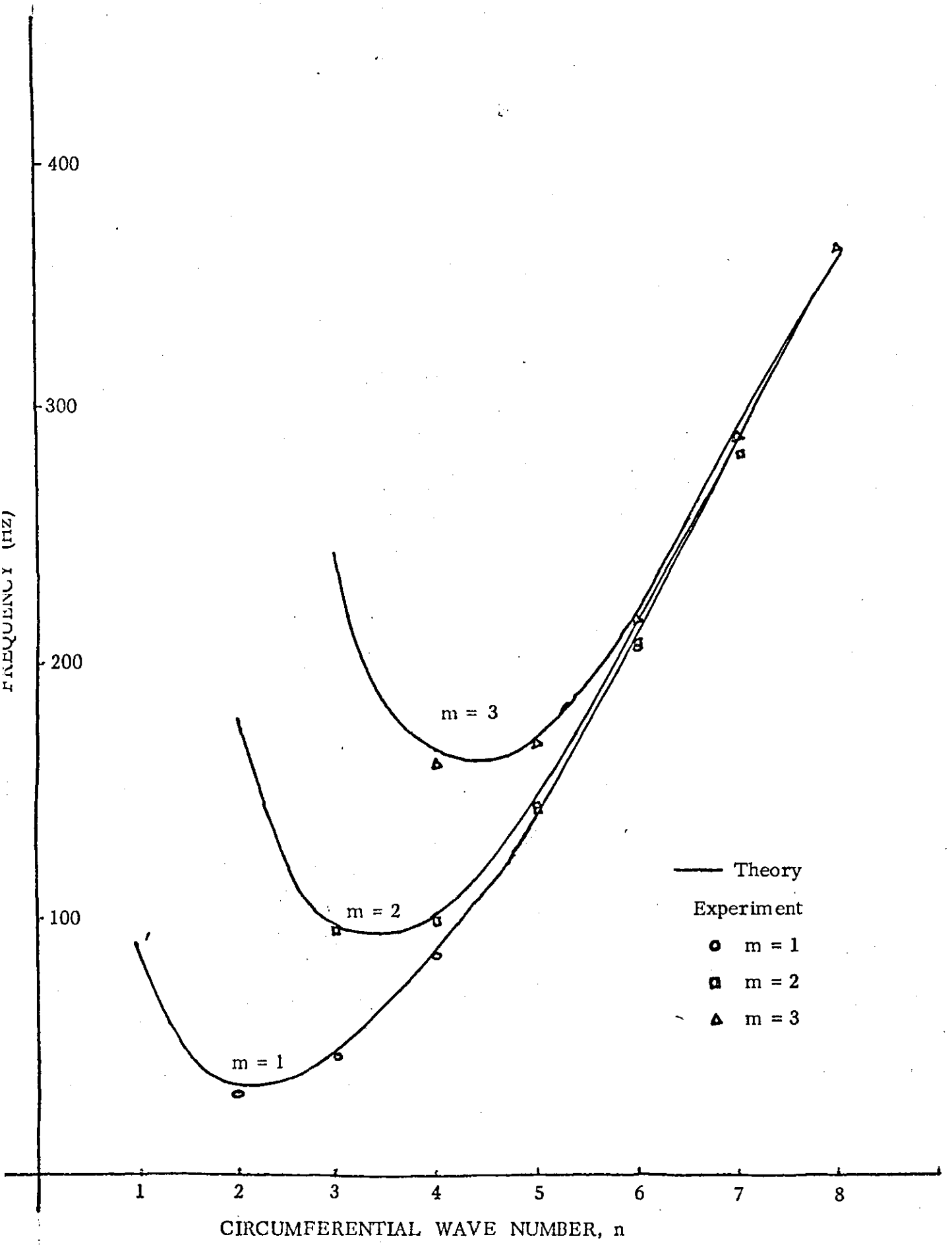

FIG. 16 EXPERIMENTAL AND ANALYTICAL FREQUENCIES OF CLAMPED-FREE SHELL (MODEL SII)

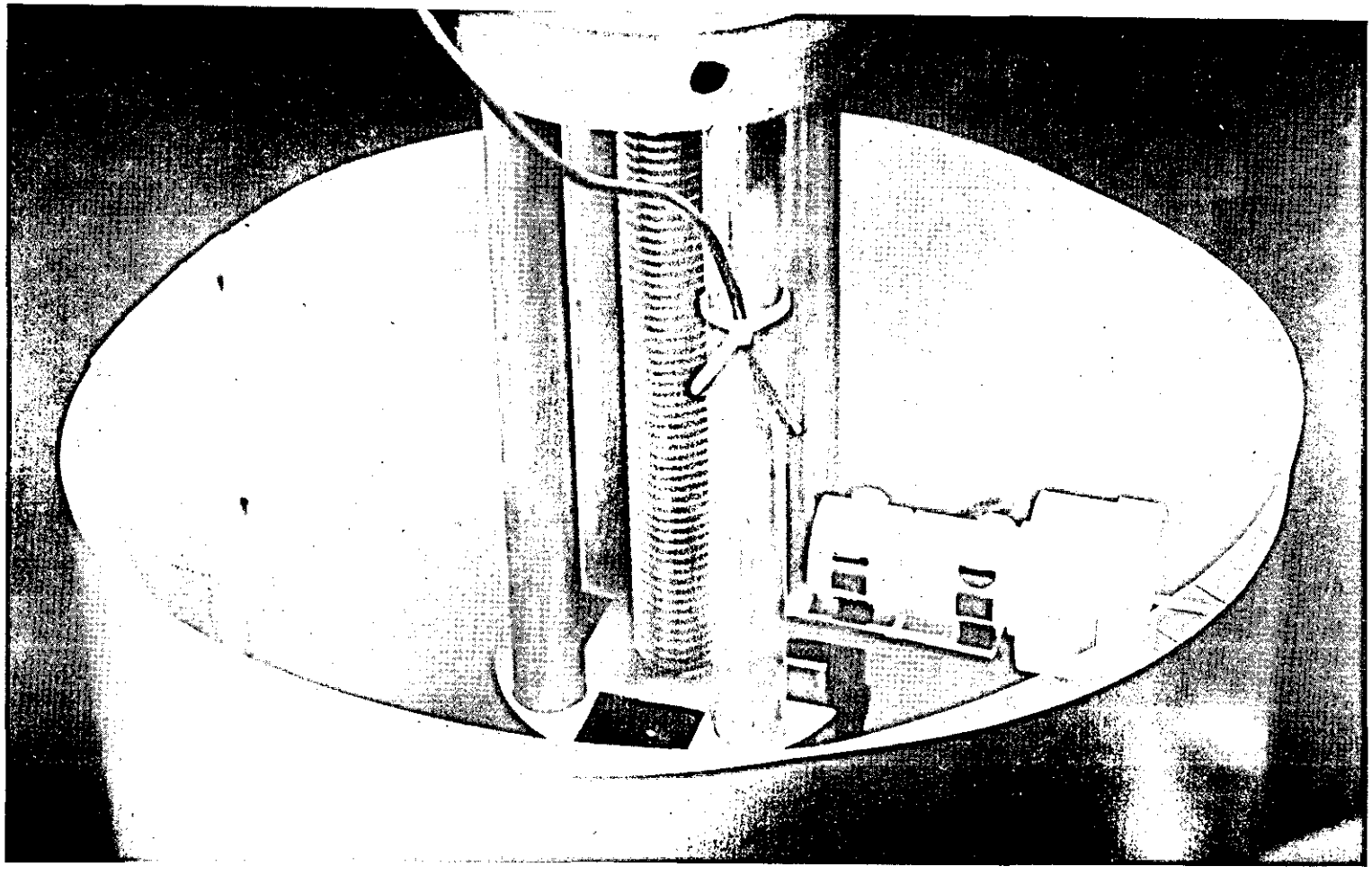

FIG.17 Pictorial View of Model Stack SII Oscillating with Three Circumferential Full Waves (n=3)

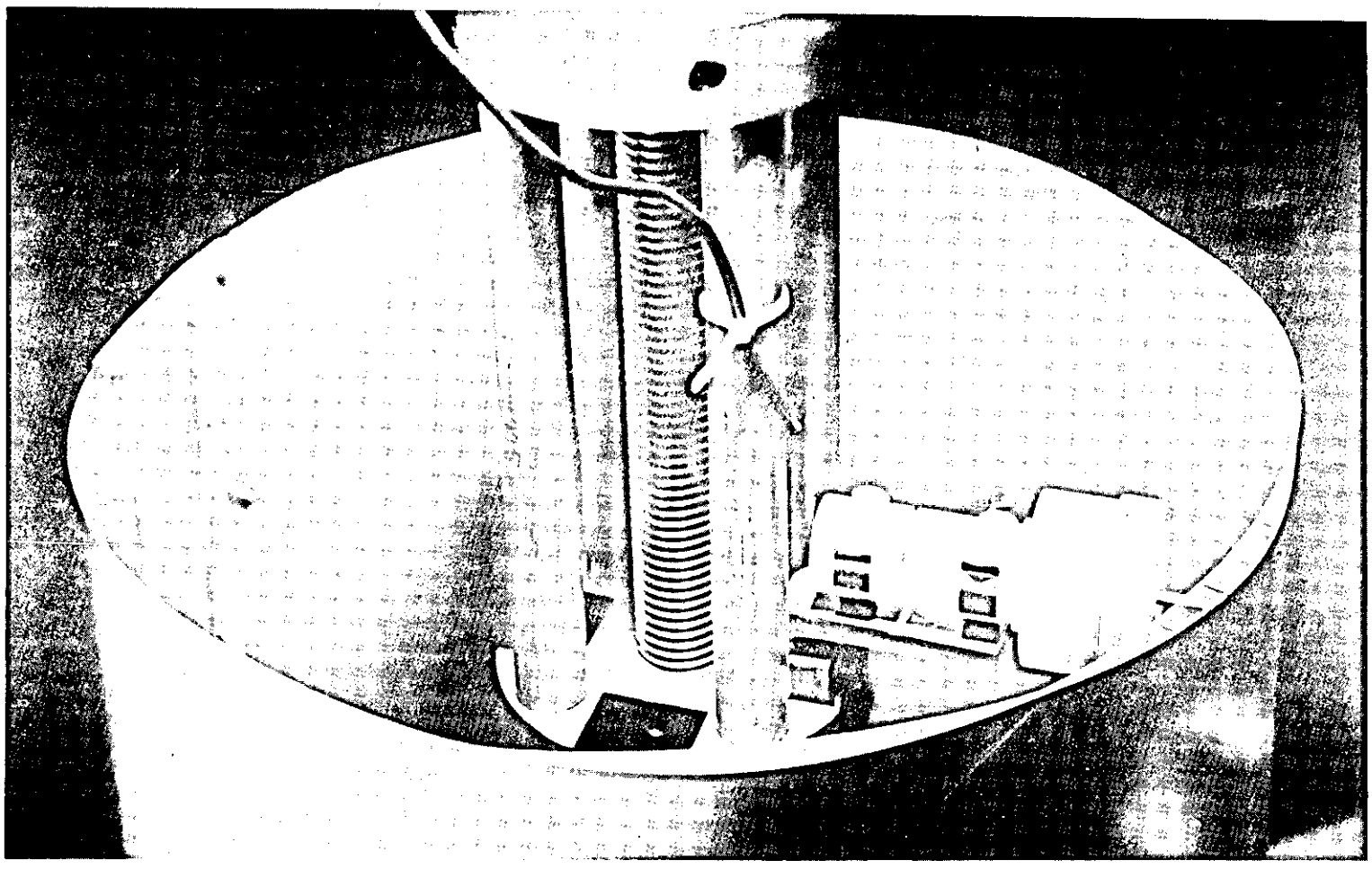

FIG.18 Pictorial View of Model Stack SII Oscillating with Four Circumferential Full Waves (n=4)

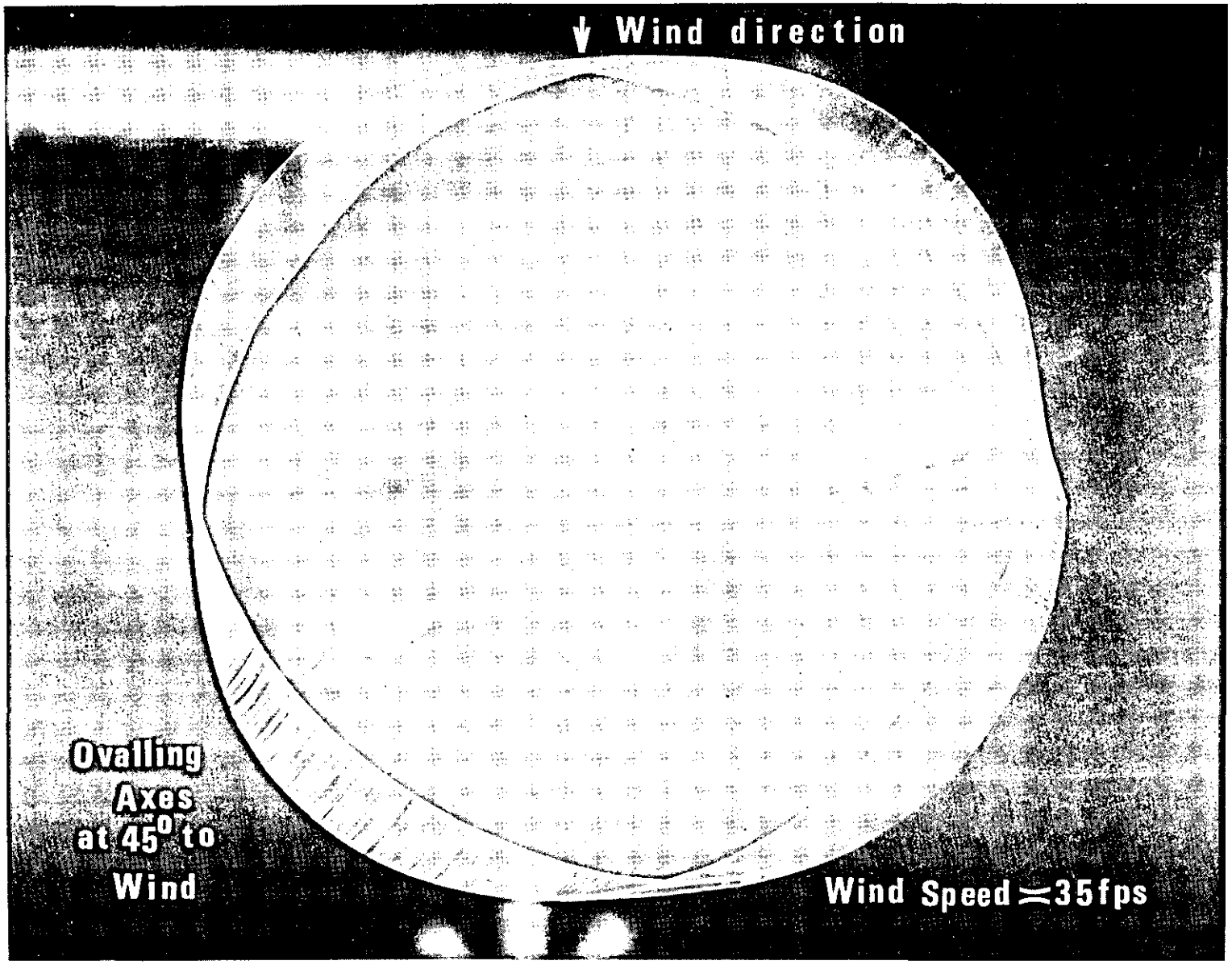

FIG.19 Photograph Showing Ovalling Oscillations of Model Stack TIV (Stage1)

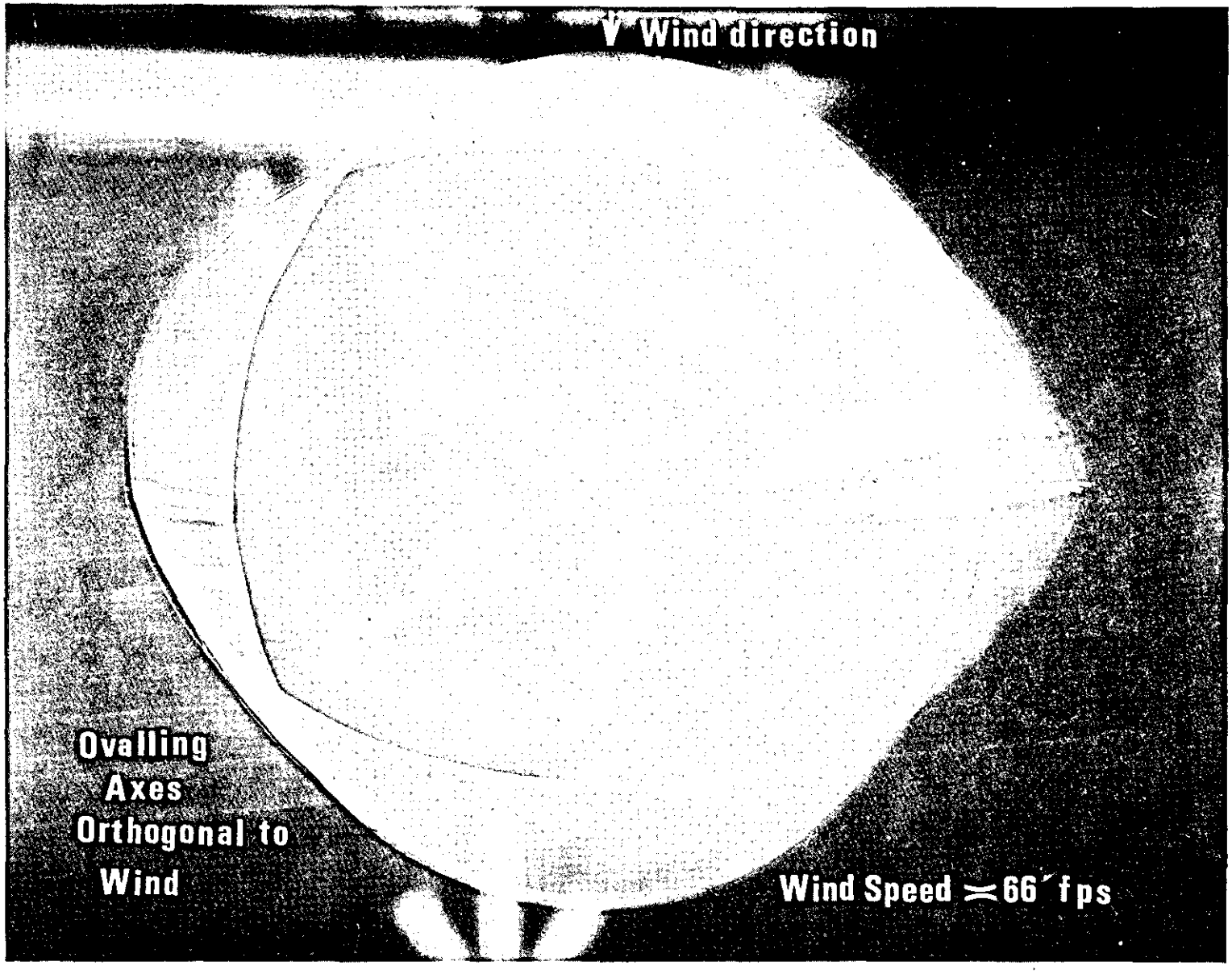

FIG.20 Photograph Showing Ovalling Oscillations of Model Stack TIV (Stage 2)

APPENDIX I (TT 7008)

EFFECT OF HELICAL STRAKES ON THE CYLINDER T IV TESTED IN THE WIND

This cylinder when tested in the wind tunnel showed quite a few interesting features which have been discussed briefly in Table 13 and shown in Figures 19 and 20.

Helical strakes, .25" wide and .5" deep were put on this cylinder on upper one third height of the cylinder. This was first tried to make strakes out of one piece material .25" wide and .5" deep. It was rather difficult to bend these strakes to bring them to size where they will reasonably fit on the body of the cylinder so this method of making one-piece strakes was abandoned. The method which was successfully tried was that of glueing 9 strips, .25" wide and .052" thick, bent individually in the desired form of helical strakes.

Wind-tunnel tests were made and observations recorded were as follows:

There was hardly any movement observed for this cylinder with strakes at a wind speed of about 76 f.p.s., unlike the plain model stack T IV which ovalled significantly at this wind speed. At about 50 f.p.s., wind speed, ovalling was seen to commence though with a very small amplitude ($\approx$ 0.1" of oscillation which rose to about 0.15" at a wind speed of about 66 f.p.s. At about 71 f.p.s., of wind, transverse sway again with very small amplitude ($\approx$ .1") was observed which in no way can be compared with swaying amplitude observed for the plain cylinder T IV which was of the order of 0.5" to 0.7". This situation persisted with increasing wind speeds and amplitude grew to about .2" for a wind speed of 94 f.p.s.

APPENDIX II

Response of the Model Shell SI (PVC Coated) with One or Two Layers of 0.005" Thick Fablon

It has been remarked on page 35 that when shell TIV (with 0.005" pvc coat and 0.005" thick fablon layer over its surface) was tested in the wind tunnel the ovalling was virtually stopped and swaying was observed with a very much reduced amplitude and with a slight decrease in frequency. This was attributed to the added structural damping due to the fablon layer. An attempt has been made since, to assess the changes in frequency and structural damping due to the addition of one or two layers of 0.005" thick fablon on a pvc coated model stack (SI) excited by an electromechanical shaker.

It can be seen from table II 1 and from the previous results for shells (Table 5) that by adding a fablon layer there is only a marginal increase in the structural damping factor and an additional layer does not make any further appreciable difference in the results. Though the increase in damping over the shell with no added fablon is small, it is perhaps sufficient to decrease the amplitudes of oscillation and to stop the ovalling of shell TIV in the wind tunnel. As is indicated in Table II 1, the frequency of oscillation decreases due to added inertia of fablon layers although the effect appears to be greater than would have been anticipated.

It should be remarked however that the experimental technique involved in measuring the structural damping factor is not as sensitive as one would wish and an error of $\pm$ 30% is possible in the quoted values.

TABLE II 1

m	1			2			3		
n	Calculated frequency plain SI	Measured Frequency (Hz) (& damping)		Calculated frequency plain SI	Measured Frequency (Hz) (& damping)		Calculated frequency plain SI	Measured Frequency (Hz) (& damping)	
		one layer fablon	two layers fablon		one layer fablon	two layers fablon		one layer fablon	two layers fablon
1	84.3	-	-	470	-	-	1120	-	-
2	28.1	21.2	20.2,(2.3)	164	-	-	446	-	
3	23.7	20.6	21.0,(2.45)	80.9	72.8,(2.4)	64.6,(2.4)	222	-	164.5(2.3)
4	38.9	36	-	59.5	50.7,(2.9)	50.5,(2.5)	135	-	100.2,(2.2)
5	62	58	-	68.8	65.2,(2.5)	-	105	87.2(2.5)	77.4(2.5)

N.B. The damping values are quoted as per cent critical and are given inside parenthesis.